

Copyright
by
John Leo Molloy
2006

**The Dissertation Committee for John Leo Molloy Certifies that this is the approved
version of the following dissertation:**

Detection of Metal Vapor Atoms in Bubbles at Room Temperature

Committee:

James A. Holcombe, Supervisor

Gary T. Rochelle

Peter J. Rossky

Jason B. Shear

Keith J. Stevenson

Detection of Metal Vapor Atoms in Bubbles at Room Temperature

by

John Leo Molloy B.S.

Dissertation

Presented to the Faculty of the Graduate School of

The University of Texas at Austin

in Partial Fulfillment

of the Requirements

for the Degree of

Doctor of Philosophy

The University of Texas at Austin

December 2006

Acknowledgements

First and foremost I would like to thank my parents for giving me the guidance, upbringing, and motivation to pursue this endeavor. Without them I would not be here, in more ways than one. I would like to thank Dr. Emily Niemeyer for mentoring me as an undergraduate, introducing me to research, and exposing me to the fact that it doesn't always work the first time. I would like to thank Dr. Holcombe for his guidance, discussions, knowledge, and believing in this project (and me) even when I was losing faith in it.

Lastly, I would like to thank Holcombe group members past and present. Bill thanks for showing me the ropes of graduate school as well as how many items in the lab that can double as a hammer when necessary. Gulay, thank you for helping me move forward on this project, giving me new ideas, and supplying the enthusiasm to make it happen. Adam and Thomas, thank you for your frank discussions regarding subjects scientific or otherwise. Nikhilesh, it was great being you colleague and friend. Carina and Brianna, thank you for your friendship, discussions, and sitting through my group meetings which inevitably went at least an hour too long. Lastly, I want to thank Jacque for being a valuable friend, colleague, and classmate. Thank you for the moral support and encouragement which helped me to stay the course and retain most of my sanity while trying to graduate.

Detection of Metal Vapor Atoms in Bubbles at Room Temperature

Publication No. _____

John Leo Molloy, Ph.D.

The University of Texas at Austin, 2006

Supervisor: James A. Holcombe

One of the largest obstacles in miniaturizing traditional atomic spectroscopic sources is the need for a thermal/electrical source for free atom production. A single article in the literature has demonstrated atomic absorption detection of Ag, Cu, and Pd in aqueous solution at room temperature for atoms in the gas phase, which may ultimately permit miniaturization. Unfortunately, several laboratories have found that reproducing the phenomenon has been difficult. Without a sound fundamental explanation of the processes leading to the signal, one must conclude that it can be done, but some unsuspected and unknown design/methodological nuances are responsible for only a single reported success.

Gas phase atoms could exist at room temperature “in solution” if the atoms were trapped in very small bubbles. A simpler system containing Hg vapor within a single 500 μL bubble was first studied using atomic absorption measurements. The use of experimental data and computer simulations revealed that metal transport out of bubbles suffers from slow diffusion through solution and limited solubility of the elemental

species. Absorption signals for Hg vapor decayed over thousands of seconds, with slower decay rates associated with solutions higher in metal concentration and reducing power.

Submicron sized bubbles were created in a flow-through cell during mixing of a 20% ethanol solution containing a reducing agent with Pd in 2% HCl. A repeatable atomic absorption signal was produced using this method. Replacement of ethanol with 1-propanol and use of a surfactant enhanced the signal through generation of more bubbles with lower internal pressures present. Limits of detection of ca. 100 ppb in Pd were achieved, although it is estimated that about 0.4% of the Pd initially added is contained within the bubbles as gaseous atoms. Further discussion includes exploration of the fundamental processes present in a procedure that delivers a repeatable signal.

Table of Contents

List of Tables	xi
List of Figures	xii
Chapter 1: Introduction	1
1.1 A brief history and overview of lab-on-a-chip technologies	1
1.2 Miniaturization of elemental analysis technologies	3
1.2.1 Adapting current atomization sources	3
1.2.1.1 Sample introduction through nebulization	3
1.2.1.2 Hydride generation	4
1.2.1.3 Cold vapor Hg analysis	5
1.2.1.4 Miniaturizing flame and furnace sources	5
1.2.1.5 Chip based plasma sources	6
1.2.2 Atomic absorption measurements in solution	7
1.2.2.1 Results of Panichev and Sturgeon	8
1.2.3 Development of a lab-on-a-chip device using cold atom solution atomic absorption (CASAA)	8
1.2.3.1 Light sources	9
1.2.3.2 Detectors	10
1.2.3.3 Detection scheme	10
1.2.3.4 Initial attempts at atomic signal production	11
1.3 Assumptions necessary for atomic signal detection in solution	13
References	16
Chapter 2: Detection of Hg within a single bubble in a stirred system	19
2.1 Introduction to mercury vapor in aqueous systems	19
2.2 Experimental	22
2.2.1 Reagents	22
2.2.2 Experimental setup and procedure	23
2.3 Results	24
2.3.1 Variation of bubble size	25

2.3.2 Mass transport into the bubble.....	27
2.3.3 Variation of pH	28
2.3.4 Variation of ionic strength	29
2.3.5 Addition of reducing agent	30
2.3.6 Addition of surfactants.....	31
2.3.7 Changing physical properties of solution	31
2.3.8 Simple diffusion out of a sphere	34
2.3.9 Monte Carlo studies	36
2.4 Limitations of experimental setup	39
References.....	39
Chapter 3: Mass transport Hg within a system governed by diffusion.....	41
3.1 Experimental	41
3.1.1 Reagents.....	42
3.1.2 Experimental setup and procedure.....	43
3.2 Experimental results.....	44
3.2.1 Variation of oxidation/reduction properties of the surrounding solution.....	45
3.2.2 Addition of Hg to the surrounding solution.....	47
3.2.3 Observation of Hg transport into a nitrogen bubble	49
3.2.4 Investigation into Hg adsorption on syringe tip and reaction cell walls	50
3.3 Computer simulations	52
3.3.1 Use of the explicit box method to simulate diffusion	52
3.3.2 Best fit of simulation and resulting diffusion coefficient used	58
3.3.3 Determination of $\text{Hg}^0_{(\text{aq})}$ solubility	60
3.3.4 Modification of the simulation to detect order at the bubble interface.....	60
3.4 Conclusions.....	61
References.....	62
Chapter 4: Generation of an atomic absorption signal for Pd within microbubbles	64
4.1 Introduction.....	64

4.1.1 Spectral properties of atoms in small bubbles	64
4.1.2 Generation of microbubbles.....	66
4.2 Experimental design.....	67
4.2.1 Reaction cell design	67
4.2.2 Experimental procedure development	71
4.2.2.1 Reagents.....	71
4.2.2.2 Procedure	73
4.3 Experimental results.....	74
4.3.1 Initial CASAA signal detection	74
4.3.2 Signal analysis	77
4.3.2.1 Signal diagnostics	77
4.3.3 Parameters leading to signal enhancement	80
4.3.3.1 Other reaction cell designs.....	81
4.3.3.2 Use of a commercially available cell design.....	84
4.3.3.3 Metal concentration	84
4.3.3.4 Addition of surfactant	86
4.3.3.5 Injection loop volume	88
4.3.3.6 Stop flow experiments	89
4.3.3.7 Signal integration.....	91
4.3.3.8 Detection efficiency.....	95
4.3.4 Increasing bubble density	95
4.4 Conclusions.....	99
References.....	99
Chapter 5: Some preliminary explorations and future directions	101
5.1 Possible avenues for future research.....	101
5.1.1 Increasing reaction cell path length	101
5.1.2 Increasing CASAA signal through more complete reagent mixing	104
5.1.3 Obtaining a CASAA signal for other metals	107
5.2 Conclusions.....	108
References.....	110

Appendix A: Data collection setup.....	111
Appendix B: Visual Basic code for simulations.....	114
B.1 Monte carlo simulation to determine time of particle loss considering only gas diffusion rates.....	114
B.2 Simulation of Hg leaving bubble in stagnant solution.....	117
B.2.1 Explicit box method.....	117
B.2.2 Crank Nicholson method.....	121
B.3 Monte carlo simulation of diffusion through cuvet.....	125
Appendix C: Alignment of Hollow Cathode and Deuterium lamps.....	128
Vita	131

List of Tables

Table 1.1 Summary of Assumptions for Cold Atom Solution Atomic Absorption (CASAA)	13
Table 2.1 Decay rate change with pH.....	28
Table 2.2 Decay rate change with ionic strength.....	29
Table 2.3 Parameters used for calculation of diffusion out of a sphere.....	34
Table 2.4 Parameters used for Monte Carlo simulation	37
Table 3.1 Parameters for simulation using box method	55
Table 4.1 Parameters used for Monte Carlo simulation of Pd particle diffusion in reaction cell.....	92

List of Figures

Figure 1.1 Possible instrument for performing atomic absorption measurements on a chip	11
Figure 1.2 Initial reaction cell design	13
Figure 2.1 System for flow of aqueous solution past Hg vapor bubble.....	21
Figure 2.2 Schematic of flow cell.....	24
Figure 2.3 Signal and line fit for Hg decay for a 0.4 mL bubble surrounded by DI water.....	24
Figure 2.4 Relationship between bubble volume and decay rate.....	26
Figure 2.5 Movement of Hg vapor through bubble interface in both directions	27
Figure 2.6 Decay of Hg signal after addition of reducing agent.....	30
Figure 2.7 Effect of viscosity on Hg vapor decay rate	32
Figure 2.8 Effect of surface tension on Hg vapor decay rate.....	33
Figure 2.9 Effect of density on Hg vapor decay rate	33
Figure 2.10 Results of calculation of Hg diffusion out of a sphere	36
Figure 2.11 Results of Monte Carlos simulation of diffusion of Hg out of a spherical bubble.....	38
Figure 3.1 Experimental design for diffusion controlled mass transport measurements..	42
Figure 3.2 Quartz reaction cell for diffusion controlled mass transport measurements ...	43
Figure 3.3 Absorbance signal decay of Hg in unstirred DI water and 1% HNO ₃	45
Figure 3.4 Hg Absorbance signal decay with the addition of SnCl ₂	47
Figure 3.5 Hg absorbance signal decay in solutions containing Hg.....	48
Figure 3.6 Transport of Hg through bubble interface in both directions	50
Figure 3.7 Effect of presence of Au wire within bubble.....	51
Figure 3.8 Explicit Box method setup	53
Figure 3.9 Diagram of simulation design	54
Figure 3.10 Effects of changing D and H parameters of simulation	57
Figure 3.11 Simulated Hg decay signal compared to experimental data for 10 mM SnCl ₂ and 10 mM SnCl ₂ and 2 ppm Hg.....	59
Figure 4.1 Calculated absorption profiles for Ag 328.068 nm line at 25 °C	65
Figure 4.2 Schematic of initial setup for CASAA	68
Figure 4.3 Schematic of final cell design.....	69
Figure 4.4 Plexiglass frame for reaction cell. All measurements are in mm.	70
Figure 4.5 PTFE pieces for control of solution flow. All measurements are in mm.	70
Figure 4.6 Illustration of flow patterns within reaction cell using dye. Picture denote 30, 70, and 110 s after plug entry into cell. Solution flow proceeds from bottom to top of the cell.	74
Figure 4.7 CASAA signal for 500 μL of 20 ppm Pd and using 20% ethanol and 0.1%NaBH ₄	75
Figure 4.8 Signal obtained for blank and 20 ppm Pd using 340.45 nm Pd line and 346.58 nm Co line 0.1% NaBH ₄ /20% ethanol reducing solution and 500 μL injection volumes were used.....	77

Figure 4.9 ICP-MS data for Pd ⁺ and Ar ₂ ⁺ (right y-axis) for procedure to produce CASAA signal. Large peak at 3500 s occurred from bubbles in reaction cell effluent, suggesting Pd is resident within the bubbles. 20 ppm Pd, 0.1% NaBH ₄ /20% ethanol reducing solution, and 500 μL injection volume were used.	79
Figure 4.10 Design of PTFE bottom piece to control solution flow into reaction cell. All measurements are in mm.	81
Figure 4.11 Schematic for cell bottom piece which fosters turbulence.	82
Figure 4.12 Calibration curve for Pd using a) integrated peak area and b) peak height 0.1% NaBH ₄ /20% ethanol reducing solution and a 500 μL injection volume were used.	86
Figure 4.13 Signal enhancement from the addition of 0.001 M DDAB to 20 ppm Pd solution and using 0.1% NaBH ₄ /20% ethanol reducing solution and 500 μL injection volume.	87
Figure 4.14 Integrated signal for 20 ppm Pd solution and 0.5% NaBH ₄ /20% ethanol reducing solution with changing injection loop volume.	89
Figure 4.15 CASAA signal resulting from 100μL of 5 ppm Pd and using 0.1% SnCl ₂ /20% ethanol reducing solution if pump is stopped after atoms enter observation zone.	90
Figure 4.16 Calibration curve using integrated signal for different integration times using 0.1% NaBH ₄ /20% ethanol reducing solution and 100 μL injection volume. ..	91
Figure 4.17 Comparison of Monte Carlo simulation results to experimental data using different concentrations of Pd and 0.1% NaBH ₄ /20% ethanol reducing solution and 100 μL injection volume.	94
Figure 4.18 CASAA signal for 5 ppm Pd using 0.1% NaBH ₄ /30% 1-propanol reducing solution and 100 μL injection volume compared to data using ethanol.	96
Figure 4.19 Calibration curve for Pd using 0.1% NaBH ₄ /30% 1-propanol reducing solution and 100 μL injection volume.	98
Figure 5.1 Cylindrical cell designed to increase effective path length. All measurements are in mm.	102
Figure 5.2 CASAA signal obtained for 100 μL of 20 ppm Pd for reaction cell with 5 cm path length.	103
Figure 5.3 Results of turbulent mixing from use of syringe needle to facilitate turbulent entry of metal analyte plug.	106
Figure A1 Schematic of data collection setup. Wires attached test point 19 on the control board of the spectrometer to Analog Input 1 on the connection block and test point 20 to ground on the connection block. The connection block was connected to a DAQ card via 68 pin cable.	111
Figure A.2 Screenshot of Cont Acq to Spreadsheet File.vi.	112
Figure A.3 Calibration curve for converting voltage to absorbance.	113
Figure C.1 Apparatus for probing beam profile. Wire was scrolled across beam in vertical and horizontal directions for all lamps used using translation stages.	128
Figure C.2 Horizontal beam profiles for Pd hollow cathode and deuterium lamps. Number at the top of each graph is the distance along the beam from the side of the spectrometer compartment.	129

Figure C.3 Results of aligning Hollow Cathode and Deuterium lamp beams. Results shown are for Pd lamp 130

Chapter 1: Introduction

This research undertakes the study of a complex procedure to generate an atomic absorption signal in solution. Data utilizing this technique was first published by another laboratory¹ whose work had not been built upon for several years. Initial plans for this project included reproduction of this signal, not to compete with traditional elemental analysis techniques such as inductively coupled plasmas or furnace atomization, but for the application of the technique to miniaturization and fabrication on a chip. After initially unsuccessful attempts to reproduce an atomic absorption signal in solution, correspondence with the original author confirmed the difficulty in signal detection,² and it was determined that exploration of the fundamental process giving rise to this signal would eventually facilitate the development of a reproducible procedure for the generation of metal vapor species in solution.

This chapter will introduce the subject material, from the motivation to perform elemental analysis on a chip to discussion of how other researchers have tried to address the problem. The following chapters will embark upon a study of the fundamental processes occurring within a similar system using Hg vapor to produce an atomic absorption signal in solution. The remaining chapters will explore some of the procedure development and eventual success in observing a cold atom solution atom absorption (CASAA) signal as well as discussion of parameters causing enhancements to this signal.

1.1 A BRIEF HISTORY AND OVERVIEW OF LAB-ON-A-CHIP TECHNOLOGIES

The area of research that now includes lab-on-a-chip technologies have existed for over twenty five years when the first example of miniaturization of laboratory devices was presented in the form of a gas chromatograph on a silicon wafer in 1979.³ However, the fruition of the concept did not occur until the development of technologies which

could move small volumes of fluid through microchannels^{4, 5} as well as standardized methods to make microchannels, such as photolithography.⁶ The concept of miniaturized total chemical analysis was first suggested in 1990,⁷ and involves efforts to miniaturize multiple laboratory techniques such as sample preparation and analysis, so that they may be performed within the confines of a small chip. This idea has energized the field, which was reinforced with breakthroughs in fabrication techniques as well as the use of capillary electrophoresis on silicon chips.⁸ In fact, research within the area of lab-on-a-chip technologies has become more prevalent in analysis of biological samples because of the small sample sizes which can be used for analysis.^{9, 10} There are many advantages to creating devices which mimic laboratory scale procedures onto a small chip. As just mentioned, smaller sample volumes can be used in these cases, leading to faster mixing and reaction times with smaller consumption of potentially expensive reagents. Small sample volumes also hold the inherent advantage of minimizing clean up after analysis, a potentially important point if either analyte or reagent happens to be dangerous to the analyst or the environment. The most obvious advantage to the development of lab-on-a-chip technologies is the creation of small, portable instruments. This can be a somewhat misleading advantage, and one must be mindful of chip technologies available that require large and/or heavy auxiliary equipment to operate. Chip technologies also allow for the production of low cost single use analytical devices, negating issues such as memory effects and reaction vessel cleaning. Lastly, by applying technologies such as microsecond capillary electrophoresis,¹¹ lab-on-a-chip technologies can offer very rapid analyses.

The field of lab-on-a-chip technology appears to have moved away from its infancy with rather complex chip designs containing many functions. In one recent example, Pal et. al. showed the analysis of DNA from an influenza virus on a 1.5 cm x

1.6 cm chip which included valves and reaction chambers for control of reagents, a heated chamber for performing polymerase chain reaction (PCR) as well as a microchannel for separation of DNA fragments using capillary electrophoresis.¹² Additionally, the authors contend that the dimensions of the device could be decreased by an order of magnitude with the same results and a cost of production of only \$1 per chip.¹² There are many other examples throughout the recent literature which, along with the aforementioned work, indicate the level of sophistication available in lab technologies that have been put on a chip.¹²⁻¹⁴

1.2 MINIATURIZATION OF ELEMENTAL ANALYSIS TECHNOLOGIES

Despite the present level of maturity of the field, the development of microchip devices capable of *elemental determinations* on a typical aqueous sample have been absent. Adaptation of conventional atomic spectroscopic techniques requires the production of gaseous atoms from a sample, which presents miniaturization difficulties for traditional thermal atomization and ionization techniques.

1.2.1 Adapting current atomization sources

Following the trends used for development of chip-based technologies for molecular spectroscopy, much effort has been made to miniaturize traditional elemental analysis technologies. Considering that the majority of samples analyzed for elemental information are aqueous, two technologies must be developed: microscale techniques for desolvation as well as atomization of the sample. Unfortunately, the adaptation of these techniques has thus far has had limited success.

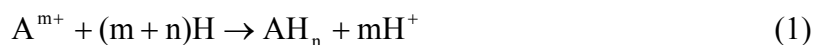
1.2.1.1 Sample introduction through nebulization

Nebulizers are the most prevalent method of turning an aqueous sample into an aerosol which can be more easily atomized. This is traditionally accompanied by the use

of a spray chamber in order to further limit the solvent reaching the atomization source. Unfortunately, by limiting solvent loading nebulizers also limit analyte reaching the atomization source, traditionally suffering from low efficiencies (~1%). This can be increased to 20% relatively easily using a conventional nebulizer at $\mu\text{L}/\text{min}$ flow rates.¹⁵, and high efficiency nebulizers have been developed¹⁶ which boost efficiencies up to 40 to 50%¹⁵. Other methods of nebulization including direct injection high efficiency nebulizers (DIHEN)¹⁷ allow virtually all of the sample to enter a plasma source, and development of specialized devices such as multiple low uptake nebulizing capillaries combined into one device also show promise.¹⁸ Such devices have been designed for use with plasma sources, specifically microwave induced plasmas (MIPs), and show promise for adaptation to chip based analysis.

1.2.1.2 Hydride generation

Hydride generation is another method of transporting the analyte to a thermal source without the solvent, thus greatly reducing the net energy needed for atomization/excitation/ionization. Using this method, a reducing agent is combined with strong acid, producing hydrogen gas. This gas reacts with the analyte to form a volatile hydride, which is commonly swept to the spectrometer using a gas such as Ar. Typical reducing agents used include SnCl_2 , NaBH_4 , and KBH_4 .¹⁹ The general reaction is as follows:¹⁹



The main drawback of this method is that it is only applicable to elements which will form volatile hydrides such as AsH_3 , GeH_4 , SnH_4 , TeH_2 , SbH_3 , PbH_4 , BiH_3 , and SeH_2 . While this method is able to make volatile hydrides which can be transported easily to a spectrometer, some method of thermally dissociating the hydrides is still necessary²⁰ with the exception of Cd.²¹ Despite these drawbacks, this method is one step

closer to a method of atomization which could be put onto a chip. Adaptation to miniaturization could be further enhanced with successful exploitation of electrochemical hydride generation²². Analysis of arsenic on a chip has been performed by Ozmen et. al.²³ with use of a traditional scale MIP for atomic emission measurements.

1.2.1.3 Cold vapor Hg analysis

Cold vapor analysis is very similar to hydride generation both in the reagents used and the overall outcome of the reaction. The volatility of elemental Hg requires only that ionic forms of mercury be reduced to the elemental form after any necessary sample pretreatment. In fact, cold vapor analysis is the most common method for quantifying Hg in a sample and exhibits detection limits as low as 0.3 pg.²⁴ Without the need of any additional thermal source, cold vapor Hg generation should be ideal for adaptation to analysis on a chip as is suggested by its determination using capillary electrophoresis coupled with atomic fluorescence.²⁵ However, this type of analysis is unique to elements, such as Hg, that have a substantial vapor pressure.

1.2.1.4 Miniaturizing flame and furnace sources

At first, it is surprising that very little effort has been made to miniaturize traditional flame atomization sources. However flame sources have integral problems which prevent reduction of size with ease. The most glaring problem is that if absorption measurements are to be taken, considerable reduction in flame size would lead to reduction in path length and comparable reduction in signal. Therefore, while development of such a device that could be interfaced with a chip might be possible, it would seem foolhardy with such a weakness initially known.

Electrothermal atomizers, ETA, (aka “graphite furnace atomizers”) are sources which are typically associated with micro-analysis. Although typical power requirements

for heating the furnace are excessive (2-5 kW) and external cooling is generally required, Young et al. have reported on an air cooled graphite furnace²⁶. Additionally, wire filament devices²⁷⁻³⁰ avoid water cooling and use only a few hundred watts of power for heating. However, the sampling is discrete and the signal is transient rather than continuous. Similarly, it is difficult to envision a chip mounted ETA, even when using a filament; and auxiliary gas supplies as well as optics would further hinder miniaturization and portability.

1.2.1.5 Chip based plasma sources

Unlike the other atomization sources discussed above, chip based plasma sources have become an area of development receiving much attention with many different methods discussed in the literature.³¹ Work focused on miniaturized plasmas have had to address reduction in the typically high Ar gas flows (20 L/min) and power requirements (1-2kW). Engel et al. has shown the feasibility of microwave induced plasmas (MIPs) with the analysis of Hg.³² Other work from this lab using this device shows a plasma can be generated a 0.8 mm diameter cavity,³³ and the issue of portability has been addressed by other authors making low power (<3 W) air-cooled microwave microstrip plasma for analysis of helium in air.³⁴ Bass. et al. have likewise shown that small capacitively coupled plasmas are also a method of atomizing or ionizing samples.³⁵ These authors have been developing a water cooled device using He as a plasma gas with a flow rate of 70 mL/min to detect species such as N₂ gas by emission. Microfabricated inductively coupled plasmas (mICPs) also show promise with power requirements as low as 1 W and relatively small sized discharge tubes (1 mm).³⁶

There are a multitude of other small plasma sources being developed, but so far all of them share the inability to analyze samples with aqueous solvents. A few review articles discuss the problems researchers have encountered when trying to analyze

samples which are not in the gas phase,^{31, 37} and even with specialized sample introduction devices such as high efficiency nebulizers, solvent loading of the plasma makes analysis difficult at best, frequently extinguishing the plasma entirely. It is not surprising that the literature published on the development of miniature plasmas always discusses the analysis of gaseous samples such as Hg vapor or effluent from a gas chromatography instrument. There is a solitary example of detection of Na in an aqueous sample using mICP methods,³⁸ which shows promise in the area of chip based plasmas if other elements can be detected..

1.2.2 Atomic absorption measurements in solution

Because of the inherent problems associated with the above techniques, it would seem prudent to circumvent the desolvation process altogether and simply detect atoms directly in solution. The detection of atoms in aqueous solution is not a recent development. Tyson and West first suggested the idea of observing atomic species in solution,³⁹ and Fujiwara et al. detected absorption peaks for Hg after reduction of the ions with NaBH₄.⁴⁰ Later, γ -radiolysis was used to produce Ag atoms which were detected using absorbance measurements^{41, 42}, and recently Hg_(aq) absorbance measurements were made through solution in conjunction with a liquid core waveguide.⁴³ However, in all of these studies the absorbance spectra showed the expected solvent broadening effects, i.e., bandwidths in excess of 10 nm. The obvious problem with this is that background correction techniques typically used in atomic spectroscopy are dependent upon the inherent narrow line profiles of atomic absorption peaks.⁴⁴ Additionally, calculations to determine absorption linewidths⁴⁵⁻⁴⁷ show that absorption lines of this magnitude suffer from attenuation of the peak intensity by several orders of magnitude. Without the ability to differentiate atomic signals from interferences such as scatter and molecular species,

and with the sensitivity and selectivity loss due to linewidths on the nanometer scale, applicability of an atomic absorption method would be very limited.

1.2.2.1 Results of Panichev and Sturgeon

In 1998 Panichev and Sturgeon described detection of atomic species in aqueous solution at room temperature via narrow line atomic absorption.¹ They reported making room temperature atomic absorption measurements for low vapor pressure metals and they measured linewidths which are typical of gas phase atoms at room temperature, in spite of the fact that such linewidth measurements were made through aqueous solution containing the analyte and NaBH₄ reducing agent. It is logical to assume that the atomic species within the solution are gas phase atoms. This would occur if the atoms exist in bubbles in the solution, which was mentioned as a possibility by the authors after a suggestion from this lab.¹ This postulate is further supported by the fact that the authors employed NaBH₄ as a reducing agent, which is also capable of converting H⁺ to H_{2(g)}. Thus, the NaBH₄ may have served a twofold purpose in their experiment: reducing the metal ions to atomic form, as well as generating small bubbles that contain the metal atoms inclusive of narrow line atomic absorption measurements.

1.2.3 Development of a lab-on-a-chip device using cold atom solution atomic absorption (CASAA)

As discussed above, the main problem contributing to the lack of chip based elemental analysis instrumentation is the lack of a viable, miniaturized atomization source. The solution-based atomization technique discussed above presents itself as an ideal solution to this problem for at least a few elements. It circumvents desolvation issues and suggests applicability to many elements which can be reduced in solution including some of the transition metals. However, since this is only part of an instrument

which would perform atomic absorption measurements, one must ponder what properties would be inherent to ideal light sources and detectors.

1.2.3.1 Light sources

Traditional atomic absorption instruments use hollow cathode lamps (HCL) as light sources. However, in trying to adapt HCLs for lab-on-a-chip use, there would likely be excessive noise levels because of the limited optical speed dictated by the chip's microchannel where absorption measurements would likely be made. If background correction were needed, then complex optics with similar optical throughput could restrict the effectiveness of the correction system. Electrodeless discharge lamps (EDLs) are more intense than HCLs but not sufficiently so to overcome the aperture imposed by the chip's small cross sectional area.

Diode lasers represent light sources that might be ideal since they can be relatively inexpensive, small, current modulated to function in background correction, and sufficiently bright and stable to yield extremely low detection limits. The impressive drop in detection limits is initially suggested by results with traditional atomization sources.⁴⁸ Later work by Liger et. al. shows detectable signals of 2×10^{-7} absorbance units, a limit imposed only by shot noise.⁴⁹ This detectable signal is 3 orders of magnitude lower than that expected from HCLs.⁴⁹

Diode lasers have wavelengths which are tunable by either changing the temperature of the diode or changing the current applied to the diode. Changing the temperature can be used to move the wavelength of the laser so that one laser might be used for multiple elements if the absorption lines are closely spaced (<20 nm). Additionally, modulation of the current around the atomic absorption line can be performed in order to achieve built in background correction of the signal using, for example, phase sensitive detection (e.g., lock-in amplification).⁴⁹⁻⁵³ Niemax et. al. have

shown that multiple diode lasers can be used for simultaneous determination of multiple elements when the detection scheme also incorporates Fourier analysis.⁵³ Currently, the largest problem with using this light source is the lack of availability of diode lasers at wavelengths below 380 nm, a region in which many elements are determined. However, it has been shown that frequency doubling and sum frequency generation have been successfully used with diode lasers to achieve wavelengths in the UV region.⁵¹ Therefore, it is possible that the ideal light source for elemental analysis on a chip-based instrument has already been developed.

1.2.3.2 Detectors

Photomultiplier tubes (PMTs) are commonly used in spectrometers because of their ability to amplify small amounts of light by large amounts and give low detection limits. While the use of a PMT would be conducive to a small instrument, semiconductor photodiodes have already been used successfully with diode lasers to achieve the shot noise limits of detection mentioned previously.⁴⁹ Photodiodes have the added benefits of being very small, inexpensive, and rugged.

1.2.3.3 Detection scheme

Given the discussions from the previous sections, much of the instrumentation conducive to performing atomic spectroscopy on a chip is already available, and the lack of a viable atomization source is the main obstacle. However, it is conceivable that the atomization technique pioneered by Panichev and Sturgeon could be adapted for a chip-based laboratory if it were reproducible and/or reliable.

With a reliable atomizer, a possible embodiment of a simplified system might be similar to that shown in Figure 1.1 in which multiple diode lasers could be used for simultaneous analysis of multiple elements with a photodiode as a detector. The

atomization source would consist of a long path length microfluidic flow cell atomizing metal ions in solution through chemical reduction.

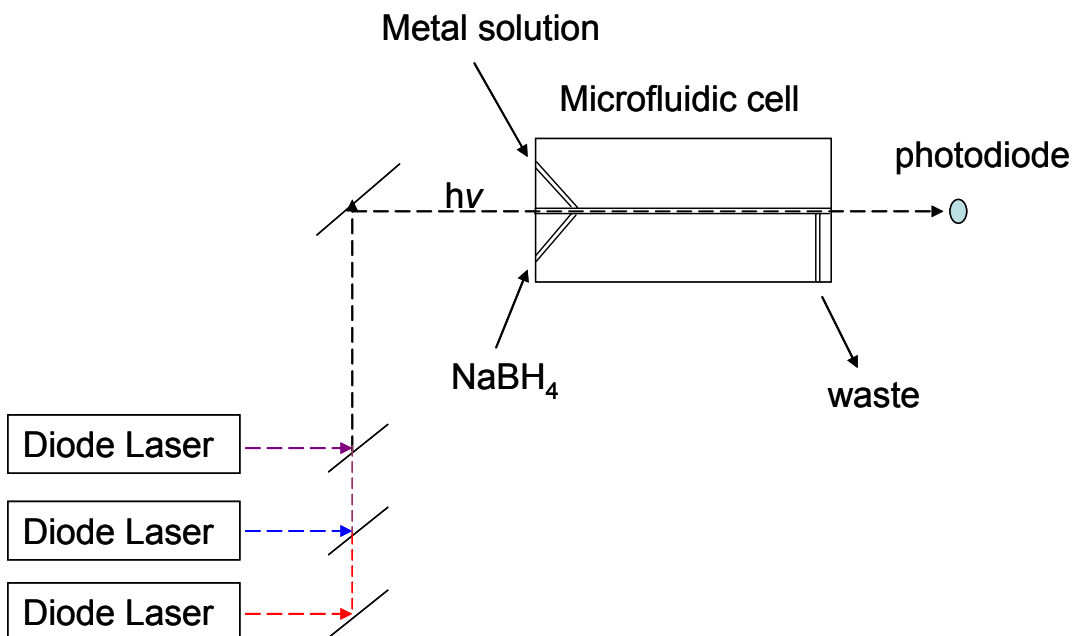


Figure 1.1 Possible instrument for performing atomic absorption measurements on a chip

While the optics, detection and physical layout of the system are relatively straightforward, the success is most strongly dependent on a means of generating gaseous atoms. While the paper of by Panichev and Sturgeon¹ demonstrated that the signal could be seen, numerous labs (including this lab) have been unable to reproduce the results. In short, the ability to produce gaseous atoms is currently more of an art than a science, and an “art” that even the originator’s lab cannot routinely reproduce.

1.2.3.4 Initial attempts at atomic signal production

Initially the goal of this research was to build a system similar to that used by Panichev and Sturgeon to detect atoms in solution and to reproduce the atomic signal for Ag. The cell designed matched the dimensions of the cell built by Panichev and Sturgeon

as closely as possible and is shown in Figure 1.2. The cell was fabricated in-house with a plexiglass frame and quartz windows which were attached using silicone adhesive. Two inlet ports in the bottom allowed entry of the reducing agent and metal ion solutions, with the channels meeting in a Y-configuration. Outlets for waste were at the top and side of the cell.

Once built, the system would then be probed to optimize it for the purpose of its application to the larger goal of instrument design, but also in order to determine some of the fundamental processes which were allowing this signal to occur and be maintained. Unfortunately, the reproduction of the atomic signal in solution was more difficult than predicted. This arose from several problems. The main difficulty present was that the production scheme was unreliable and many of the experimental parameters of the published system were unknown. While it is seen from Figure 1.2 as well as the original paper¹ that the general reaction cell design was reproduced, spectroscopic as well as chemical details of the original working system were not known, such as the observation height within the cell, solution flow and mixing patterns within the cell, and pH values used for successful detection of a signal. Even simple parameters such as impurities in the original authors' water could have been critical to giving rise to a signal. Working for several months changing many different parameters within the system produced no appreciable signals except perhaps those erroneously observed due to the scatter from NaBH_4 producing bubbles. Communication with one of the original authors² confirmed the difficulty in producing the atomic signal was not confined to this lab.

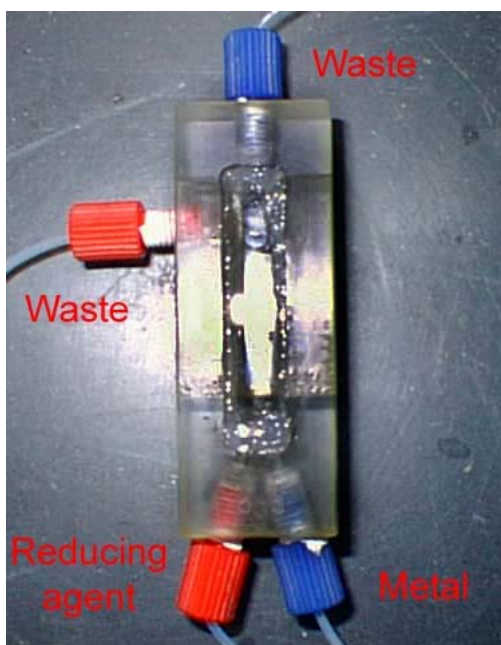


Figure 1.2 Initial reaction cell design

1.3 ASSUMPTIONS NECESSARY FOR ATOMIC SIGNAL DETECTION IN SOLUTION

Because it is impossible to optimize a signal that cannot be generated, the plan of the project was shifted to try to determine what key factors must be present to produce an atomic signal in solution. Some assumptions are necessary before evaluating the criteria needed to observe an atomic absorption signal in solution. These will be inferred from the production and shape of the signal reported by Panichev and Sturgeon.¹ These assumptions are summarized in Table 1.1, beginning with the obvious need for a reducing agent capable of converting the solvated cations to their elemental state.

Table 1.1 Summary of Assumptions for Cold Atom Solution Atomic Absorption (CASAA)

Production of metal atoms	<p>The solvated, free metal is produced in solution by reduction of a soluble cation to the relatively insoluble metal or unstable hydride.</p> $M^{n+}(\text{aq}) + ne^{-} \rightarrow M(\text{aq})$ $M^{n+}(\text{aq}) + mH^{+} + (n+m)e^{-} \rightarrow MH_m(\text{aq})$ <p>In the case of hydride production, decomposition within the solution or inside the gaseous bubble must occur within the time scale of the observation period.</p>
Metal form	The free metal must exist as a vapor inside the bubbles to provide the previously observed ¹ narrow absorption line profile.
Bubble size	Many, if not all, of the bubbles must be sufficiently small that buoyancy forces permit residence times in solution of several seconds.
Metal transport	Transfer of the metal (or hydride) across the interfacial boundary of the bubble must be rapid, and bubble density in solution must be high enough that solvated atoms must diffuse on short distances to the bubble interface.
Number of atoms per bubble	Atom density within the bubbles must be small enough to avoid significant nucleation and formation of dimers, trimers, etc. on the time scale of the observation period.

It is also reasonable to assume that the metal transport within bulk solution as well as across the interfacial boundary of the bubbles must be fast, so that metal atoms created in solution can be transported into the gas and be detected. This is a problem which will be addressed in Chapters 2 and 3. Lacking an atom source for the metals of initial interest (Ag, Pd, Cu), Hg vapor will be used due to it being easily obtainable and not subject to homonucleation processes.

As stressed earlier, in order to have gas phase atoms dispersed in aqueous solution, the atoms must exist in bubbles. While generation of bubbles is not difficult,

creating stable bubbles of the correct size is more challenging. Preferably the bubbles should be small enough so that they rise slowly through solution. Additionally, the bubbles must remain small, a difficult problem to solve due to collisions between bubbles causing coalescence. Production of micro and nanoscale bubbles is not well understood, partially due to the difficulty of optical detection. Even if one were to create sub-micrometer sized bubbles, detection would be difficult due to their continuous movement from buoyancy, as well as growth in size due to coalescence. This problem will be addressed in Chapter 4.

Finally, one must consider whether there is a maximum number of atoms that can be accommodated in a single bubble. If too many atoms are formed and move inside a limited number of bubbles, homonucleation is likely to occur, causing a reduction or loss of the atomic absorption signal. In short, the metal vapor density within the bubbles must be low enough so that almost all collisions within the bubble are with nonreactive gas molecules rather than other metal atoms.

Atomization techniques conducive to analysis of aqueous sample on a chip are not presently available, but a solution based atomization technique presented in the literature shows promise. Unfortunately, several laboratories have found that reproducing the phenomenon has been difficult. Without a sound fundamental explanation of the processes leading to the signal, one must conclude that it can be done, but some unsuspected and unknown design/methodological nuances are responsible for only a single reported success. In order to study fundamental processes within the system, Chapter 2 will probe the mass transport processes present in a similar system by observing Hg absorbance signals in a system with a single larger bubble. In this way, production of the aforementioned elusive system might be possible if all the critical factors are known and assembled.

REFERENCES

- (1) Panichev, N.; Sturgeon, R. E. *Analytical Chemistry* **1998**, *70*, 1670-1676.
- (2) Sturgeon, R. E., 2004.
- (3) Terry, S. C.; Jerman, J. H.; Angell, J. B. *IEEE Transactions on Electron Devices* **1979**, *ED-26*, 1880-1886.
- (4) Van de Pol, F. C. M.; Van Lintel, H. T. G.; Elwenspoek, M.; Fluitman, J. H. J. *Sensors and Actuators A: Physical* **1990**, *21*, 198-202.
- (5) Smits, J. G. *Sensors and Actuators A: Physical* **1990**, *21*, 203-206.
- (6) Madou, M. J. *Fundamentals of Microfabrication: The Science of Miniturization*, 2nd ed.; CRC Press: Boca Raton, 2002.
- (7) Manz, A.; Graber, N.; Widmer, H. M. *Sensors and Actuators, B: Chemical* **1990**, *B1*, 244-248.
- (8) Manz, A.; Harrison, D. J.; Verpoorte, E. M. J.; Fettingner, J. C.; Paulus, A.; Luedi, H.; Widmer, H. M. *Journal of Chromatography* **1992**, *593*, 253-258.
- (9) Auroux, P.-A.; Iossifidis, D.; Reyes, D. R.; Manz, A. *Analytical Chemistry* **2002**, *74*, 2637-2652.
- (10) Reyes, D. R.; Iossifidis, D.; Auroux, P.-A.; Manz, A. *Analytical Chemistry* **2002**, *74*, 2623-2636.
- (11) Jacobson, S. C.; Hergenroder, R.; Koutny, L. B.; Ramsey, J. M. *Analytical Chemistry* **1994**, *66*, 1114-1118.
- (12) Pal, R.; Yang, M.; Lin, R.; Johnson, B. N.; Srivastava, N.; Razzacki, S. Z.; Chomistek, K. J.; Heldsinger, D. C.; Haque, R. M.; Ugaz, V. M.; Thwar, P. K.; Chen, Z.; Alfano, K.; Yim, M. B.; Krishnan, M.; Fuller, A. O.; Larson, R. G.; Burke, D. T.; Burns, M. A. *Lab on a Chip* **2005**, *5*, 1024-1032.
- (13) Verpoorte, E. *Electrophoresis* **2002**, *23*, 677-712.
- (14) Broyles, B. S.; Jacobson Stephen, C.; Ramsey, J. M. *Analytical chemistry* **2003**, *75*, 2761-2767:.
- (15) Todoli, J.-L.; Hernandis, V.; Canals, A.; Mermet, J.-M. *Journal of Analytical Atomic Spectrometry* **1999**, *14*, 1289-1295.
- (16) Liu, H.; Montaser, A. *Analytical Chemistry* **1994**, *66*, 3233-3242.
- (17) Westphal, C. S.; Kahen, K.; Rutkowski, W. F.; Acon, B. W.; Montaser, A. *Spectrochimica Acta, Part B: Atomic Spectroscopy* **2004**, *59B*, 353-368.
- (18) Huang, M.; Hirabayashi, A.; Shirasaki, T.; Koizumi, H. *Analytical Chemistry* **2000**, *72*, 2463-2467.
- (19) Dedina, J. *Hydride generation atomic absorption spectrometry*; Wiley: Chichester (England), 1995.
- (20) Holak, W. *Analytical chemistry* **1969**, *41*, 1712-1713.
- (21) Sanz-Medel, A.; Valdes-Hevia y Temprano, M. C.; Bordel Garcia, N.; Fernandez de la Campa, M. R. *Analytical Chemistry* **1995**, *67*, 2216-2223.

- (22) Brockmann, A.; Nonn, C.; Golloch, A. *Journal of Analytical Atomic Spectrometry* **1993**, *8*, 397-401.
- (23) Ozmen, B.; Matysik, F.-M.; Bings, N. H.; Broekaert, J. A. C. *Spectrochimica Acta, Part B: Atomic Spectroscopy* **2004**, *59B*, 941-950.
- (24) Bloom, N.; Fitzgerald, W. F. *Analytica Chimica Acta* **1988**, *208*, 151-161.
- (25) Li, F.; Wang, D.-D.; Yan, X.-P.; Lin, J.-M.; Su, R.-G. *Electrophoresis* **2005**, *26*, 2261-2268.
- (26) Young, J. P.; Shaw, R. W. *Institute of Physics Conference Series* **1992**, *128*, 347-350.
- (27) Bruhn, C.; Berndt, H.; Tristao, M. L. *Analytica Chimica Acta* **1987**, *193*, 361-365.
- (28) Ezer, M.; Elwood, S. A.; Jones, B. T.; Simeonsson, J. B. *Analytica Chimica Acta* **2006**, *571*, 136-141.
- (29) Rust, J. A.; Nobrega, J. A.; Calloway, C. P., Jr.; Jones, B. T. *Analytical Sciences* **2005**, *21*, 1009-1013.
- (30) Rust, J. A.; Nobrega, J. A.; Calloway, C. P., Jr.; Jones, B. T. *Analytical Chemistry* **2005**, *77*, 1060-1067.
- (31) Franzke, J.; Miclea, M. *Applied Spectroscopy* **2006**, *60*, 80A-90A.
- (32) Engel, U.; Bilgic, A. M.; Haase, O.; Voges, E.; Broekaert, J. A. C. *Analytical Chemistry* **2000**, *72*, 193-197.
- (33) Bilgic, A. M.; Voges, E.; Engel, U.; Broekaert, J. A. C. *Journal of Analytical Atomic Spectrometry* **2000**, *15*, 579-580.
- (34) Hopwood, J.; Iza, F. *Journal of Analytical Atomic Spectrometry* **2004**, *19*, 1145-1150.
- (35) Bass, A.; Chevalier, C.; Blades, M. W. *Journal of Analytical Atomic Spectrometry* **2001**, *16*, 919-921.
- (36) Hopwood, J.; Iza, F.; Coy, S.; Fenner, D. B. *Journal of Physics D: Applied Physics* **2005**, *38*, 1698-1703.
- (37) Broekaert, J. A. C. *Analytical and Bioanalytical Chemistry* **2002**, *374*, 182-187.
- (38) Ichiki, T.; Koidesawa, T.; Horiike, Y. *Plasma Sources Science & Technology* **2003**, *12*, S16-S20.
- (39) Tyson, J. F.; West, T. S. *Nature (London, United Kingdom)* **1974**, *250*, 139-140.
- (40) Fujiwara, K.; Umezawa, Y.; Fujiwara, S.; Fuwa, K.; Shima, N.; Kamimura, H. *Nature (London, United Kingdom)* **1978**, *276*, 47-48.
- (41) Ershov, B. G.; Janata, E.; Henglein, A.; Fojtik, A. *Journal of Physical Chemistry* **1993**, *97*, 4589-4594.
- (42) Janata, E.; Henglein, A.; Ershov, B. G. *J. Phys. Chem.* **1994**, *98*.
- (43) Tao, S.; Gong, S.; Xu, L.; Fanguy, J. C. *Analyst (Cambridge, United Kingdom)* **2004**, *129*, 342-346.
- (44) Welz, B.; Sperling, M. *Atomic absorption spectrometry*; Wiley-VCH: Weinheim, 1999.
- (45) Lovett, R. J.; Parsons, M. L. *Spectrochim. Acta, Part B* **1980**, *35B*, 615-630.
- (46) Lovett, R. J.; Parsons, M. L. *Applied Spectroscopy* **1977**, *31*, 424-434.
- (47) Lovett, R. J. *Applied Spectroscopy* **1985**, *39*, 778-786.
- (48) Hergenroeder, R.; Niemax, K. *Spectrochimica Acta, Part B: Atomic Spectroscopy* **1988**, *43B*, 1443-1449.

- (49) Liger, V.; Zybin, A.; Kuritsyn, Y.; Niemax, K. *Spectrochimica Acta, Part B: Atomic Spectroscopy* **1997**, *52B*, 1125-1138.
- (50) Zybin, A.; Schnurer-Patschan, C.; Bolshov, M. A.; Niemax, K. *TrAC, Trends in Analytical Chemistry* **1998**, *17*, 513-520.
- (51) Niemax, K.; Zybin, A.; Eger, D. *Anal. Chem.* **2001**, 135A-139A.
- (52) Niemax, K.; Zybin, A.; Schnuerer-Patschan, C.; Groll, H. *Analytical Chemistry* **1996**, *68*, 351A-356A.
- (53) Niemax, K.; Schnuerer-Patschan, C.; Groll, H. *Spectrochimica Acta Rev.* **1993**, *15*, 349-377.

Chapter 2: Detection of Hg within a single bubble in a stirred system

2.1 INTRODUCTION TO MERCURY VAPOR IN AQUEOUS SYSTEMS

The previous chapter discussed a method for detection of atomic species in solution at room temperature. There are numerous areas of the published procedure which could cause difficulty in reproducing the atomic signal, such as production of bubbles in adequate numbers and of minimal size, reduction of metal ions to atomic form, and metal atom transport into the bubbles. In this chapter the last issue will be explored, while the other problems will be addressed in Chapter 4.

The original work by Panichev and Sturgeon¹ never addressed how the atomic signal is maintained over time. The linewidth suggested gas phase atoms and yet the signals observed were of metals that would likely condense at ambient temperatures, viz., Ag, Cd and Pd. If uniquely adsorbed at the interface then some interface property would have to negate solvent broadening effects on the absorption lines.

Both experimental studies using Raman spectroscopy²⁻⁴ and theoretical⁵ studies agree that the water molecules at an air/water interface are arranged in an ordered fashion. While order such as a common axis of water molecules aligning parallel to the air/water interface occurs only over a few monolayers,⁵ perhaps this is enough to significantly affect mass transport of atoms through the bubble interface. This explanation lacks the ability to address linewidth broadening and solvation issues, but perhaps it can explain the equally important processes allowing the atomic signal to persist over time.

Since the signals of Panachev and Sturgeon were definitely observed but are unable to be reproduced in our laboratory, there must be some subtle nuance in the original system which has escaped observation by this researcher as well as others. The

system presented within this chapter was designed to explore basic processes that may explain the inability to reproduce the results originally reported. In order to circumvent some of the problems that have been encountered with the system presented in the literature, a much simpler system will be studied. To isolate the chemistry of atom production from transport and other processes, Hg was chosen as the analyte because of its relatively high vapor pressure at 20 °C (1.702×10^{-6} atm).⁶

Hg is routinely determined at room temperature by atomic absorption by Cold Vapor Atomic Absorption Spectroscopy (CVAAS), which is used only for Hg.⁷⁻⁹ Because of its toxicology, it is the objective of various studies, e.g., its behavior in the environment,^{10, 11} its solubility in water,¹² and its reactivity with various aqueous species.¹³⁻¹⁷ Mercury equilibrium in aqueous solution includes the atomic form (Hg^0) as well as the Hg^+ and Hg^{2+} ions.¹³ These equilibria can be pushed toward Hg^0 by adding reducing agents to the solution. This can be accomplished by reducing Hg^{2+} directly to the atomic form, or the easier reduction of Hg^{2+} to Hg_2^{2+} which has been shown to spontaneously disproportionate to the atomic form.¹⁸ The atomic form of Hg has a very low solubility in aqueous solution,¹⁹ so the addition of reducing agents should cause elemental Hg to favor a gaseous state once equilibrium is reached.

The general design of the system that was used to initiate these studies is shown schematically in Figure 2.1. The ultimate system of interest¹ is assumed to be small hydrogen bubbles produced by borohydride reduction of H^+ that move by buoyant forces through the solution. In an attempt to simulate that system while permitting time-dependent monitoring of the Hg absorption signal, a bubble was inserted into a vertical quartz tube so that the flow of aqueous solution from top to bottom could counteract the buoyancy of the Hg-containing bubble and maintain its height within the optical path of an atomic absorption spectrometer.

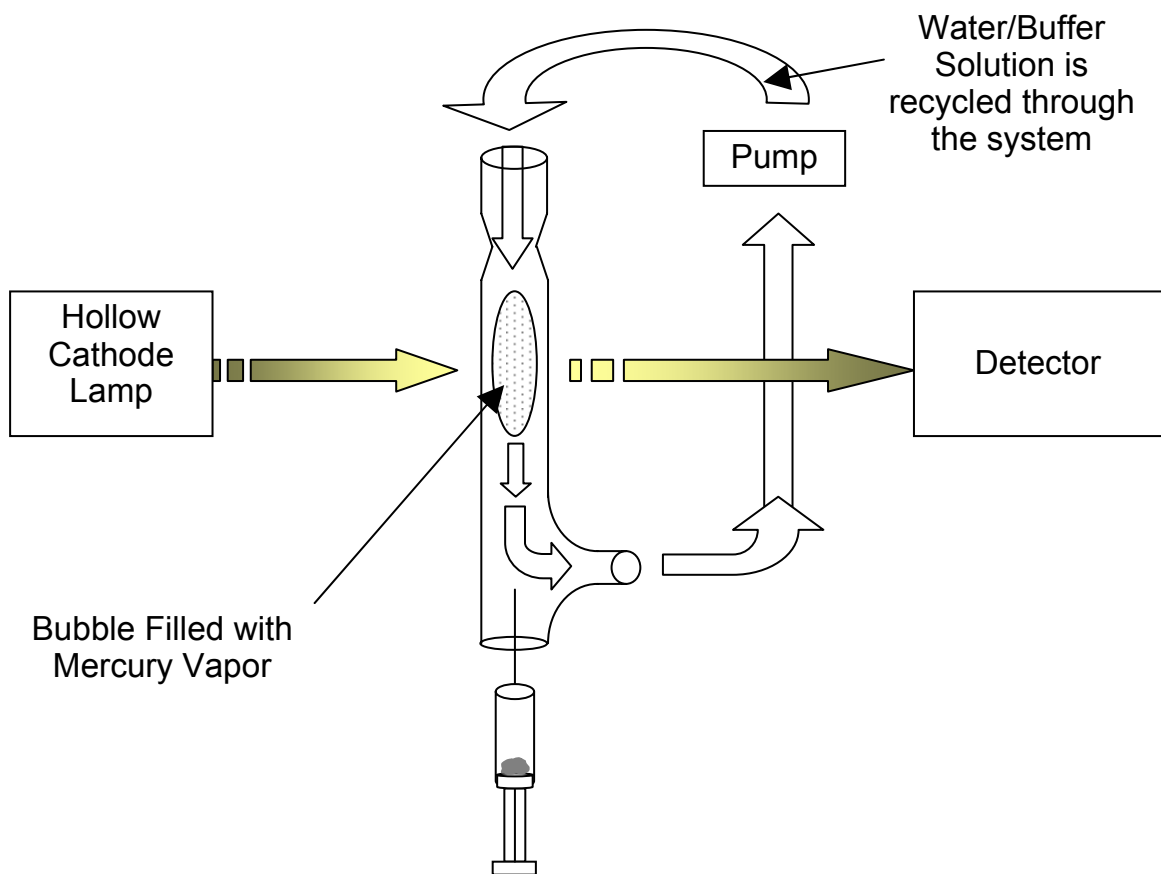


Figure 2.1 System for flow of aqueous solution past Hg vapor bubble

This design should allow information about decay of atomic signals within a bubble to be obtained, information which may be applicable to other systems with smaller bubbles. However, one must be cautious in equating the two systems. A key difference is highlighted by looking at the rise velocity of bubbles of various sizes. Using Navier-Stokes equation,²⁰ the bubble diameter needed to produce a specific rise velocity can be calculated:

$$d = \sqrt{\frac{18\nu\eta}{(\rho_{water} - \rho_{air})g}} \quad (1)$$

where d is the bubble diameter, v is velocity, η is viscosity of water, ρ is density, and g is the gravitational constant. This predicts that a bubble with a diameter of 0.4 cm such as the one used in many of these experiments, will have a velocity of 10 m/s. This is an extremely high velocity, however once bubbles are larger than ~ 0.7 mm, the Stokes equation which treats a bubble as a hard sphere, no longer applies. Larger bubbles are subject to processes such as internal circulation²¹ which can vary based on the makeup of the surrounding solution. Experimental data has shown that the bubble velocity for a 0.4 cm bubble in water is much lower than what would be predicted using the Stokes equation, around 23 cm/s.²¹ This highlights some key differences between the prototype system and that present if very small bubbles are the object of concern.

2.2 EXPERIMENTAL

All experiments were performed using a modified Varian SpectrAA 400 Plus FAAS which had its burner head removed. Measurements were taken using Hg hollow cathode lamp (SCP Science) operated at the manufacturer's recommended setting using a reduced slit height and a bandpass of 0.5 nm. For detection of Hg atoms, 253.7 nm was monitored. The deuterium background correction was turned on for all experiments. Data collection was accomplished using LabView™ software made by National Instruments, and Microsoft Excel® was used for data analysis. Data was collected 16 times a second, and the smoothing was performed using a 10 point moving average and exponential smoothing algorithm using a 0.9 damping factor.

2.2.1 Reagents

Aqueous solutions were made using distilled, deionized water from a mixed bed ion exchange column (Barnstead Thermolyne). pH adjustment was accomplished using sodium hydroxide (EM Science), nitric acid (Fisher Scientific), or hydrochloric acid

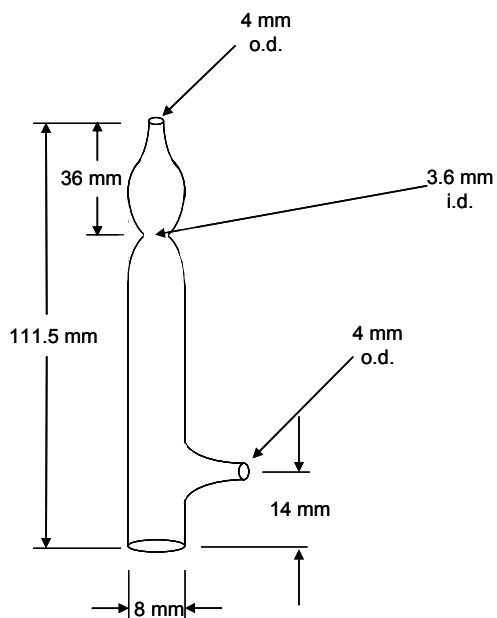
(Fisher Scientific). Phosphate buffer (Fisher Scientific) was used to change the ionic strength of various sample solutions. pH and temperature were monitored using a Ion 6 pH/temperature meter (Oakton). Some experiments required reducing agents to be added to solutions, with sodium borohydride (Fisher Scientific) being used. The organic solvents methanol (Fisher Scientific), ethanol (Aaaper Alcohol and Chemical Co.), glycerol (Fisher Scientific), and hexane (Fisher Scientific) were used to change the physical properties of various solutions. Triton X-100 (Acros Organics) and Sodium Dodecyl Sulfate (Electrophoresis Grade, Fisher Scientific) surfactants were also used for some experiments. Dimethyldichlorosilane (Fisher Scientific) was also used to make reaction cell walls hydrophobic in some experiments.

2.2.2 Experimental setup and procedure

The cell used is shown in Figure 2.2 and is made out of quartz with a rubber septum placed in the bottom for easy injection of a bubble containing Hg vapor. One third of the way down the quartz cell a narrow section was inserted to insure solution flow rates sufficient to keep the bubble from contacting the quartz wall. The quartz cell was placed in the optical path of the spectrometer and held at a constant height using 3 prong clamps. Hg vapor for each experiment was obtained by allowing a small amount of elemental Hg_(l) (~0.25 g) to equilibrate with a nitrogen headspace inside a 3 mL disposable plastic syringe (Fisher Scientific). Aqueous solution was prepared fresh before each experiment and the total volume of solution used within the flow system was 250 mL. The pump remained off during bubble injection into the system, but was immediately started (flow rate: 3.1 mL/min) after bubble injection. Solution flow occurred from top to bottom of the cell in Figure 2.2 with the sidearm diverted to waste. The spectrometer monitored the absorbance signal after the bubble had entered optical path and data was recorded using a data acquisition card (Labview, model PCI6023E) run

on a PC. Details of data acquisition procedure can be found in Appendix A. Hg atomic absorption signal was monitored until the signal had decayed entirely.

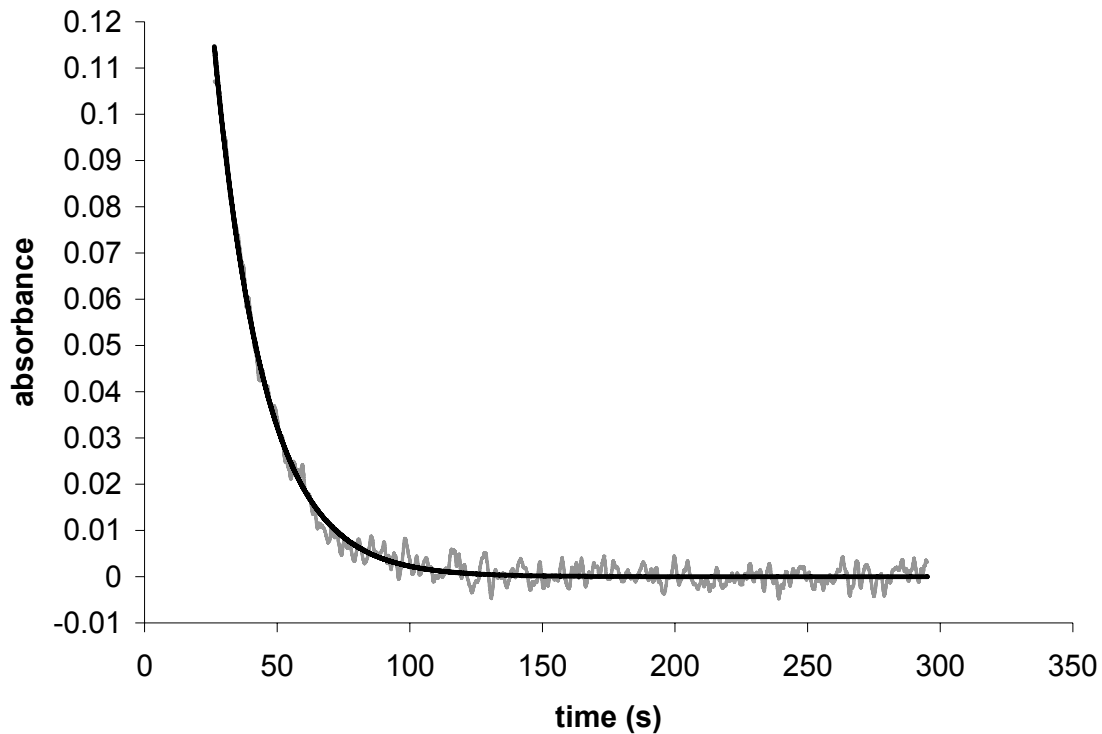
Figure 2.2 Schematic of flow cell



2.3 RESULTS

Initial results for a 0.4 mL bubble containing Hg vapor are shown in Figure 2.3. Due to the noise present within the signal even after smoothing, it was found that Excel's Solver function could be used to fit a curve to $A = ae^{-kt} + b$. The results of such a fitting program are also shown in Figure 2.3. The decay rate (k) is used throughout the rest of this chapter as an indicator of the effect of changes in the flowing solution composition. It is important to note that the b term was generally 0 and a was a nonzero constant throughout experiments (~ 0.89 regardless of surrounding solution).

Figure 2.3 Signal and line fit for Hg decay for a 0.4 mL bubble surrounded by DI water



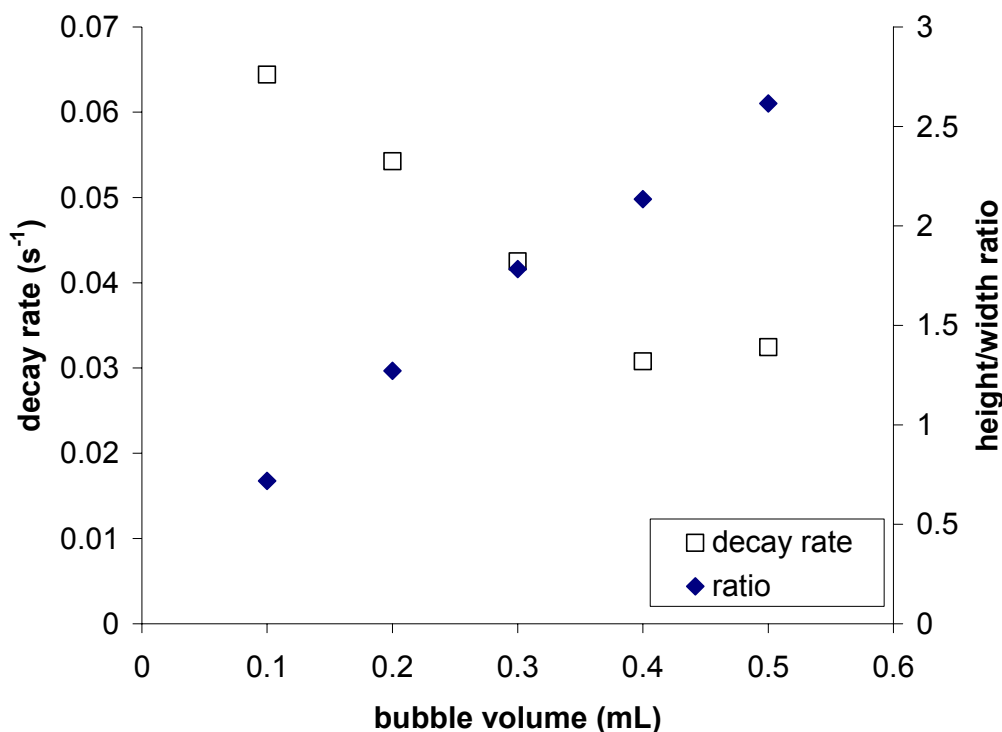
For the experiments which follow, $t = 0$ was designated by the entry of the bubble into the optical path of the spectrometer, and erratic behavior of the atomic absorption signal from scattering of the HCL beam is not included. The absorbance was then normalized to the starting absorbance for a DI water solution so that the change of the decay constant k could be compared upon the change or addition of various experimental parameters.

2.3.1 Variation of bubble size

The result of changing the bubble volume is shown in Figure 2.4. The measurements of the bubbles' heights and widths were made with a micrometer and are also shown. As the width of each bubble is constrained by the 0.813 cm diameter walls of the reaction tube, it makes sense that the ratio of height to width increases linearly with

volume (since only the height actually increases). The decay rate decreases relatively linearly from 0.1 to 0.4 mL with it remaining unchanged from 0.4 to 0.5 mL.

Figure 2.4 Relationship between bubble volume and decay rate



Bubbles smaller than 0.1 mL oscillated in and out of the optical beam due to solution flow and could not be monitored. Bubbles larger than 0.5 mL had a large enough height that they would end up within the cell side arm (Figure 2.2) and break apart. A larger diameter flow cell was constructed to allow larger bubble sizes, but the solution flow rate required to keep a bubble vertically immobile was enough to cause the bubble to be broken apart. Bubble sizes used in this chapter were 0.4 mL unless otherwise specified.

2.3.2 Mass transport into the bubble

While it is quite simple to monitor the absorbance signal decay as the Hg leaves the bubble, it is also imperative to determine if Hg vapor will move into the bubble, and on what time scale. In order to achieve this, DI water was saturated in Hg by allowing liquid Hg to sit in a container filled with water for 2 weeks. After this, a normal experiment was performed, inserting a 0.4 mL Hg vapor bubble, as well as a separate experiment inserting a bubble filled only with nitrogen. The results are shown in Figure 2.5.

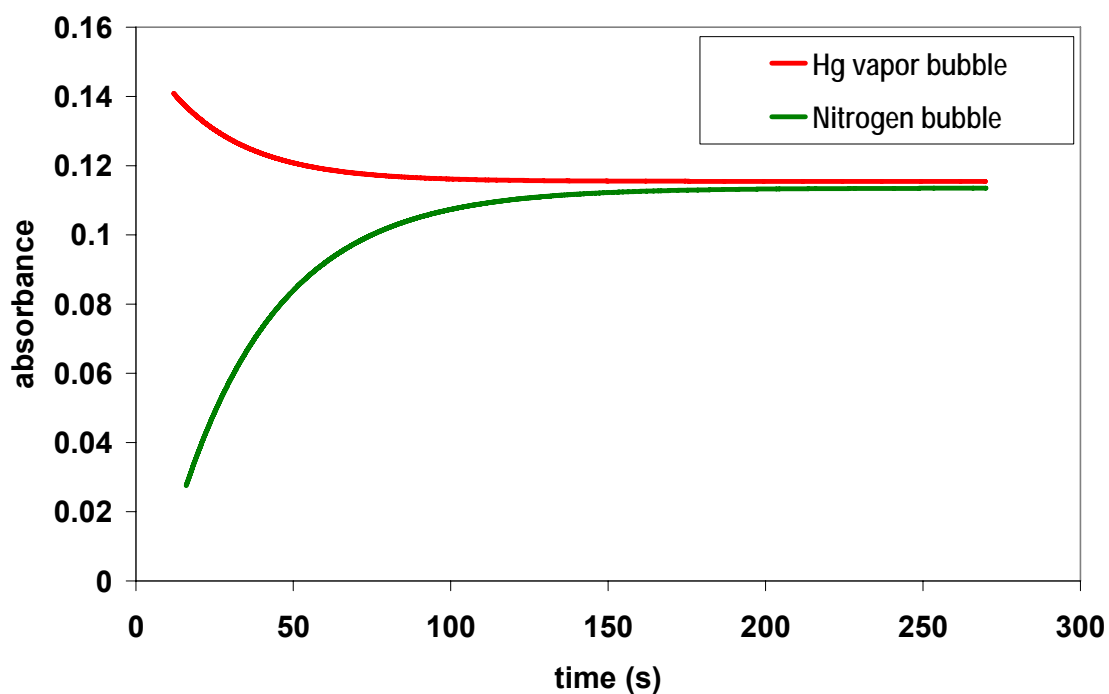


Figure 2.5 Movement of Hg vapor through bubble interface in both directions

It is immediately evident that the movement of Hg from the saturated solution into the N₂ bubble occurs on the same time scale as loss of Hg from a bubble into water. The movement of the Hg into the bubble from solution is reasonable considering the low solubility of Hg.¹⁹ However, this was an important experiment to perform since eventually movement of metal atoms *into* many small bubbles will be an under investigation.

2.3.3 Variation of pH

Table 2.1 Decay rate change with pH

	Decay Rate (s ⁻¹)	Normalized to Water
Water	0.047	1.0
pH 1.5	0.050	1.1
pH 11.5	0.047	1.0

As can be inferred from Table 2.1, pH did not appear to significantly affect the decay rate of Hg within the bubble. This is quite curious because the pH 1.5 solution was made using nitric acid, which would be considered an oxidizing environment. The alkaline solution was made using NaOH and should present a less favorable environment into which the Hg would move. This is because a higher concentration of elemental Hg would be present rather than easily oxidized to Hg²⁺ and Hg₂²⁺. The effect of the reducing power of solution will be discussed in more detail when looking observing decay signals while reducing agents are in the surrounding solution. While pH is considered a critical parameter for other cold vapor generation methods,^{1, 22, 23}, it is generally a factor controlling reducing agent strength.

It was also noted that the noise present in the pH 1.5 experiment was much higher. It appeared that the bubble would sometimes drag along the reaction cell wall,

suggesting an increase in the hydrophobicity of the wall. This behavior was less apparent in neutral solutions and absent when using basic solutions. Silanization of the reaction cell wall using a solution of 1% dimethyldichlorosilane in hexane to intentionally make the cell walls hydrophobic also produced signal decays which were noisy and, again, the bubble tended to stick to the cell walls. Because the pH 11.5 decay rate was identical to that of DI water, subsequent experiments were performed at pH 11.5 to insure the integrity of the bubble walls.

2.3.4 Variation of ionic strength

Table 2.2 Decay rate change with ionic strength

Buffer Strength	Decay Rate (s^{-1})	Normalized to Water
Unbuffered	0.047	1.0
0.02 M	0.047	1.0
0.1 M	0.037	0.8
1.0 M	0.024	0.5

Ionic strength of the solution surrounding the bubble was changed through the addition of buffer solutions containing Na_2HPO_4 and Na_3PO_4 at pH 11.9. While lower ionic strength solutions gave identical decay curves to DI water, higher ionic strengths slowed the decay rates. Other authors have investigated how changing the salt concentration of solution affected the uptake of Hg vapor from the atmosphere,²⁴ but it is curious that they did not see as pronounced results, especially at higher pH levels.

2.3.5 Addition of reducing agent

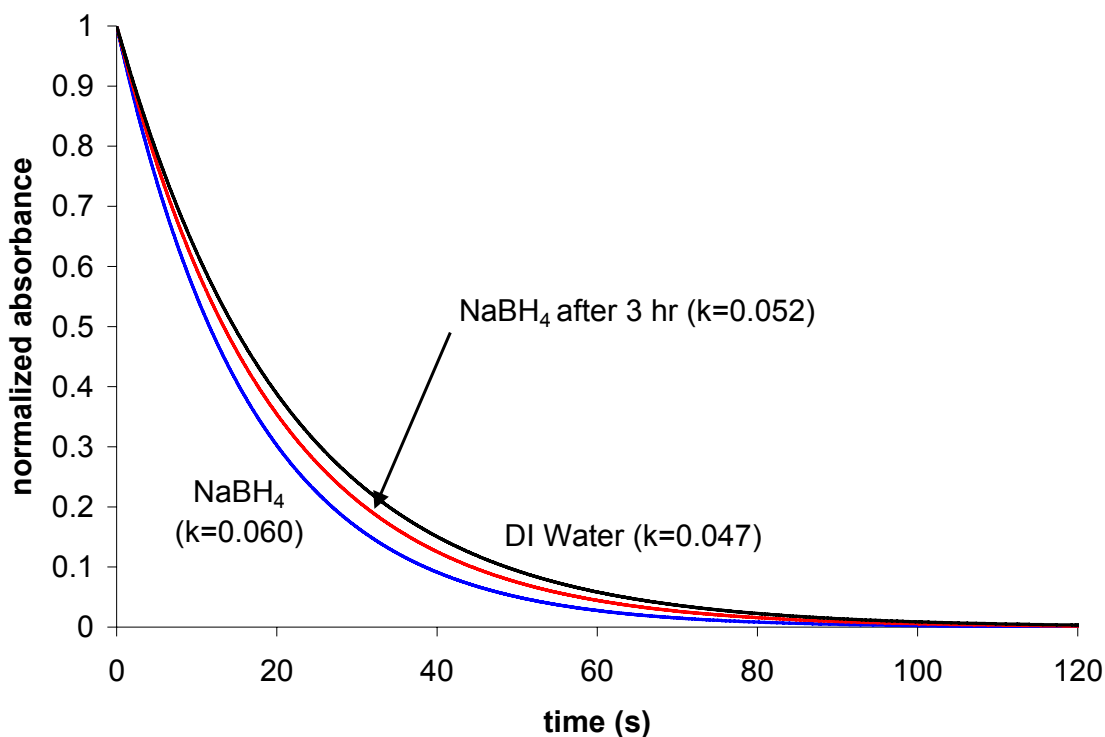


Figure 2.6 Decay of Hg signal after addition of reducing agent

The decay rate increased with the addition of a reducing agent, NaBH₄, to the solution. NaBH₄ evolves H₂ when dissolved in aqueous solution with more gas generated at lower pH values. The experiments shown in Figure 2.6 were performed at neutral pH, so H₂ evolution was noticeable. The initial decay rate of the solution for 0.005% NaBH₄ was higher than that of DI water. If the solution was left to sit for 3 h before the Hg-laden bubble was injected, the decay rate became more similar to that of DI water, suggesting that the reducing agent was consumed upon standing. Typically it would be expected that a more oxidizing environment would increase Hg loss to solution²⁵ and a reducing solution would slow uptake by solution. However, it appears that in this case

the amount of Hg present to be absorbed is small enough that the reducing agent does not affect the decay rate. Normally Hg within a reducing solution would be more likely to remain in the very insoluble elemental form which could be volatilized back into the vapor, but the system is set up in such a way that any Hg transported to the solution is carried away from the interface by the flowing solution. It remains unclear why the signal decay would *increase* in presence of a reducing agent, unless it simply reflects incorporation of H₂ from the borohydride reduction into the gas bubble and subsequent decrease in Hg_(g) density simply because of the increase in the bubble's volume.

2.3.6 Addition of surfactants

Triton X-100 (25 mM) and sodium dodecyl sulfate (20 mM) surfactants both had no effect on the Hg decay rate. Surfactants have been used in the past to stabilize cold vapor experiments involving Cd²² and it was thought that the decay rate might be affected in this system. However, Panichev and Sturgeon¹ did notice enhancements in their signal intensity and duration with the addition of Triton X-100. Additionally, it was reasonable to assume that any surfactant should change the surface tension at the bubble-solution interface which might impact the decay rate.

2.3.7 Changing physical properties of solution

Even though changing the surface tension through the addition of surfactants showed no change in the signal decay, a more controlled change in the surface tension as well as viscosity and density of surrounding solutions might give information about the system. The values for many of these properties are known for aqueous/organic solvent mixtures containing methanol, ethanol, and glycerol at various concentrations.⁶ Figure 2.7 shows the effect of changing solution viscosity on decay rates for mixtures of each of these solvents and water. The decay rate seems increase with increasing viscosity for

methanol and ethanol. However glycerol shows an opposite trend, suggesting that viscosity may not be the parameter that is causing the decay rate change.

Figure 2.7 Effect of viscosity on Hg vapor decay rate

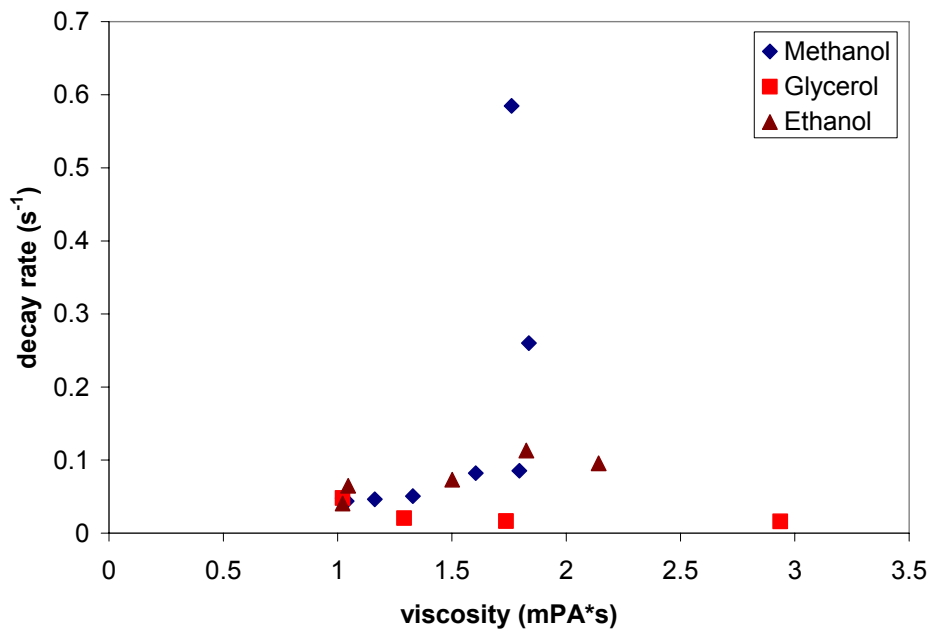


Figure 2.8 shows the effect of changing the solution's surface tension, and it is evident that one trend is not common for the different solutions, although the similar tendencies again seen for ethanol and methanol suggest that some correlation with surface tension might be present.

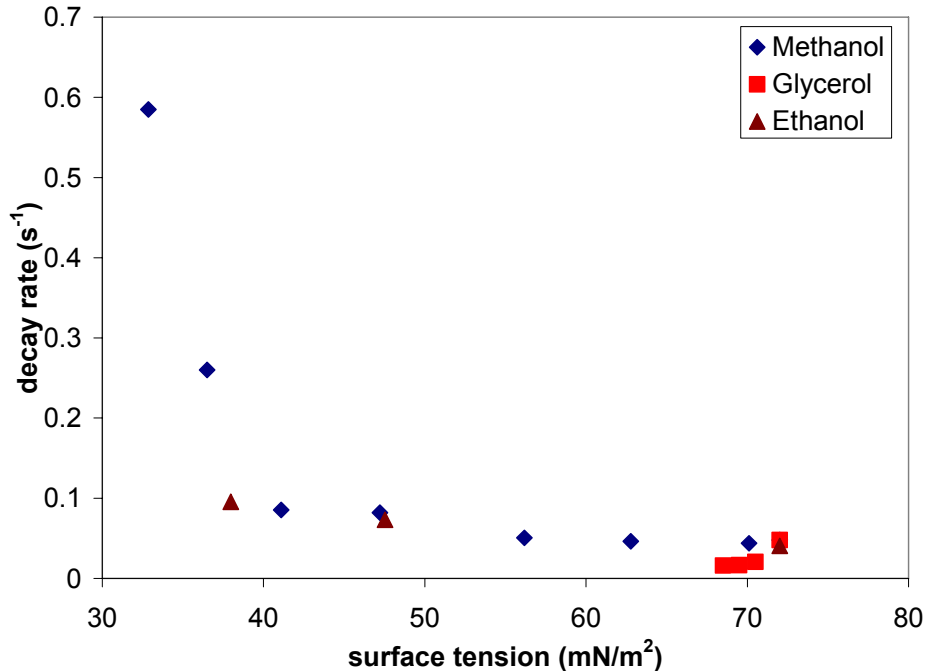
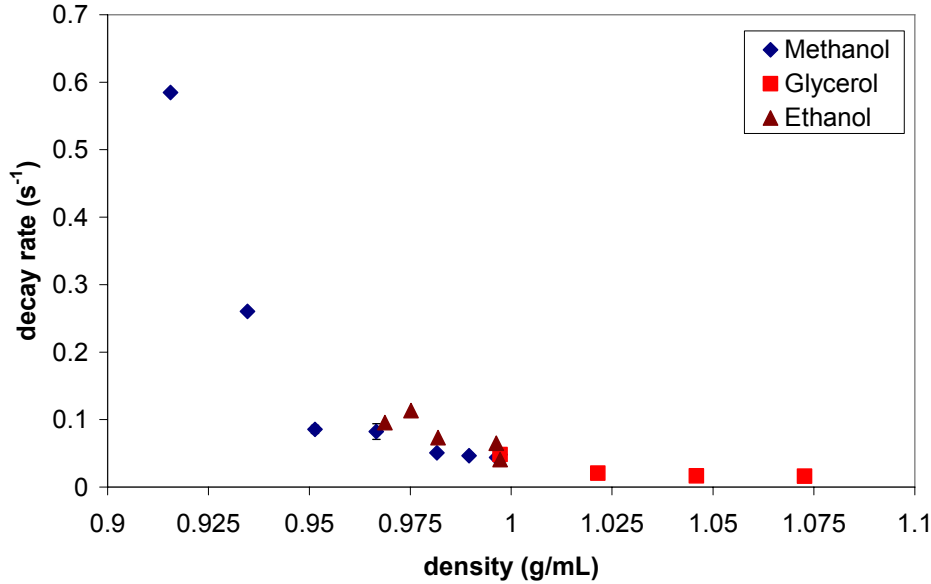


Figure 2.8 Effect of surface tension on Hg vapor decay rate

Finally, Figure 2.9 shows the results when the solution density was altered in a controlled manner. In this instance a very good correlation between density and decay rate is seen for all three solvents with faster signal decay with lower density solutions. While it appears that density has a significant effect on the rate of decay, an explanation is not obvious. If diffusional mass transport in solution were to govern the rate of Hg loss from the bubble, then this trend would suggest that Hg atoms are diffusing more rapidly into less dense solutions. A few methods exist for calculating diffusion coefficients^{26, 27} which incorporate density. These calculations suggest that the decreased density should increase diffusion rate. However, it is surprising that diffusion should have such a significant impact on mass transport since the solution is *flowing* by the bubble and would suggest that convection would play a dominant role.

Figure 2.9 Effect of density on Hg vapor decay rate



2.3.8 Simple diffusion out of a sphere

If diffusion does have a bearing on the transport of Hg vapor out of the bubble, even in this somewhat turbulent system, it would be prudent to also consider gas phase diffusion in the bubble. In order to do this, the system model will be simplified and the time for 90% loss of the Hg vapor from a sphere will be calculated. The equation for diffusion out of a sphere is:²⁸

$$\frac{C - C_1}{C_0 - C_1} = 1 + \frac{2D}{\pi} \sum_{n=1}^{\infty} \frac{(-1)^n}{n} \sin \frac{n\pi r}{a} e^{-\frac{Dn^2\pi^2 t}{a^2}} \quad (1)$$

where C is the concentration at a given radius r , C_1 is the initial concentration within the sphere, C_0 is the concentration at the sphere surface, D is the diffusion coefficient, a is the sphere radius, and t is time. The variables used are summarized in Table 2.3.

Table 2.3 Parameters used for calculation of diffusion out of a sphere

Parameter	Setting used
Sphere radius	0.50 cm
D_{Hg} in air ²⁹	0.14 cm ² /s
Surface Concentration	0
Initial Concentration	1.07×10^{-4} mol/L
Time	0 - 100 s

The initial concentration used was obtained from the vapor pressure of Hg at 25°C.⁶ Some assumptions were made such as the Hg behaving as an ideal gas, the bubble being spherical and the surface concentration always being zero. The results of the calculation are shown in Figure 2.10. It is immediately obvious that this calculation does not adequately describe the mass transport of the Hg vapor out of the bubble. The 90 % loss of Hg occurs in only 0.5 s, about 2 orders of magnitude faster than the decay observed experimentally. The assumptions made should not affect the decay time to this extent, so it would be advantageous to design a more complex modeling method in order to better approximate the experimental setup.

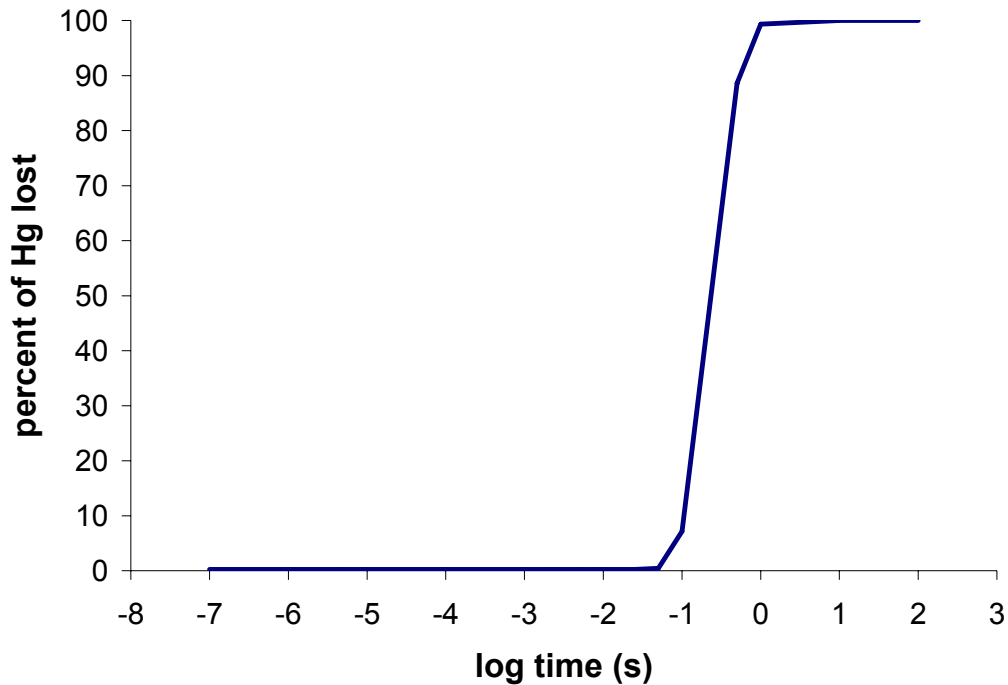


Figure 2.10 Results of calculation of Hg diffusion out of a sphere

2.3.9 Monte Carlo studies

Using Monte Carlo methods it is easy to calculate how long an atomic signal would last if we were to assume any atoms colliding with bubble walls would be lost to the surrounding solution. The equation used to simulate diffusion in Monte Carlo simulations is:³⁰

$$\Delta d_i = R_{g_i} (6D_{T_i} \Delta t)^{1/2} \quad (2)$$

where R_{g_i} is a random number from a Gaussian distribution, D_{T_i} is the temperature dependent diffusion coefficient, and Δt is time increment used in the simulation and Δd_i is the distance in the X, Y, or Z direction during a given Δt . The parameters used for the simulation are shown in Table 2.4 and the Visual Basic code used for the simulation is

available in Appendix B. Mercury was the element used for the simulation so results could be compared to experimental data and because its gaseous diffusion coefficient was known.²⁹ The simulation tracks a number of particles which start out randomly distributed within the spherical bubble. During each Δt , each particle is moved in each of the 3 dimensions according to equation 2. If a particle moves further than the radius of the sphere it is considered to be lost to solution. The percentage of the starting atoms remaining within the spherical bubble is monitored as time passes with the time where 90% of the particles lost being recorded.

Table 2.4 Parameters used for Monte Carlo simulation

Parameter	Setting used
Bubble Volume	0.50 cm ³
D _{Hg} in air	0.14 cm ² /s
Temperature	25 °C
Δt	0.01 s
Number of Particles	1000 particles

For example, when no more atoms enter the bubble over time, this method predicts that 90% of the atoms are lost in ~ 0.2 s, a much shorter duration than the ~ 50 s observed experimentally for Hg as well as the ~ 120 s observed in the literature for other metal species.¹

The simulation was then changed so that some of the collisions of the atoms with the bubble walls are completely elastic and the colliding atom remains in the gas. In this particular case the particle is moved back to its starting position for a given Δt . The results are shown in Figure 2.11 and showed that if only 0.07% of the wall collisions resulted in atoms being lost to solution then simulated decay times approximate our

experimental decay times for Hg. A 0.025% probability of loss with wall collision would approximately match the signal duration observed in the Panichev and Sturgeon experiment.¹ It is not obvious why almost perfectly elastic collisions would occur between Hg atoms and the bubble walls.

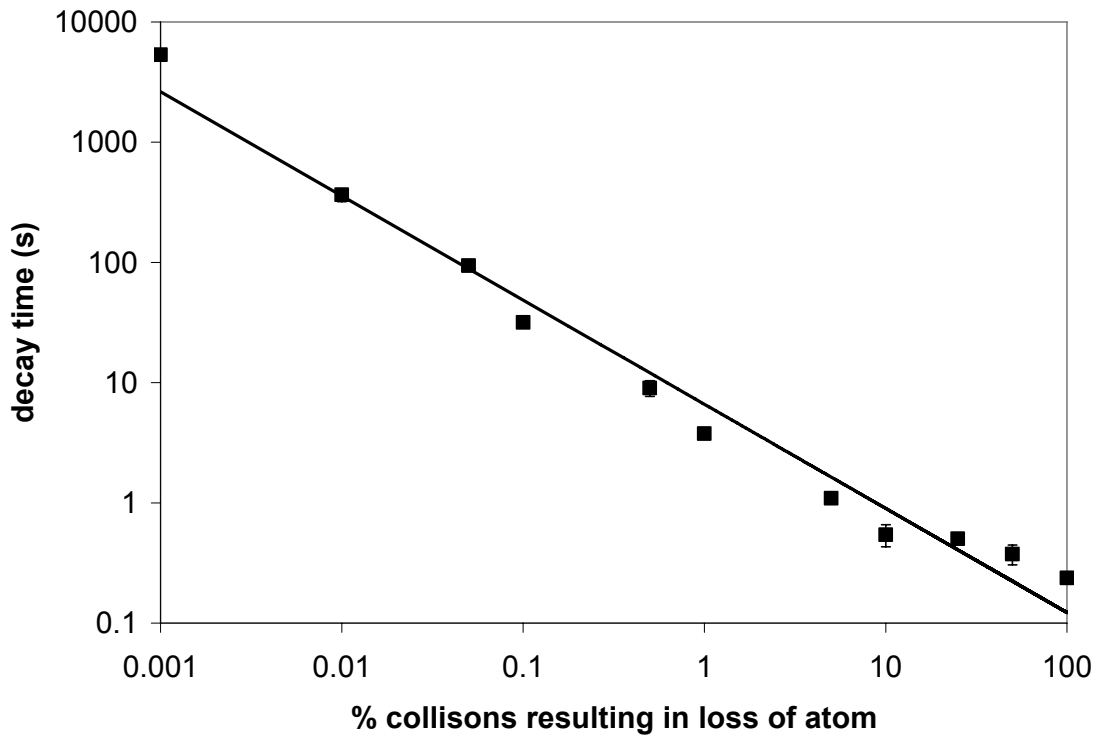


Figure 2.11 Results of Monte Carlo simulation of diffusion of Hg out of a spherical bubble

The results of the Monte Carlo simulations detailed above pointed out some problems with the hypothesis that atomic species could exist in bubbles surrounded by solution for more than a few hundred milliseconds. Because of this disagreement between the experimental results and the model built to describe the system, another logical step would be to look at diffusion of the atomic species after they leave the bubble and diffuse in solution. This would address the question of whether the atomic signal

could exist as one event which decayed slowly over time, or a series of short events with a continuous exchange of analyte with the surrounding solution. The later explanation would make much more sense, not relying upon 99.975% of the collisions with bubble walls to be perfectly elastic to keep the atoms out of solution. Lastly, another omission within this model would be the absence of any type of mechanism to account for the energy required to solvate the metal atoms in the surrounding solution, the activation energy of which could be significant.

2.4 LIMITATIONS OF EXPERIMENTAL SETUP

In attempting to model the experimental system described in this chapter, it was found that some key parameters such as solution flow around the bubble were ill defined, thus complicating the model. More experiments with an even simpler system were performed to avoid using these ill defined parameters which control metal transport. These experiments will be described in the next chapter.

While the experimental setup used in this chapter did not ideally mimic the conditions for the Panechev and Sturgeon experiment, the original exploratory purpose has been partially fulfilled. The importance to the absorbance signal on parameters such as solution density, ionic strength and perhaps surface tension have been separated from parameters such as pH and surfactant concentration.

REFERENCES

- (1) Panichev, N.; Sturgeon, R. E. *Analytical Chemistry* **1998**, *70*, 1670-1676.
- (2) Miranda, P. B.; Shen, Y. R. *Journal of Physical Chemistry B* **1999**, *103*, 3292-3307.
- (3) Du, Q.; Superfine, R.; Freysz, E.; Shen, Y. R. *Physical Review Letters* **1993**, *70*, 2313-2316.
- (4) Shultz, M. J.; Baldelli, S.; Schnitzer, C.; Simonelli, D. *Journal of Physical Chemistry B* **2002**, *106*, 5313-5324.

- (5) Wilson, M. A.; Pohorille, A.; Pratt, L. R. *Journal of Physical Chemistry* **1987**, *91*, 4873-4878.
- (6) *CRC Handbook of Chemistry and Physics*, 83 ed.; CRC Press: New York, 2002.
- (7) Wood, R. W. *Philosophical Magazine (1798-1977)* **1912**, *24*, 316-322.
- (8) Hughes, A. L.; Thomas, A. R. *Physical Review* **1927**, *30*, 466-472.
- (9) Hatch, W. R.; Ott, W. L. *Analytical Chemistry* **1968**, *40*, 2085-2087.
- (10) Lin, C.-J.; Pehkonen, S. O. *Atmospheric Environment* **1999**, *33*, 2067-2079.
- (11) Brosset, C. *Water, Air, and Soil Pollution* **1987**, *34*, 145-166.
- (12) Clever, H. L.; Johnson, S. A.; Derrick, M. E. *Journal of Physical and Chemical Reference Data* **1985**, *14*, 631-680.
- (13) Morita, H.; Mitsuhashi, T.; Sakurai, H.; Shimomura, S. *Analytica Chimica Acta* **1983**, *153*, 351-355.
- (14) Kobayashi, T. *Taiki Osen Gakkaishi* **1987**, *22*, 230-236.
- (15) Munthe, J., McElroy, W.J. *Atmospheric Environment, Part A: General Topics* **1992**, *26A*, 553-557.
- (16) Zhao, L., 1997.
- (17) Zhao, L. L.; Rochelle, G. T. *Industrial & Engineering Chemistry Research* **1998**, *37*, 380-387.
- (18) Toribara, T. Y.; Shields, C. P.; Koval, L. *Talanta* **1970**, *17*, 1025-1028.
- (19) Feng, Y.-L.; Lam, J. W.; Sturgeon, R. E. *Spectrochimica Acta, Part B: Atomic Spectroscopy* **2004**, *59B*, 667-675.
- (20) Beek, W. J.; Muttzall, K. M. K.; Van Heuven, J. W. *Transport Phenomena*, 2nd ed.; John Wiley & Sons, LTD.: New York, 1999.
- (21) Clift, R. *Bubbles, drops, and particles*; Academic Press: New York, 1978.
- (22) Sanz-Medel, A.; Valdes-Hevia y Temprano, M. C.; Bordel Garcia, N.; Fernandez de la Campa, M. R. *Analytical Chemistry* **1995**, *67*, 2216-2223.
- (23) Dedina, J. *Hydride generation atomic absorption spectrometry*; Wiley: Chichester (England), 1995.
- (24) Waite, D. T. S., A. D.; Liu, Y.; Huang, G. H. *Chemosphere* **2002**, *49*, 341-351.
- (25) Zhao, L.; Rochelle, G. T. *AIChE Journal* **1996**, *42*, 3559-3562.
- (26) Wilke, C. R.; Chang, P. *Am. Inst. Chem. Eng. J.* **1955**, *1*, 264-270.
- (27) Sitaraman, R.; Ibrahim, S. H.; Kuloor, N. R. *Journal of Chemical and Engineering Data* **1963**, *8*, 198-201.
- (28) Crank, J. *The mathematics of diffusion*, 2nd ed.; Clarendon Press: Oxford, 1975.
- (29) Spier, J. L. *Physica (The Hague)* **1940**, *7*, 381-384.
- (30) Guell, O. A.; Holcombe, J. A. *Analytical Chemistry* **1990**, *62*, 529A-534A, 536A, 538A, 540A-542A.

Chapter 3: Mass transport Hg within a system governed by diffusion

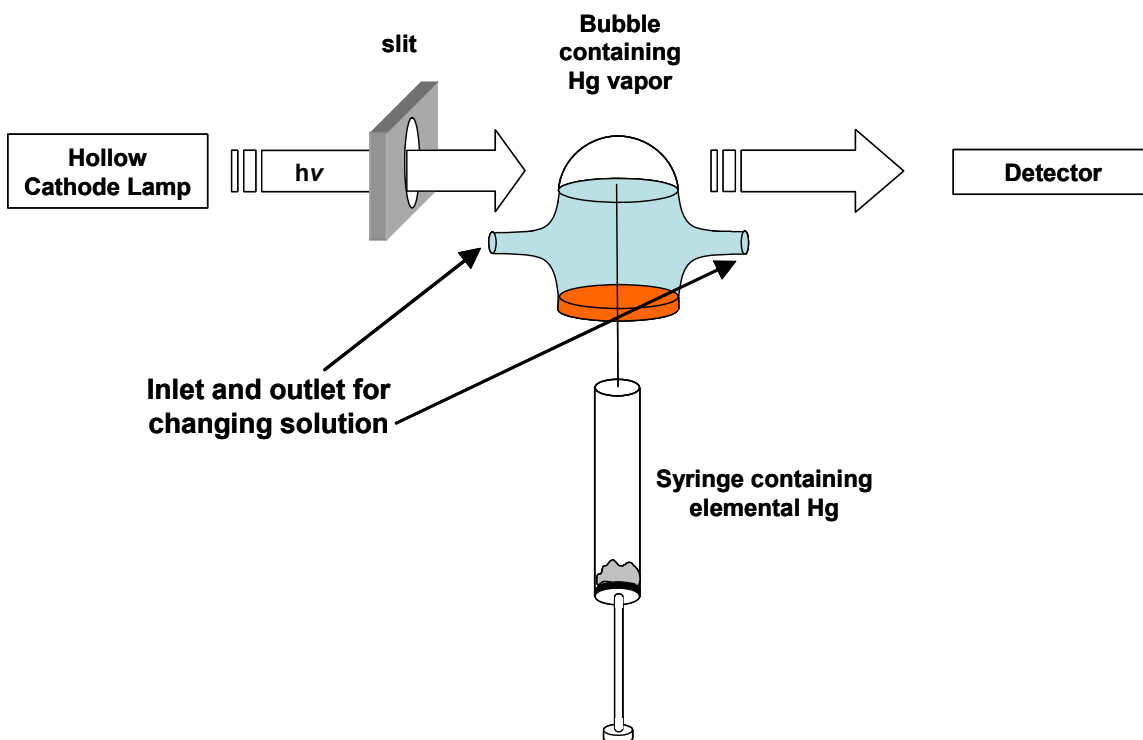
The experimental design presented in the previous chapter was successful in providing a variety of information about mass transport within a system containing a free floating bubble. However, the system was difficult to model due to unknown variables present. This chapter will delve more deeply into a simpler, albeit similar system. In order to minimize convection and focus on mass transport due to diffusion, the present system will contain a bubble in stagnant solution. By changing the surrounding solution and building a more complex model of the system, important information can be gleaned to address the larger problem of generating and maintaining an atomic signal for other elements. While this is the overall goal of the study, there is other information that can be obtained in the process which may be useful in its own right. This includes both the study of Hg transport into solutions which might be analogous to aqueous systems in the environment, as well as elucidation of fundamental parameters of the system such as the diffusion coefficient of elemental Hg through water and its solubility in aqueous solution, the former not present in the literature and the later contested among those authors who have studied it.

3.1 EXPERIMENTAL

The general experimental setup is shown in Figure 3.1. All experiments were performed using a modified Varian SpectrAA 400 Plus FAAS which had its burner head removed. Measurements were taken using Hg Hollow Cathode Lamp (SCP Science) operated at the manufacturer's recommended setting using a reduced slit height and a bandpass of 0.5 nm. For detection of Hg atoms, 253.7 nm was monitored. The deuterium background correction was turned on for all experiments. Data collection was accomplished using LabView™ software made by National Instruments, and Microsoft

Excel[®] was used for data analysis. Data was collected at a rate of 16 Hz, and the smoothing was performed using a 10 point moving average and exponential smoothing algorithm using a 0.9 damping factor.

Figure 3.1 Experimental design for diffusion controlled mass transport measurements



3.1.1 Reagents

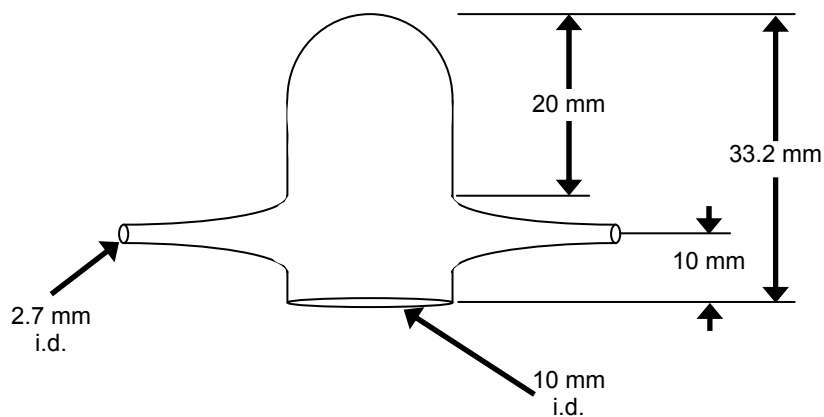
Aqueous solutions were made using distilled, deionized water from a mixed bed ion exchange column (Barnstead Thermolyne). pH adjustment was accomplished using sodium hydroxide (EM Science), nitric acid (Fisher Scientific), or hydrochloric acid (Fisher Scientific). pH and temperature were monitored using a Ion 6 pH/temperature meter (Oakton). Some experiments required reducing agents to be added to solutions, with either sodium borohydride (Fisher Scientific) or stannous chloride (Technical Grade, Fisher Scientific) being used.

Mercury was added to solutions for some experiments using a 1000 ppm Hg Standard (AA grade, Acros Organics). For 10 ppm Hg solutions, the Hg standard was diluted 100-fold with DI water. Solutions containing both Hg and reducing agents were prepared fresh each day by diluting the Hg standard to 2 ppm with a 10 mM solution of SnCl₂ in 2% HCl. Reductant solutions were prepared fresh daily and contained either NaBH₄ or SnCl₂ and NaBH₄ solutions were adjusted to pH 11 using NaOH while solutions using SnCl₂ were adjusted to pH 1 using HCl.

3.1.2 Experimental setup and procedure

The experimental setup for studying Hg loss from a 500 μ L bubble consisted of a home built quartz cell (Figure 3.2) which was hemispherical in shape, with a rubber septum (Fisher Scientific) inserted in the bottom. The cell measured 10 mm (i.d.) and had an inlet and outlet on each side to allow for addition and removal of solution. The quartz cell was positioned in the optical path of the spectrometer so that the bubble would rest at the top of the cell with the optical beam passing through it. An aperture (3.18 mm x 25.2 mm) placed 29 mm in front of the cell center was used to limit the area that was monitored.

Figure 3.2 Quartz reaction cell for diffusion controlled mass transport measurements



The inside of the quartz cell was silanized using a solution of 1% dimethyldichlorosilane (Fisher Scientific) in hexane (Fisher Scientific) and a rinse solution of methanol (Fisher Scientific). Mercury vapor for each experiment was obtained by allowing a small amount of elemental Hg_(l) (~0.25 g) to equilibrate with a nitrogen headspace inside a 1 mL Hamilton SampleLock™ syringe (Fisher Scientific). For each experiment, the cell was filled with the desired solution which had been degassed using in-house nitrogen. To start the experiment, the Hg vapor was injected into the cell using the syringe to make a bubble with a volume of 500 μL. The syringe was removed, and only the bottom part of the bubble was exposed to solution. The earlier silanization of the inside of the quartz cell caused the meniscus to flatten out, giving a disc-shaped interface. The height of the solution was measured within the cell and masked with electrical tape to prevent the HCL beam from reaching the detector after passing through the interface or any solution. The decay of the Hg signal was monitored as Hg atoms left the bubble and were transported into solution which was not stirred.

Computer simulations were written on a PC running Windows XP® using Microsoft Visual Basic and Microsoft Excel.

3.2 EXPERIMENTAL RESULTS

The absorbance decay curves produced by this experimental setup initially looked similar to those produced in the previous chapter, but having an order of a magnitude longer decay times. Initial signal analysis revealed that each signal decay could not be accurately described by a pure exponential decay. While it was eventually determined that the signal could be described by a more complex model, comparison of experiments to DI water runs will be the methodology used in the next section since no simple decay constant accurately describes the curves.

3.2.1 Variation of oxidation/reduction properties of the surrounding solution

As shown in Figure 3.3, Hg atomic absorbance signal obtained from observing a 500 μL bubble that was initially saturated with $\text{Hg}_{(\text{g})}$ at 25 $^{\circ}\text{C}$ can last for several thousand seconds. Because the solution was stagnant, only mass transport by diffusion is significant unless oxidation of elemental Hg in the solution occurs. If oxidation takes place, such as in the solution of 1% HNO_3 shown in Figure 3.3, the rate of Hg^0 transport through the interface is a function of the Hg ion concentration and the chemical potential of the solution, i.e., the redox character of the solution would dictate closeness to equilibrium at any given spatial zone. It is important to note that while no deliberate mixing of the solution occurred, the solution was not temperature controlled and slight temperature variations (± 0.5 $^{\circ}\text{C}$, as monitored by a thermocouple) of the solution around the bubble could have caused minor convection.

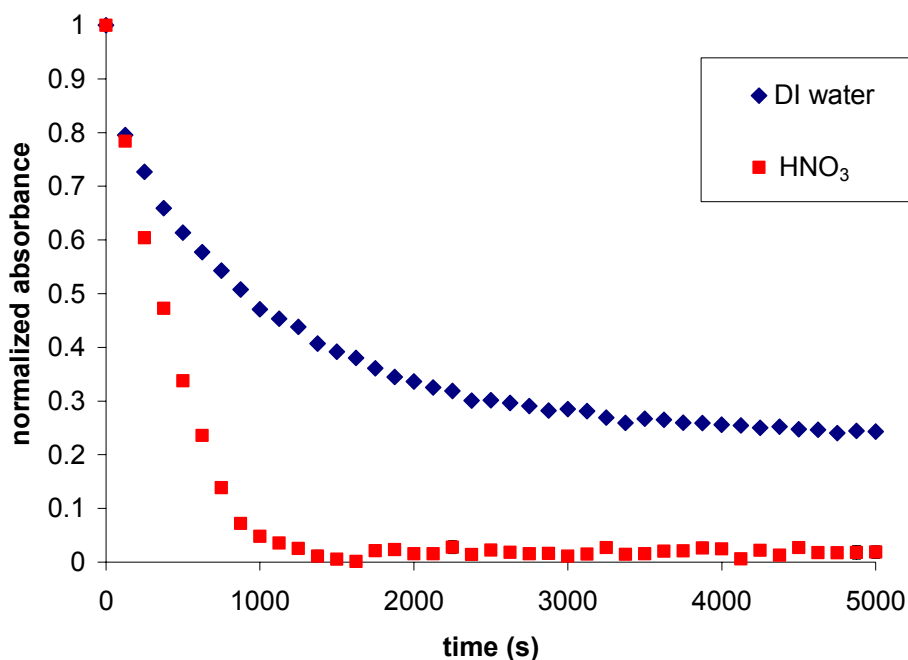


Figure 3.3 Absorbance signal decay of Hg in unstirred DI water and 1% HNO_3

In order to make the principal species in solution elemental Hg, the solution surrounding the bubble could be made reducing in nature by adding SnCl₂. While the use of NaBH₄ would make the system analogous to that of Panichev and Sturgeon,¹ it evolves hydrogen in solution and alters the volume of the 500 μL bubble. NaBH₄ also creates many small bubbles in the solution that also attach to the container walls, thus making the system much more difficult to model because of the other “traps” where Hg_(g) can be scavenged. For this reason, 10 mM SnCl₂ was primarily used for the reducing solution data seen in Figure 3.4. With the SnCl₂ present, the signal decays slower than in the DI water, although it should be pointed out that HCl was used to dissolve the SnCl₂ salt, and the pH of the resulting solution is ca. 0.8. However, Zhao et al.² have shown that while lower pH solutions may increase the rate of transport of Hg out of the gas phase, the type of acid matters more than the pH, with an oxidizing acid such as HNO₃ increasing elemental mercury uptake by solution, and HCl causing the oxidation to Hg²⁺ to slow down or even reducing Hg²⁺ in solution. For this system, the decay curve for 2% HCl falls between the nitric acid (Figure 3.3) and 10mM SnCl₂ curves. Therefore, the slower decay observed in Figure 3.4 for the SnCl₂ containing solutions is likely due to the strongly reducing environment around the bubble. This is consistent with the very low solubility of the Hg_(aq) which will be discussed in more detail in a later section.

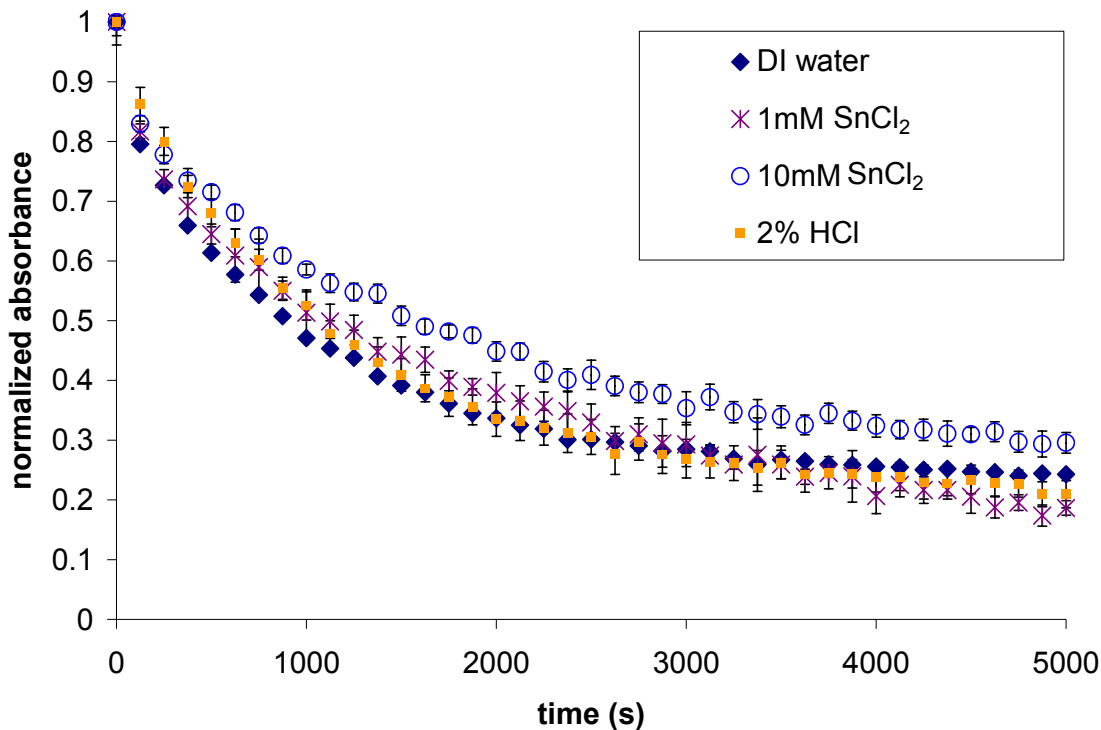
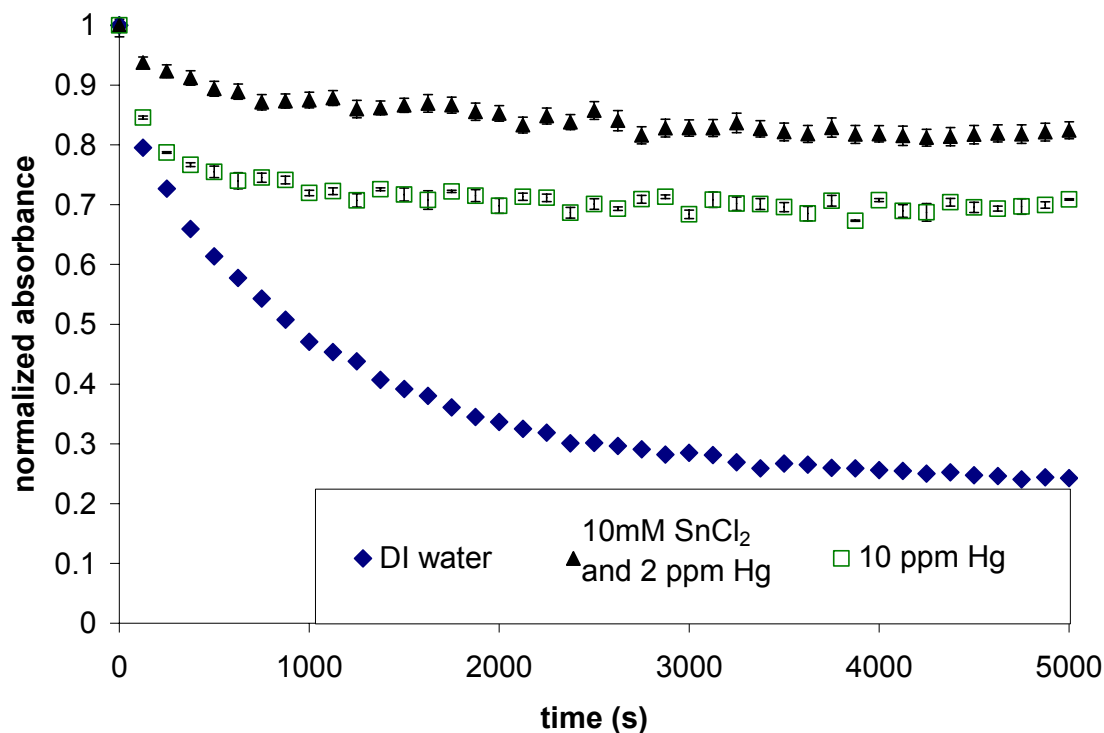


Figure 3.4 Hg Absorbance signal decay with the addition of SnCl₂

3.2.2 Addition of Hg to the surrounding solution

Shown in Figure 3.5 are the effects Hg loss from the bubble when a 10 ppm Hg solution is used. In this instance there is a drop in the Hg_(g) absorbance signal within the first 100-200 s but the rate of signal decay decreases beyond that point, probably as a result of the counter balancing effect of Hg moving from solution into the bubble. As one would expect, Hg leaves the bubble much more slowly because there are already Hg ions and atoms in solution. The addition of SnCl₂ to the Hg solutions slowed the decay of the Hg signal even more. This solution is analogous to reduction solutions used in conventional Hg cold vapor analysis,^{3, 4} so that Hg atoms that leave the bubble are replaced by Hg ions that have been reduced and volatilized from solution.

Figure 3.5 Hg absorbance signal decay in solutions containing Hg



Others have noticed an increase in the $\text{Hg}_{(g)}$ absorption rate when Hg^{2+} is present in solution.^{2, 5} It is curious that a slower decay of the Hg absorption signal is observed in Figure 3.5 for the solution containing Hg. Zhao et al. showed results within a stirred system where the presence of Hg^{2+} species catalyzed $\text{Hg}^0_{(g)}$ absorption with a rate that was near second order.² In the present system, the quiescent solution brought the solution interface closer to saturation with the observed slower decay, and interestingly, the decay rate is slower than that observed for 10mM SnCl_2 in Figure 3.4 as well as the DI water solution (Figure 3.5). This would indicate that the Hg species already present in solution did not increase absorption rate of $\text{Hg}^0_{(g)}$ as observed by other authors.^{2, 5} This disparity would suggest that the preparation of the solutions using 0.5 M sulfuric acid⁵ or 0.8 M

nitric acid² has a much larger effect on the decay rate than simply the presence of Hg²⁺ species, as observed by this work for Hg solutions which are diluted with 0.01% HNO₃ (1.5 mM). However, one of these authors² goes on to monitor the decay rate change at lower acid concentrations similar to the solution present in this system. Unfortunately, the results are not comparable as the Hg concentrations used in the present system are lower. Additionally, the experimental set up used in the present work may have contributed to the different results. The surface area through which Hg transport occurs is 2 orders of magnitude smaller in this work and the solution is unstirred, compared the experimental setup used by Zhao et al.² This indicates that the ease of saturating the interface with Hg species is a large contributor to slowing the signal decay, outpacing processes observed by other authors, such as absorption catalyzed by Hg²⁺ speeding up the decay.

3.2.3 Observation of Hg transport into a nitrogen bubble

Figure 3.6 shows that the mass transport into and out of a bubble is slow, with Hg moving into a nitrogen filled bubble over a period of few thousand seconds for a solution of 10mM SnCl₂ and 2 ppm Hg²⁺. The lack of precision in the N₂ bubble experiment may result from variations in the loss of Hg from solution during preparation. While discussion of this data seems a trivial point, it is necessary to consider because it is an environment similar to that created by Sturgeon and Panichev¹ where the metal atoms detected were surrounded by a solution of metal ions in a reducing environment. In Figure 3.6, a similar environment allowed the signal to last an extended period of time; any metal atoms lost to solution could be immediately replaced because the environment surrounding the bubbles was rich in Hg atoms.

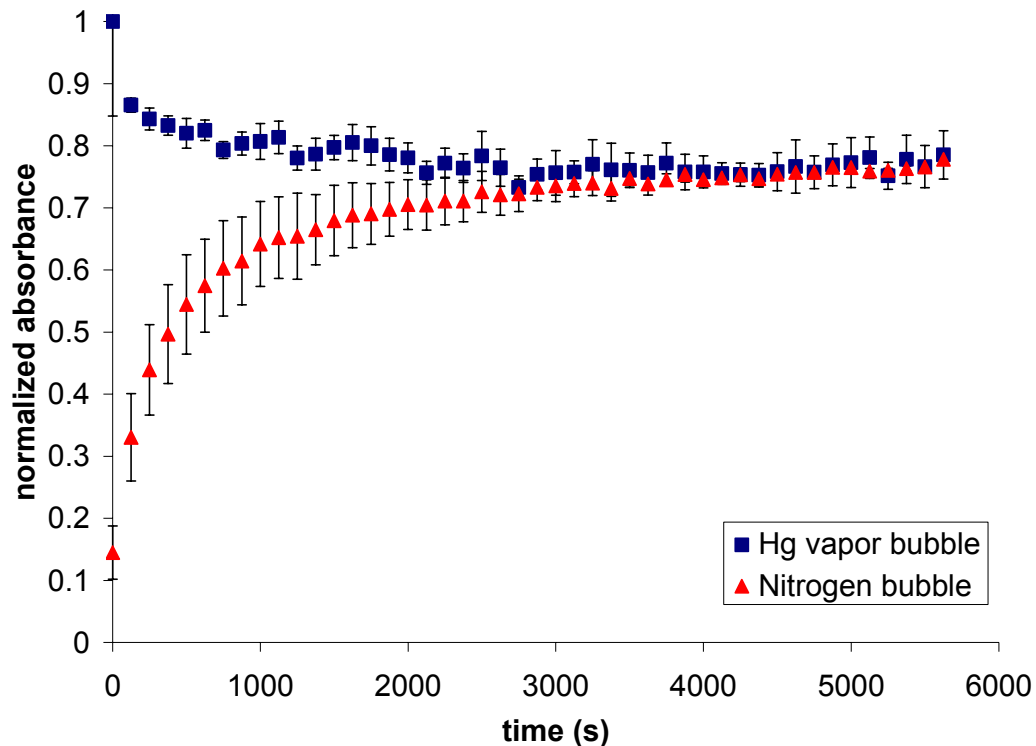


Figure 3.6 Transport of Hg through bubble interface in both directions

3.2.4 Investigation into Hg adsorption on syringe tip and reaction cell walls

There was some concern that some Hg may be lost by adsorption of $\text{Hg}_{(g)}$ onto the metal syringe tip and/or the reaction cell walls. To simulate Hg adsorption to metal in a case where Hg has a high affinity for a metal,⁶ a piece of Au wire (0.2 mm dia.) was placed in direct contact with the Hg vapor inside the bubble. The resulting decay is shown in Figure 3.7. Although there is a rapid decrease in Hg vapor due to adsorption onto the Au wire occurred within the first two minutes, a significant Hg signal was observed for a few thousand seconds. In fact, this decay rate was almost identical to that present with only DI water present. The adsorption process was considerably faster than loss from diffusion showing that Hg loss would be considerable if the vapor were

exposed to metal (such as the syringe tip) for a few hundred seconds. This would also indicate that the presence of the syringe tip for < 3 s during initial bubble formation would not have a large effect on the signal if length of exposure was reproduced for every run.

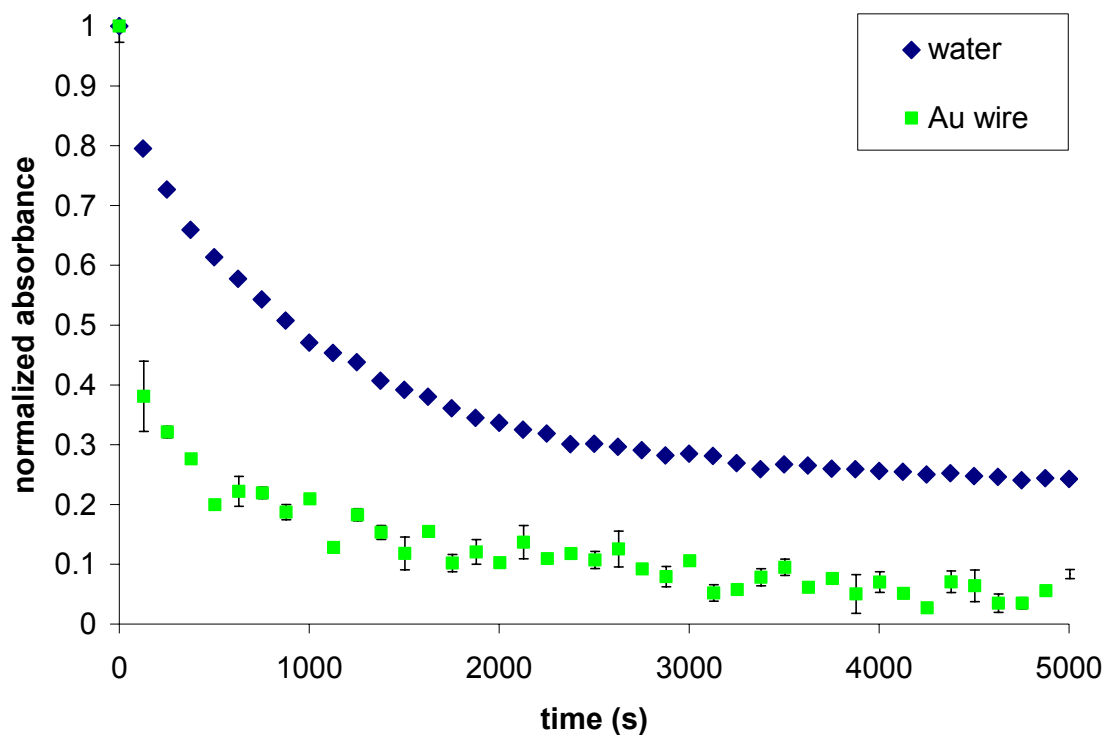


Figure 3.7 Effect of presence of Au wire within bubble

Hg adsorption to the reaction cell walls was considered as another process contributing to Hg loss. The first precaution taken to prevent this from occurring was the silanization of the cell walls using dimethyldichlorosilane. This is frequently used in analytical labs to prevent the adsorption of trace metal ions onto glassware.⁷ To confirm that significant amounts of Hg were not adsorbing to the cell walls, a normal run was performed and resulted in a relatively constant nonzero signal present after 10,000 s. The pump was turned on to move any Hg away from the interface without pushing the bubble

out of the reaction cell. The pump was stopped and heat was applied to the cell using a heat gun (Master Heat Gun, Model HG-501A) to increase the temperature inside the bubble as well as on the reaction cell walls. If Hg had adsorbed on the surface of the reaction cell, an increase in the absorbance signal would be expected as the Hg was desorbed off of the surface. The absorbance signal did not increase in this case, thus it was assumed that adsorption on the cell walls was negligible.

3.3 COMPUTER SIMULATIONS

The experimental data described above suggests which variables are significant for an aqueous system containing metal vapor in bubble(s). It appears that having a high metal concentration to make Hg species available to move back into the bubble in conjunction with a reducing agent to control the oxidation state of the metal will prolong the signal. However, it is obvious from this chapter and the previous chapter that mass transport into and out of the bubble is quite slow, lasting 100-10,000 s before an equilibrium partial pressure is reached. Obviously, increasing the interfacial area (e.g., using a large number of very small bubbles) and encouraging convection will foster rapid equilibration.

The previous experimental probing of the Hg system with a stationary bubble permitted qualitative identification of some of the mechanisms and trends. In the next section a more quantitative look at these transport processes will be pursued using simulation and modeling.

3.3.1 Use of the explicit box method to simulate diffusion

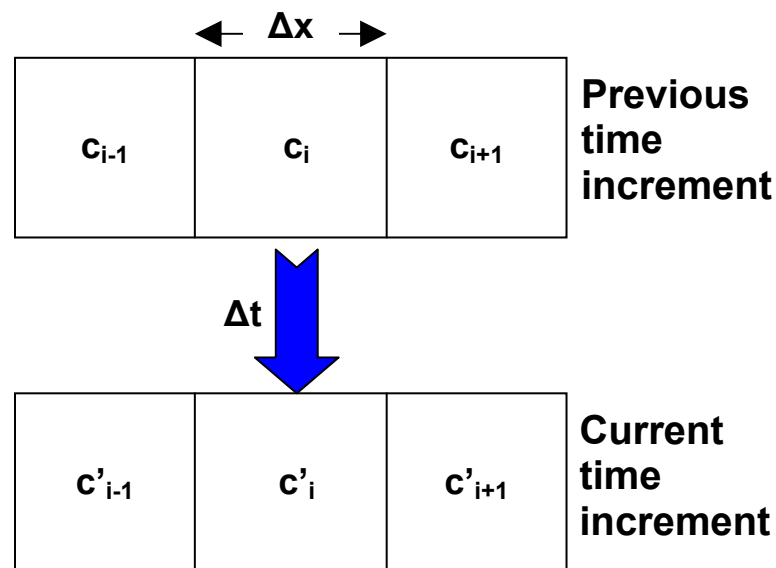
The results of the Monte Carlo simulations detailed in the previous chapter pointed out some problems with only modeling diffusion of the gaseous species out of the bubble. Because of this, another logical step would be to look at diffusion of the atomic

species after they leave the bubble and diffuse through solution. While previously used Monte Carlo simulations provided some insight, the stagnant bubble system was amenable to other discrete methods that would permit more direct comparison between simulation and experiment. In particular, the Explicit Box Method of diffusion simulation from electrochemistry⁸ was adapted to the system of interest. This type of simulation simply divides the solution surrounding the bubble into a series of discrete boxes through which the analyte makes simulated movements. The equation for diffusion through solution is:

$$c'_i = c_i + \frac{D\Delta t}{\Delta x^2}(c_{i-1} - 2c_i + c_{i+1}) \quad (1)$$

where c'_i is the new concentration for a box at position i , c_i is the previous concentration, c_{i+1} and c_{i-1} are boxes on either side of box i , Δx is the length of each box, Δt is the time increment, and D is the diffusion coefficient. The general layout of the algorithm is shown in Figure 3.8.

Figure 3.8 Explicit Box method setup

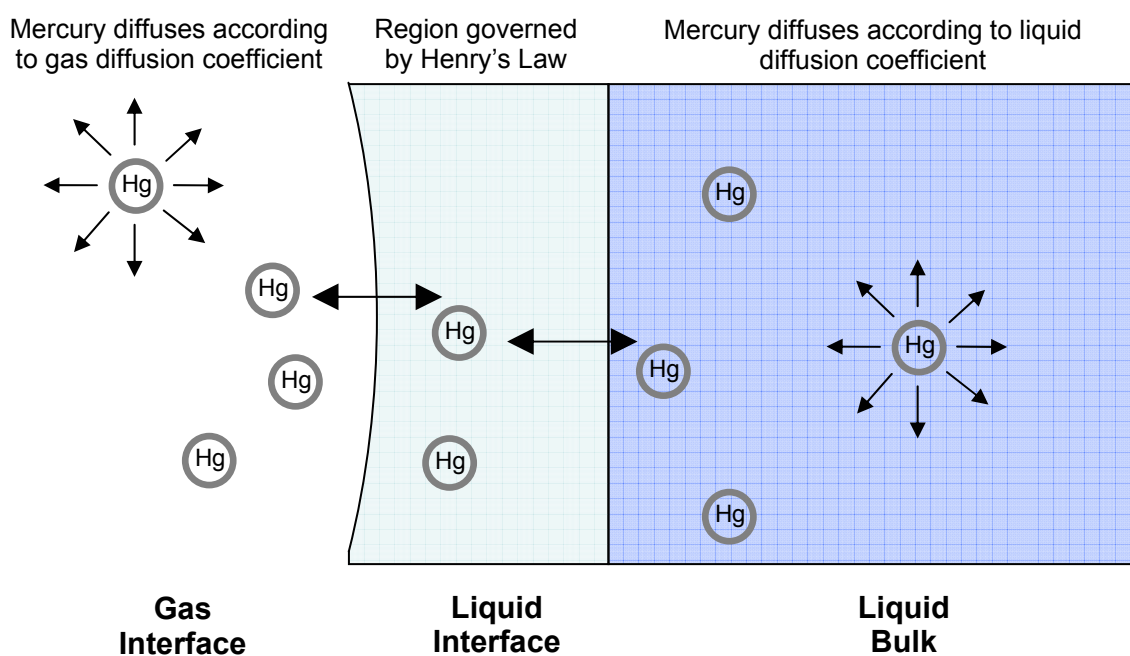


Instead of using an electrode as a source of Hg atoms, a 500 μL bubble was used, where diffusion of $\text{Hg}_{(\text{g})}$ inside the bubble was assumed to happen very quickly compared to the Δt values used for the simulation, as shown in the previous chapter by the Monte Carlo methods. This yielded the equation for the first box, c_1 , which was simply:

$$c_1 = \frac{[\text{Hg}_{\text{bubble}}]}{H} \quad (2)$$

where H is the Henry's constant for Hg^9 . A pictorial diagram of the overall simulation is shown in Figure 3.9, the parameters used for this simulation are shown in Table 3.1, and the Visual Basic code is available in Appendix B.

Figure 3.9 Diagram of simulation design



One parameter that did not have an obvious value is the coefficient of diffusion for elemental Hg in water. One value, obtained experimentally for diffusion of elemental Hg through isoctane¹⁰ was $1.6 \times 10^{-6} \text{ cm}^2/\text{s}$. Another value used by Zhao et al. during an extensive study of Hg in aqueous solutions,^{2, 11-13} used a generalized equation for

diffusion in liquids¹⁴ to predict a value of $1.19 \times 10^{-5} \text{ cm}^2/\text{s}$ for elemental Hg in water. Because of this inconsistency, the simulation was used to solve for the diffusion coefficient of Hg in water, by fitting the simulation to the experimental data. The rationale rests with related studies that suggest aqueous interfaces may contain an ordering of the water molecules at the interface which could affect the diffusion of species into solution.^{15, 16} All atoms must pass through the interface, so even if diffusion in bulk solution was very fast, a slow diffusion rate through the interface would slow the overall rate of analyte removal from the vapor phase.

Table 3.1 Parameters for simulation using box method

Parameter	Setting used
Δt	1.00 s
Δx	$1.0 \times 10^{-2} \text{ cm}$
run time	$1.0 \times 10^4 \text{ s}$
P_{Hg}	$1.71 \times 10^{-6} \text{ atm}$
Henry's Constant	0.29
Bubble Volume	0.50 cm^3
Temperature	$24.0 \text{ }^\circ\text{C}$
D_{Hg} in water	$1.30 \times 10^{-5} \text{ cm}^2/\text{s}$

Before commenting on the results of the computer simulations, it would be prudent to point out their limitations. The simulations only looked at the diffusion of the atomic form of Hg, not at any of the ionic forms that the atoms could have been converted to in solution. Also, the solution outside of the bubble was assumed to be

completely stagnant, ignoring possible convection that may arise due to small temperature differences in solution.

Initial results are shown in Figure 3.10 for different values of D and H compared to the experimental data for DI water. The D value used while varying H was 2.00×10^{-5} cm²/s and the H value used when varying D was 0.30, since these values seemed reasonable given studies in the literature.^{14, 17} While the variations of D and H shown below are quite large, even smaller variations did not give an optimal fit.

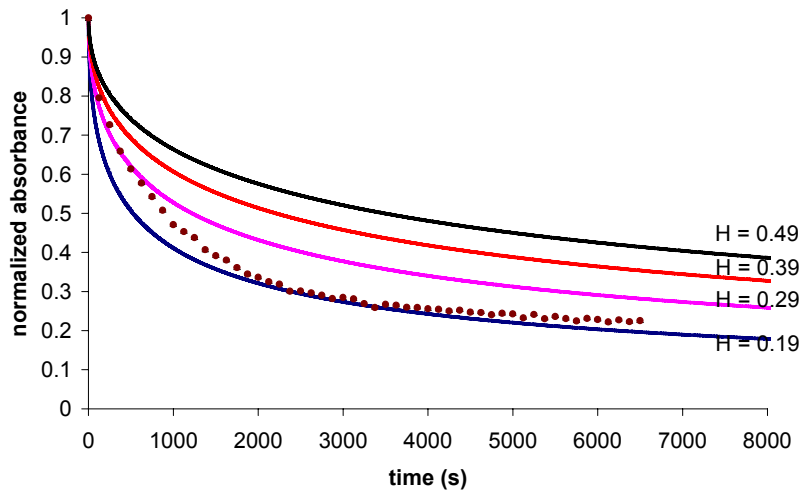
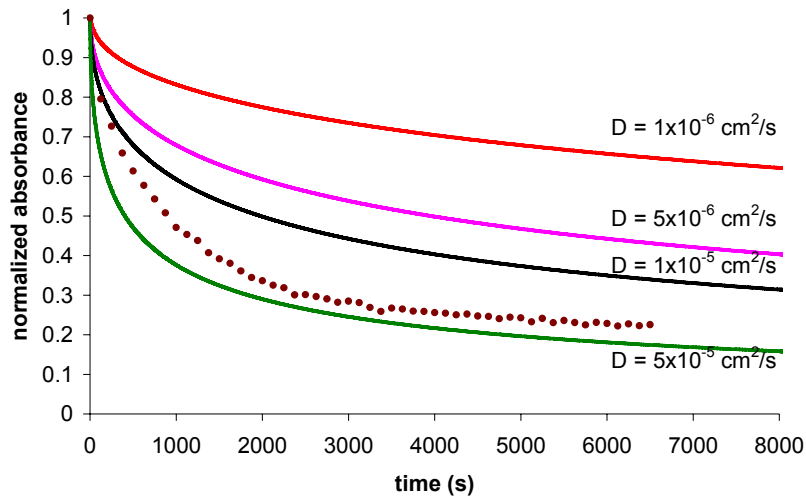


Figure 3.10 Effects of changing D and H parameters of simulation

A more sophisticated algorithm, known as the Crank-Nicholson method,⁸ was used in an attempt to improve the fit between simulated and experimental data. This method is similar to the explicit box method in that it splits the system into discrete boxes, each with an associated concentration. However, instead of solving for the

concentration of each box in a stepwise fashion for a given time increment, the Crank-Nicholson algorithm solves for all concentrations simultaneously. The Crank-Nicholson method is faster and considered to be a more robust method of calculation since it is able to handle a wider variety of Δt and Δx values without suffering from discretization errors. In the end, this method gave identical results as the explicit box method. The Visual Basic code for this method can be found in Appendix B.

3.3.2 Best fit of simulation and resulting diffusion coefficient used

The simulation and experimental data are compared in Figure 3.11. The experimental data set represents a solution containing 10 mM SnCl₂. This solution with the reducing agent represents conditions most similar to the simulation constraints, i.e., having the least number of Hg ions, which is assumed to be zero in the simulation. The diffusion coefficient found for elemental Hg through aqueous solution is 1.3×10^{-5} cm²/s although it is immediately obvious that the simulation does not give an exact fit even if it is very close to its experimental counterpart. The diffusion coefficient which gave a best fit is only 9% higher than the value calculated from a general equation for diffusion in liquids.¹⁴

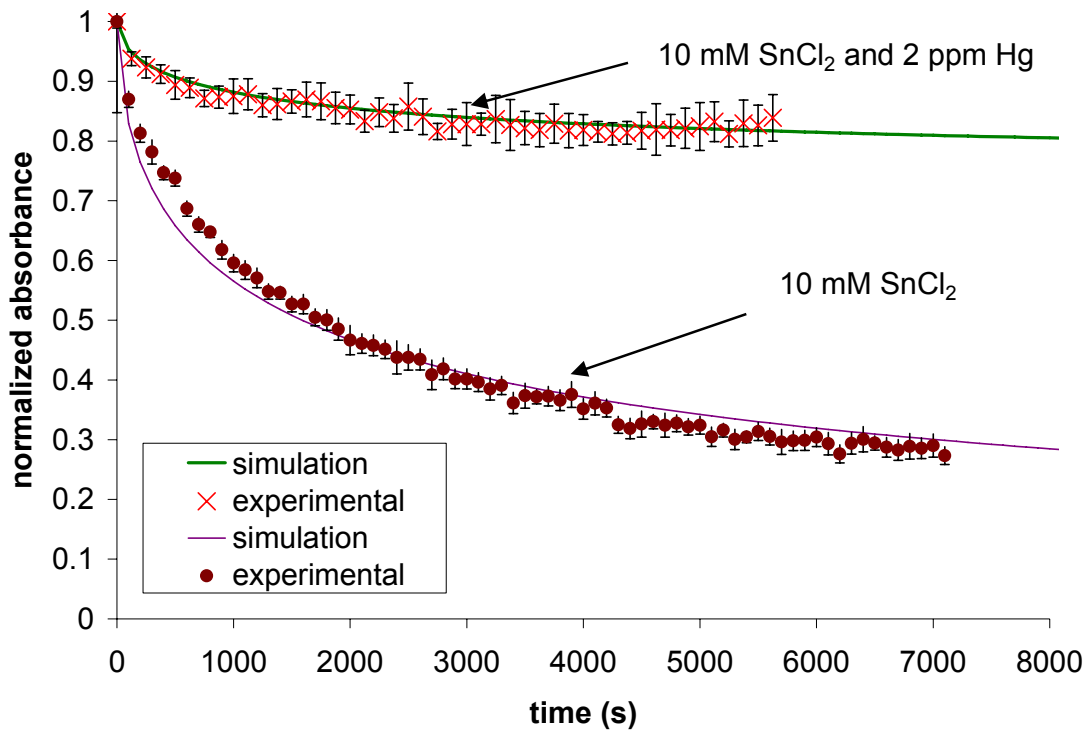


Figure 3.11 Simulated Hg decay signal compared to experimental data for 10 mM SnCl₂ and 10 mM SnCl₂ and 2 ppm Hg

The Henry's constant of 0.29 provided the best fit and is the same value reported in the literature⁹ where, interestingly, the procedure used was very similar to the experiments in the current study. The main reason for disagreement on the Henry's constant in literature sources is due to different methods of measuring the solubility of Hg in water. One very thorough review¹⁷ of solubility values for atomic as well as ionic forms of Hg discusses this topic, giving solubility values for atomic Hg of 25-81 ppb for the temperature range of interest (20-30 °C) with values not necessarily in agreement for a given temperature. However, this variance is quite small when compared to the change in solubility when Hg is in ionic form. For example, one of the relatively insoluble Hg salts, Hg₂Cl₂ has a solubility of 4 ppm while HgCl₂ has a solubility of 7.3×10^4 ppm.¹⁷ Therefore, the main

driving force keeping the Hg atoms from leaving the bubble quickly is not only how quickly the atoms can diffuse away from the bubble, but also the limited solubility of Hg^0 . The limitations of the computer simulation pointed out above could be one cause of the imperfect fit, although the difference between the 1% HNO_3 and SnCl_2 data shows the significance of simulation of the ionic forms of Hg. These results should be applicable to other cold vapor species as well and some solubility values have recently been obtained by other authors for noble metal vapor species, showing even lower solubility values than atomic Hg, with elements such as Pd yielding values of 2.6-4.2 ng/L.¹⁸

3.3.3 Determination of $\text{Hg}^0_{(\text{aq})}$ solubility

With an awareness of the variability in H, a simulation was run in an attempt to match the data with an experimental solution containing 10 mM SnCl_2 and 2 ppm Hg^{2+} surrounding a mercury filled bubble ($P_{\text{Hg}} = 1.71 \times 10^{-6}$ atm). The same D and H values were used as the other fit, but the simulation was changed so that some amount of Hg started out in solution. Since the experimental data is representative of a solution which is saturated in $\text{Hg}^0_{(\text{aq})}$, a best fit by the simulation should give an indication of the solubility of $\text{Hg}^0_{(\text{aq})}$ within the system. The concentration of $\text{Hg}^0_{(\text{aq})}$ which gave the best fit was 43 ppb. While it is expected that this value should be similar to that obtained (45 ppb) in the study that gave the Henry's constant used,⁹ this value is also very similar to the value of 40 ppb more recently determined independently by other researchers.¹⁸

3.3.4 Modification of the simulation to detect order at the bubble interface

Another point that should be commented upon is the earlier mention of ordered molecules at the interface and their effect on the overall Hg loss rate. The computer simulation was modified so that a variable diffusion coefficient could be used in the first

10 boxes of the simulation (shown in Appendix B), thus giving a gradient of diffusion coefficients that could be manually adjusted to improve the simulation's fit to experimental data. It should be noted that the 10 μm box depth used in the simulation where much larger than that of the ordered molecules at the interface, which were suggested to be only tens of monolayers.^{15, 16} For the purposes of this study, larger box sizes should have magnified any changes to the fit. Considering that changing these values did not change the fit to the experimental data appreciably unless extreme values for D were used, no conclusion can be drawn regarding the presence of such an ordered layer. This does however indicate that any order present did not contribute significantly to the overall Hg loss decay curve. The main piece of information obtained from the simulation is that the rate limiting step for the loss of Hg is due more to the Henry's constant than the diffusion near the interface. Minor changes to the Henry's constant had considerable effects on simulation results, and would be akin to changing the solubility of Hg in solution, since the Henry's constant was obtained experimentally by other authors⁹ from $\text{Hg}_{(\text{aq})}^0$ solubility. This would indicate that the largest barrier to Hg vapor transport out of the gas phase is getting the atoms to solubilize in solution before they can diffuse into the bulk.

3.4 CONCLUSIONS

Through the observation of Hg loss from a single bubble and modeling using computer simulations, a diffusion coefficient for Hg has been determined for Hg atom through water to be $1.3 \times 10^{-5} \text{ cm}^2/\text{s}$. This value is very similar to a literature value that uses a simple equation for diffusion through liquids.¹⁴ The simulation also suggests that the solubility of $\text{Hg}_{(\text{aq})}$ in aqueous solution is 43 ppb. Because of the simplicity of this system, it should be easily applicable to other species which can be trapped in a bubble,

even molecular species, in order to solve for the solubility or diffusion coefficient if either the former or later is known.

When applying what has been shown throughout the chapter to the original problem of mass transport of atoms between many small bubbles and solution, it appears that overall mass transport between the two phases is slow because of the slow diffusion of the atoms away from the interface. Gaseous diffusion within a bubble is relatively fast, and complex interfacial order of the solvent molecules does not significantly affect transport. However, diffusion of the atomic form is slow which, when combined with its low solubility, can contribute to a long lived atomic absorption signal when other transport processes such as convection are absent. Conversely, diffusion of atoms into the gas phase can be a very slow process as well, as shown by Figure 3.6.

In a practical analytical system where one is attempting to rapidly transport solvated free metal atoms from solution into a vapor phase, a large interfacial area and small distance between any point in solution and this interface is crucial. To this end, a solution with a very high density of small bubbles would appear to be optimal.

REFERENCES

- (1) Panichev, N.; Sturgeon, R. E. *Analytical Chemistry* **1998**, *70*, 1670-1676.
- (2) Zhao, L. L.; Rochelle, G. T. *Industrial & Engineering Chemistry Research* **1998**, *37*, 380-387.
- (3) Wood, R. W. *Philosophical Magazine (1798-1977)* **1912**, *24*, 316-322.
- (4) Hatch, W. R.; Ott, W. L. *Analytical Chemistry* **1968**, *40*, 2085-2087.
- (5) Morita, H.; Mitsuhashi, T.; Sakurai, H.; Shimomura, S. *Analytica Chimica Acta* **1983**, *153*, 351-355.
- (6) Biltz, W.; Meyer, F. *Zeitschrift fuer Anorganische und Allgemeine Chemie* **1928**, *176*, 23-46.
- (7) Yu, L.-P.; Yan, X.-P. *TrAC, Trends in Analytical Chemistry* **2003**, *22*, 245-253.
- (8) Britz, D. *Digital Simulation in Electrochemistry*; Springer-Verlag: New York, 1988.
- (9) Sanemasa, I. *Bulletin of the Chemical Society of Japan* **1975**, *48*, 1795-1798.

- (10) Kreevoy, M. M.; Scher, H. B. *Journal of Physical Chemistry* **1965**, *69*, 3814-3816.
- (11) Zhao, L. L.; Rochelle, G. T. *Chemical Engineering Science* **1999**, *54*, 655-662.
- (12) Zhao, L., 1997.
- (13) Zhao, L.; Rochelle, G. T. *AIChE Journal* **1996**, *42*, 3559-3562.
- (14) Sitaraman, R.; Ibrahim, S. H.; Kuloor, N. R. *Journal of Chemical and Engineering Data* **1963**, *8*, 198-201.
- (15) Wilson, M. A.; Pohorille, A.; Pratt, L. R. *Journal of Physical Chemistry* **1987**, *91*, 4873-4878.
- (16) Shultz, M. J.; Baldelli, S.; Schnitzer, C.; Simonelli, D. *Journal of Physical Chemistry B* **2002**, *106*, 5313-5324.
- (17) Clever, H. L.; Johnson, S. A.; Derrick, M. E. *Journal of Physical and Chemical Reference Data* **1985**, *14*, 631-680.
- (18) Feng, Y.-L.; Lam, J. W.; Sturgeon, R. E. *Spectrochimica Acta, Part B: Atomic Spectroscopy* **2004**, *59B*, 667-675.

Chapter 4: Generation of an atomic absorption signal for Pd within microbubbles

4.1 INTRODUCTION

The previous chapters have explored a system using Hg vapor to study the mass transport of metal atoms through bubble interfaces. This chapter will address the application of what has been learned to the similar system containing microbubbles in solution. This chapter will also address some of the other issues in producing a CASAA signal such as generating bubbles of the correct size, procedure design and eventual signal detection.

4.1.1 Spectral properties of atoms in small bubbles

Gaseous atoms at room temperature will show different linewidth characteristics than those traditionally seen in other atomic techniques that use thermal sources for atomization. Calculation of theoretical atomic linewidths¹⁻⁴ show that at 25 °C, doppler broadening contributes only 0.4 pm to the linewidth for Ag atoms in a hydrogen atmosphere. The main contributor in this instance is collisional or pressure broadening²

$$\delta\nu_c = \frac{n\sigma_c\bar{u}}{c} \quad (1)$$

where $\delta\nu_c$ is the shift in wavenumbers, n is the number density of the perturber species (H_2), σ_c is the analyte optical collisional cross section, \bar{u} is the mean velocity and c is the speed of light. If we consider Ag in 1 atm H_2 , the pressure broadening would be 6.2 pm at 298 K, giving a total linewidth of 6.8 pm. As a basis for comparison, a graphite furnace-type environment using 1 atm Ar at 2,500 K yields a linewidth of only 2.4 pm.

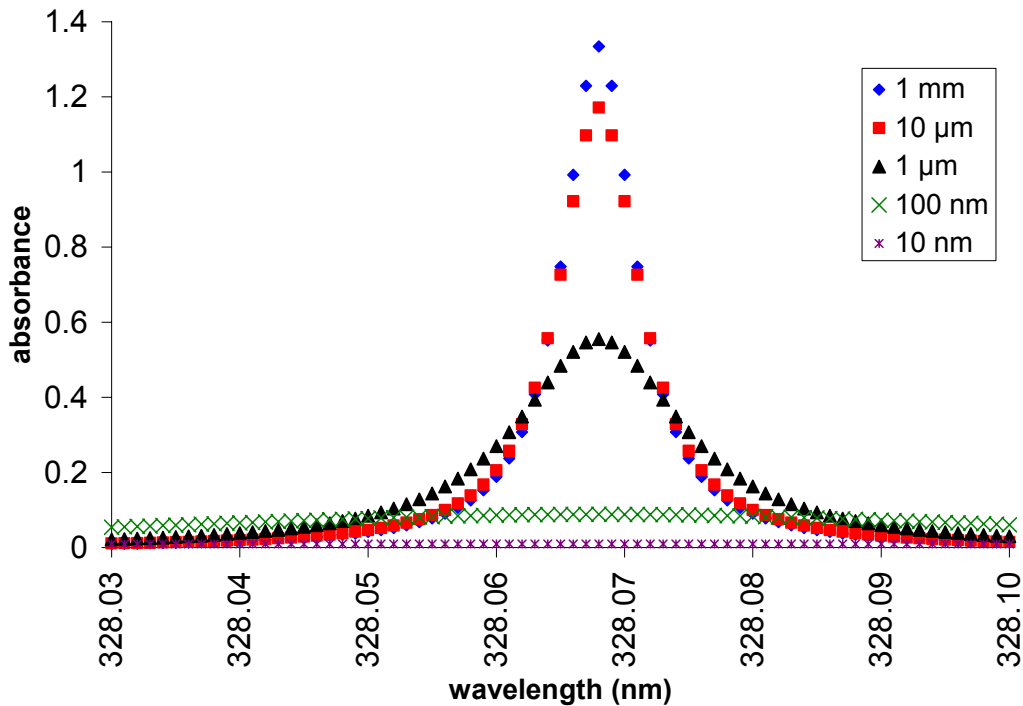
A linewidth of 6.8 pm is still less than the 11-13 pm linewidth measured by Panichev and Sturgeon.⁵ This may be the result of the pressure inside the bubbles being

greater than 1 atm, which would occur if the bubbles containing the atoms were very small. The surface tension of the surrounding solution causes an increase in the interior gas pressure according to LaPlace's Law:

$$P = \frac{2\gamma}{r} \quad (2)$$

where P is the additional pressure, γ is the surface tension of the surrounding solution (71.99 mN/m for water), and r is the radius of the bubble. Also, theoretical absorption profiles for Ag atoms can be calculated using approximations for the Voigt profile of a collisionally broadened line^{6, 7} calculated for Ag at 25 °C for various bubble sizes as shown in Figure 4.1.

Figure 4.1 Calculated absorption profiles for Ag 328.068 nm line at 25 °C



Combining equations 1 and 2 with the gas law provides a reasonable dependence of the Ag linewidth on bubble radius (expressed in m):

$$\Delta\lambda = \frac{8.8 \times 10^{-18}}{r} + 6.8 \times 10^{-12} \quad (3)$$

Bubble radii below 10 μm significantly broaden the absorption line, with 100 nm bubbles producing a width of 94 pm for Ag. If bubble size was the primary cause of the 11-13 pm Ag linewidth measured by Panichev and Sturgeon, their average bubble diameter can be estimated as ca. 4 μm .

4 μm bubbles should scatter the incident beam and may account for Panichev and Sturgeon's observed background signal. Creating smaller bubbles should reduce scatter and improve residence time by reducing bubble buoyancy; although significantly smaller bubbles could also produce an excessive amount of linewidth broadening. Thus, it seems logical to strive for bubbles in the range of $\sim 1 \mu\text{m}$ in diameter to minimize buoyancy and scatter without significantly broadening the absorbing line profile. Calculation predicts that the pressure in this size bubble would result in a ~ 14 pm linewidth for Pd.

4.1.2 Generation of microbubbles

While generation of bubbles is not difficult, creating bubbles of the correct size is challenging. The bubbles should be small enough so that they rise slowly through solution, and they must remain small, a difficult problem to solve due to collisions causing coalescence. Production of micro and nanoscale bubbles is not well understood, partially due to the difficulty of optical detection. However, Lou and coworkers were able to use atomic force microscopy (AFM) to detect bubbles as small as 20 nm in diameter formed on a mica surface.^{8, 9} The production of these bubbles was accomplished by filling a reaction cell with DI water, replacing it with an ethanol/water solution, and again replacing with DI water. The bubbles were formed due to the difference in solubility of gases within the ethanol/water and water solutions, so that when the solutions were quickly exchanged, very small bubbles were formed.

The size of the bubbles produced decreases with increasing ethanol amounts,^{8,9} to apply the procedure to this system 20% ethanol solutions will be used to generate bubbles throughout the solution. Judging from the literature, this should produce bubbles which are actually smaller than 1 μm in size; but because it is in bulk solution, coalescence should make bubble size increase. Bubble formation will be caused by the movement of the dissolved gasses from the ethanol to the water during solution mixing. The limited solubility of the gasses in aqueous solution will cause supersaturation, promoting bubble formation. While it is possible for bubbles to form in homogenous solution with no nucleation point, indications in the literature suggest that the level of supersaturation must be high, 100 times the saturation level or more.¹⁰ It is much more likely that particulates or even the reaction cell walls would act as nucleation points for bubble formation and growth.

4.2 EXPERIMENTAL DESIGN

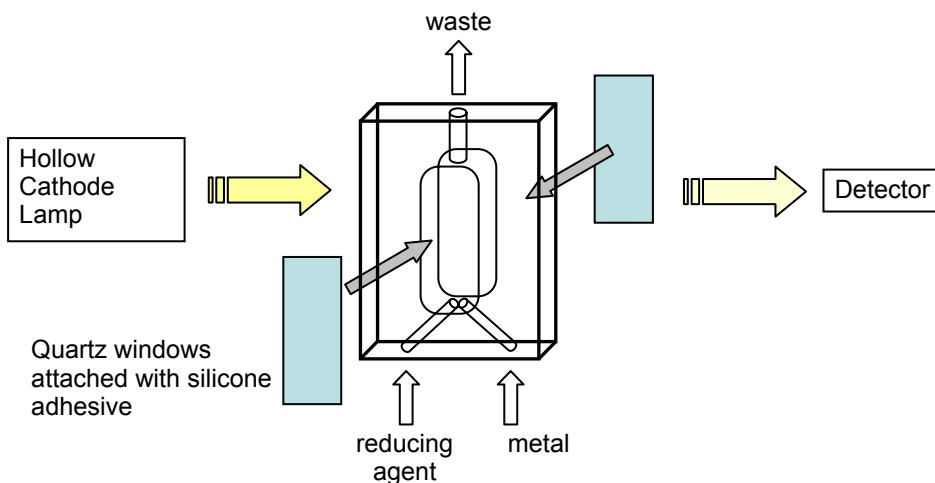
Considering that a viable procedure to generate microbubbles has been found, working reaction cell design and experimental procedure must be developed to facilitate the bubble formation as well as proper reagent mixing in order to produce atoms in solution. Furthermore, the atoms and bubbles must be generated in the same spatial area of the cell and on a time scale that allows detection.

4.2.1 Reaction cell design

Figure 4.2 shows a diagram of the original cell design taken from other authors' work.⁵ The cell is made out of plexiglass with two quartz windows made from spectrophotometric cuvetts on either side. The windows were glued to the frame using silicone adhesive. The reducing solution and metal containing solution entered the cell at

the bottom in a Y shaped configuration. Waste exited the cell at the top. The cell was mounted in the optical path of an atomic absorption spectrometer.

Figure 4.2 Schematic of initial setup for CASAA



This cell design had several problems: The Y shaped inlet at the bottom of the cell was not an easy system to reproduce. The original authors⁵ used a similar configuration, but missing details such as the angles of entry for the channels into the cell, the length of the channels and if the two channels join together before entering into the cell were all missing, possibly because the authors deemed them unimportant. Additionally, the attachment of the cell windows to the cell frame with adhesive insured that the cell could not be taken apart and reassembled reproducibly, and cell cleaning was inadequate after many experiments without disassembly. Because of this, and the fact that the original authors' procedure was not reproducible, the reaction cell was redesigned to allow more precise measurement of the physical characteristics of the reaction vessel as well as simpler replacement or addition of various cell parts.

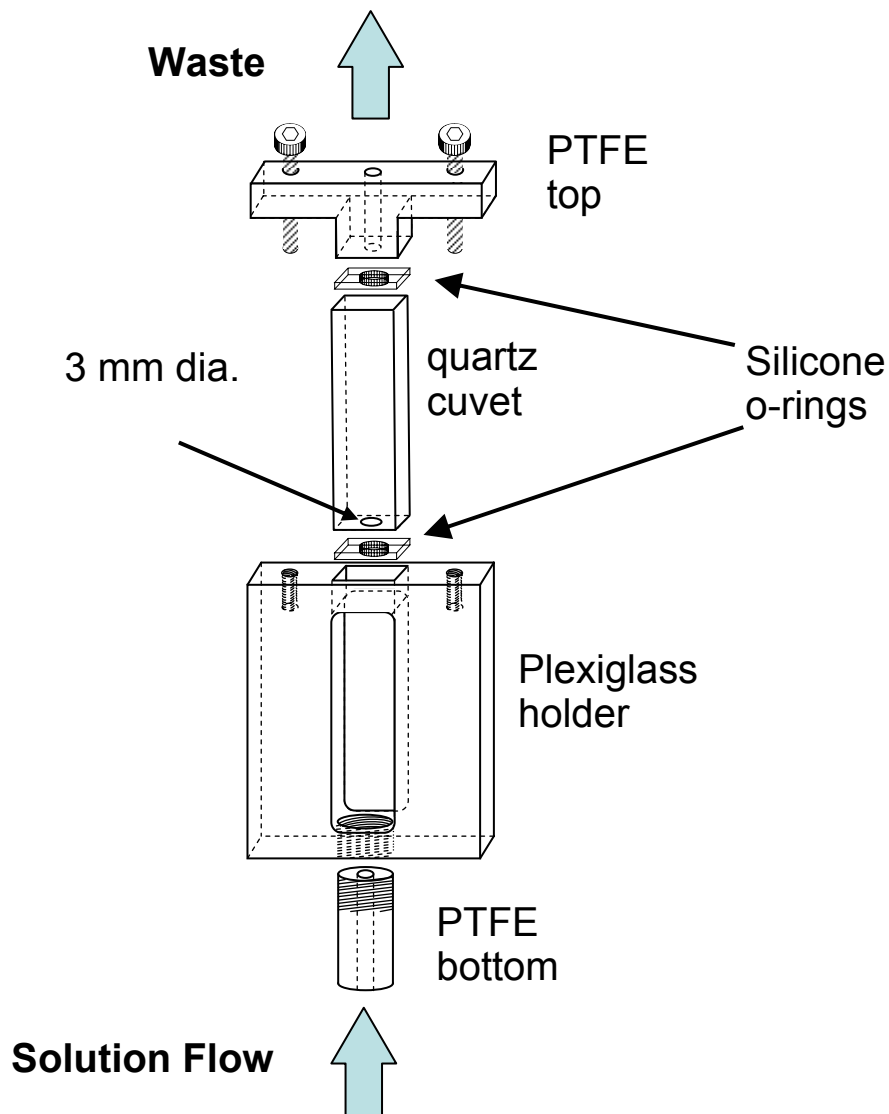


Figure 4.3 Schematic of final cell design

Due to the problems detailed above the reaction cell was redesigned completely. Figure 4.3 depicts the cell design, which is similar in its general form to that discussed previously in the literature⁵. The reaction cell is a standard 1 cm quartz cuvet (Fisher Scientific) with a lab-designed plexiglass frame which permits cell mounting in the optical path of the AA spectrometer. The cuvet fit into a plexiglass frame and had PTFE

top and bottom pieces attached to it. The plexiglass frame is shown in Figure 4.4 and the two PTFE pieces are shown in Figure 4.5.

Figure 4.4 Plexiglass frame for reaction cell. All measurements are in mm.

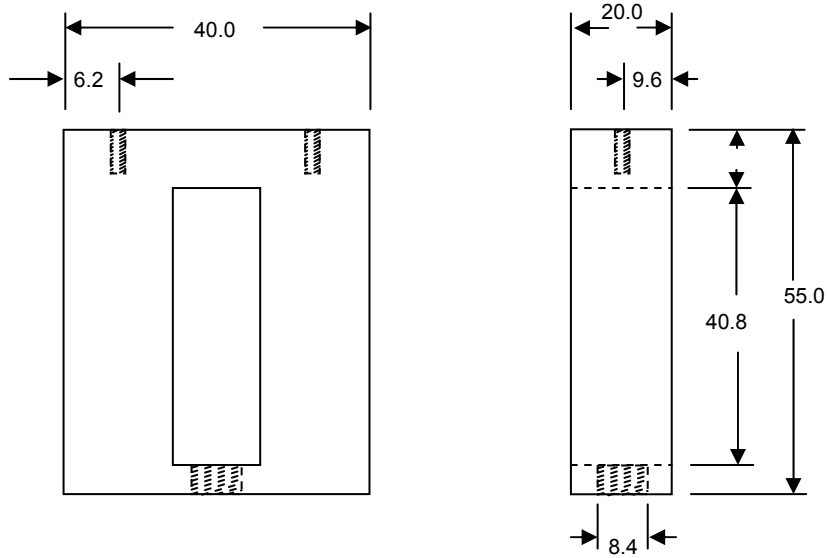
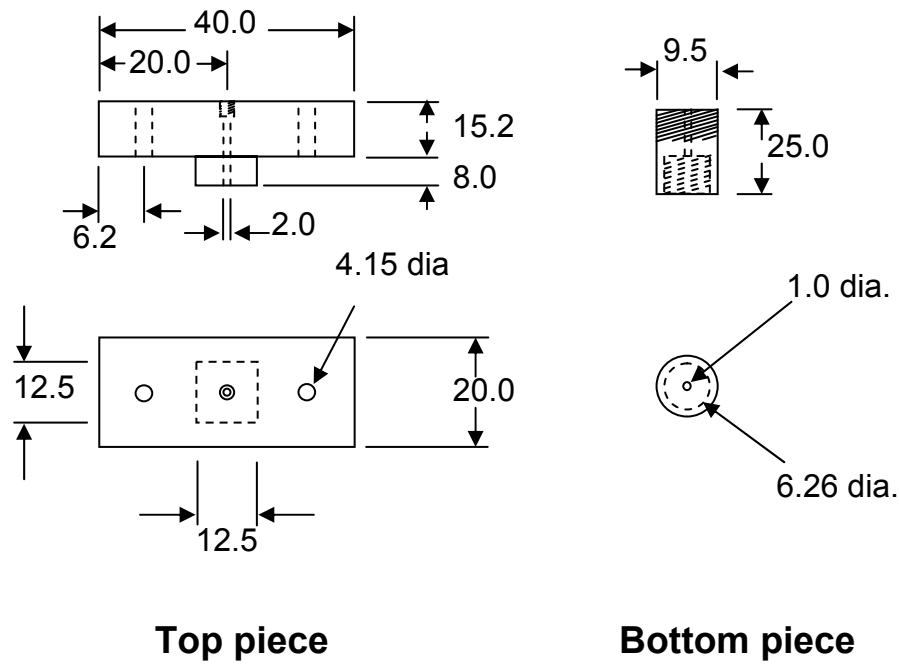


Figure 4.5 PTFE pieces for control of solution flow. All measurements are in mm.



Top piece

Bottom piece

A seal between the cuvet and plexiglass frame was made with a combination of silicone o-rings and machine screws applying pressure between the PTFE top and bottom pieces and the cell. The solution only contacted the quartz cell, PTFE pieces and o-rings.

This cell design did have some limitations. While the previous problems regarding differences in the cell properties from each reassembly after cleaning were solved, overtightening of the screws in Figure 4.3 could crush the cuvet. There was a fine line between the system being water tight and shattering the cell from the pressure. Also, the tightness of the cell dictated some of the flow patterns of the solution once it entered the cell. If the bottom o-ring was not fitted snugly against the cuvet bottom, a small chamber could remain below the entry into the cuvet where erratic mixing of solutions could occur. If care was not taken when assembling the cell, the reactions occurring within could be affected significantly. Discussion of further modifications to the cell design is found in the experimental results section.

4.2.2 Experimental procedure development

4.2.2.1 Reagents

Aqueous solutions were made using distilled, deionized water from a mixed bed ion exchange column (Barnstead Thermolyne). pH adjustment was accomplished using reagent grade sodium hydroxide (EM Science) or hydrochloric acid (Fisher Scientific). pH and temperature were monitored using a Ion 6 pH/temperature meter (Oakton). Experiments requiring reducing agents employed either sodium borohydride (Fisher Scientific) or stannous chloride (Technical Grade, Fisher Scientific). Absolute ethanol (Aaper Alcohol and Chemical Co.) and 1-propanol (Fisher Scientific) were also used in experiments.

For Pd standard solutions, a 1000 ppm Pd Standard (AA grade, Acros Organics) was diluted with 5% HCl solution. Ethanol/reductant solutions were prepared immediately before use and contained either NaBH₄ or SnCl₂. Reducing solutions containing NaBH₄ were adjusted to pH 11 using NaOH, and solutions using SnCl₂ were adjusted to pH 1 using HCl. In both cases solutions were sonicated for 3 min. 1-propanol/reducing solutions were also prepared using this method. Didodecyldimethylammonium bromide, DDAB, (98%, Aldrich) was dissolved in DI water to make a 0.05 M stock solution which was then added to Pd metal standard solution for select experiments to make the solution 0.001 M DDAB.

The choice of reducing agent was critical for the formation of atomic species in solution. Two reducing agents were considered, NaBH₄ and SnCl₂. SnCl₂ is a commonly used reducing agent for chemical vapor generation and is a stronger reducing agent than NaBH₄. Conversely, NaBH₄ has the added side effect of producing hydrogen gas in solution, as well as being used for production of metal clusters in solution.¹¹ Both reducing agents were used for cold atom generation, but NaBH₄ was primarily used because it was successful for Panichev and Sturgeon⁵ and hydrogen gas could be produced. Since bubble formation is a primary objective of this project, additional hydrogen gas would not only help initial formation of the bubbles, but also make the gaseous environment within the bubble more reducing in character.

The two reducing agents also offered the opportunity to look at cold atom generation in varying pH environments. This is because the SnCl₂ reducing solutions had to be prepared in an acidic solution (pH 1) so that the SnCl₂ salt would stay dissolved. The NaBH₄ was prepared in solution adjusted to pH 11 because lower pH values caused excessive H₂ bubble production.

Pd was chosen as the analyte for cold atom generation for two reasons: It was one of the three elements for which cold vapor atoms had already been detected, along with Cu and Ag;⁵ and among these 3 elements, Pd is the easiest to reduce.

4.2.2.2 Procedure

PTFE tubing (0.95 mm i.d, Cole Parmer) was attached to the PTFE bottom and top pieces of the reaction cell shown in Figure 4.3, and a peristaltic pump (Rainin) used to pump solution from the bottom to the top of the cell. An injection loop with volumes ranging from 100 - 500 μ L was used for the addition of the metal plug to the system. Additionally, after some of the nuances of cell design had been explored in more detail, experiments were performed with a commercially available cell designed for flow through absorption measurements (Hellma, Catalog # 130).

The cell was flushed with DI water before each run. An aqueous reducing solution containing 20% ethanol (or in some cases 30% 1-propanol) was then pumped through the cell at 17.1 mL/min for 1 minute. The injection loop was loaded with the metal solution and which was then injected into the flow system. DI water was then added at a flow rate of 1.5 mL/min. The flow patterns in the reaction cell can be visualized using a red dye (Direct red 81, Sigma) in the analyte plug volume (Figure 4.6). The pump rate was maintained throughout the continuous flow experiments. In some experiments, solution flow was stopped once the absorbing layer was in the optical path.

The D₂ lamp and Pd HCL were aligned so that they passed through the same volume within the cell to insure that background correction was occurring in the same spatial location in the cell. A more complete procedure detailing how the lamps were aligned can be found in Appendix C. The atomic absorption signal was monitored 22 mm above the bottom of the cell.

Figure 4.6 Illustration of flow patterns within reaction cell using dye. Picture denote 30, 70, and 110 s after plug entry into cell. Solution flow proceeds from bottom to top of the cell.



4.3 EXPERIMENTAL RESULTS

4.3.1 Initial CASAA signal detection

Figure 4.7 shows the absorbance signal obtained using the procedure described above. The reaction cell initially contains a reducing solution made up in 20% ethanol. After the metal plug enters the flow system, but before entry into the reaction cell, both the atomic and background signals remain low since the analyte has not yet entered the homogeneous, 20% ethanol solution. Figure 4.7 shows a small spike (~80 s) in the background absorbance signal, indicating entrance of the metal plug. This spike could result from scatter by large bubbles created at the ethanol/reductant - acidified DI water/analyte interface passing quickly through the observation zone.

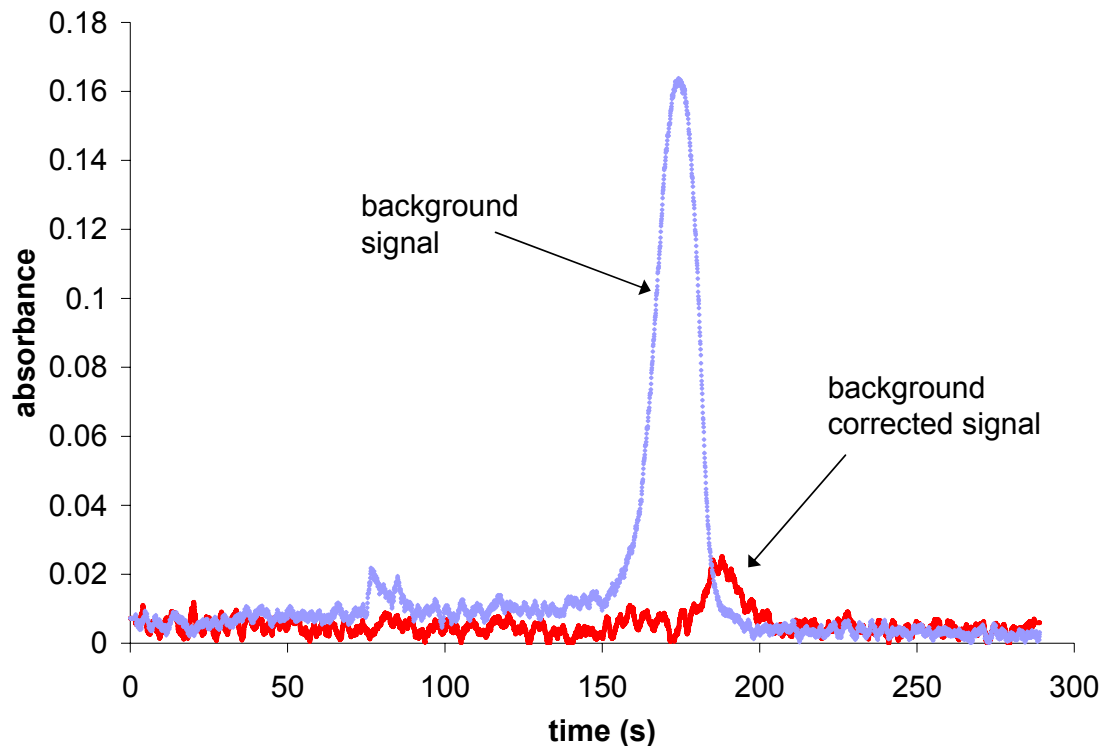


Figure 4.7 CASAA signal for 500 μL of 20 ppm Pd and using 20% ethanol and 0.1% NaBH_4

The metal plug enters the cell, disperses at the bottom of the to fill the full cross section of the cuvet and flows upward relatively undisturbed with the exception of the aforementioned bubbles mixing the solution slightly. Validation of this flow pattern was confirmed visually using a dye in place of the metal plug. Some mixing does occur because the aqueous analyte-containing plug is followed by ethanol/reducing solution (~1 mL) as a result of using the injection loop for sample introduction. Density differences cause the ethanol/reducing solution to pass through the metal plug, which sponsors analyte exposure to the reducing agent and likely contributes to bubble formation from the mixing of the acidified metal plug and ethanol solution. This flow pattern and perhaps some larger bubble formation provide mixing that transports some metal into the bulk of

the ethanol/reducing solution. This results in an atomic absorption peak signal coincident with the front edge of the background peak. This peak lacks reproducibility except at higher concentrations of reducing agent ($>0.5\%$ NaBH_4) or with use of SnCl_2 in place of NaBH_4 . The useful atomic absorption signal peak typically occurs on the trailing edge of the background peak as shown in Figure 4.7.

The background signal increases with increasing Pd concentration, and the absence of a significant background during blank runs suggests contributions to the background peak from broadband absorption from molecular species or nucleating Pd. It must be noted that the traces in Figure 4.7 were collected sequentially since the instrument used will not output the background corrected signal and background simultaneously to the computer data collection hardware.

The appearance time of the background peak in Figure 4.7 would indicate that a large part of the metal plug passes by the observation zone before any atoms are detected. Measuring the linear flow rate of the atoms as 1.41 cm/min and taking into account the height of the spectrometer entrance slit, the absorbing region is 3.1 mm (FWHM). Considering the combination of the background and signal peaks, a thickness of 6.8 mm is calculated for the entire metal plug. An undisturbed $500\text{ }\mu\text{L}$ sample plug would be 5 mm wide, which suggests some mixing and/or broadening because of slower solution flow along the walls of the reaction cell. Therefore, the large background peak could be due to metal species carried into the bulk of the ethanol/reducing solution after which reduction and nucleation occur. Atomic signal peaks only occur on the sides of this peak, because high metal concentration fosters the competing process of nucleation, thereby reducing the number of free atoms in solution. Because of this, the bubble density must be high enough within the solution so Pd atoms can diffuse to a bubble before competing reactions can occur.

4.3.2 Signal analysis

4.3.2.1 Signal diagnostics

The background-corrected blank shown in Figure 4.8 gives no absorption peak, although there appears to be a slight negative fluctuation in the signal where the absorption peak would normally appear. This could be due to refractive index gradients within the solution that cause divergence of the D₂ and HCL optical beams since perfect alignment of two separate sources is not possible in spite of the alignment precautions taken.

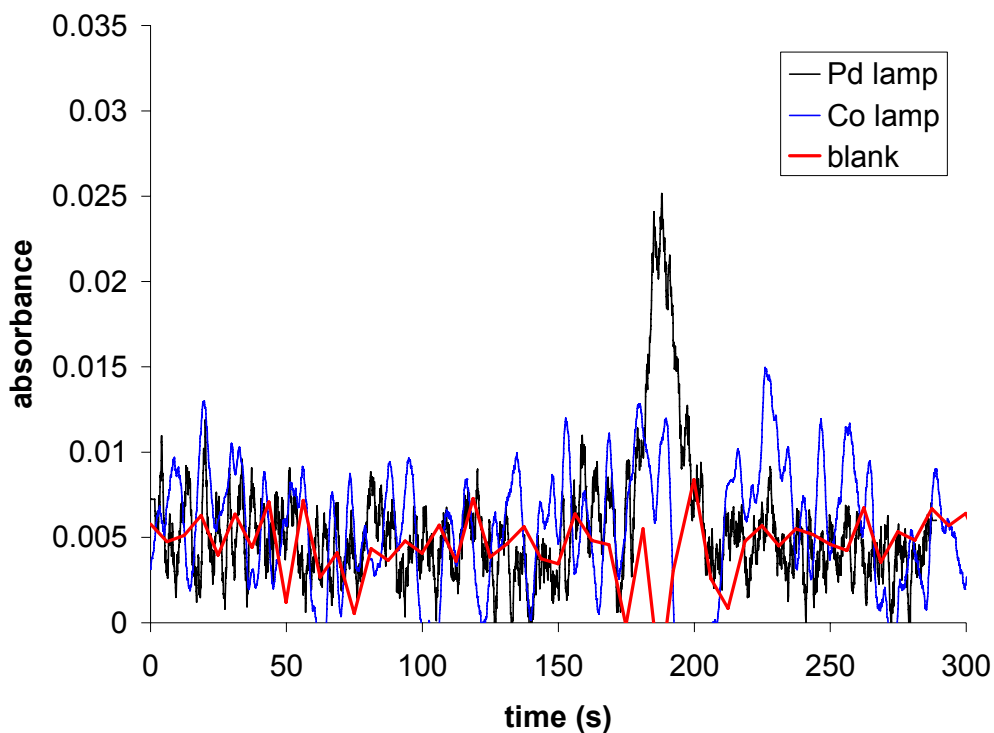


Figure 4.8 Signal obtained for blank and 20 ppm Pd using 340.45 nm Pd line and 346.58 nm Co line 0.1% NaBH₄/20% ethanol reducing solution and 500 μ L injection volumes were used.

To confirm that the signal obtained is from atomic Pd, the experimental parameters used to produce the atomic absorption signal in Figure 4.8 were used while HCL lines near the Pd resonance line at 340.45 nm, i.e., Co line at 340.51, 346.58 nm and the Ni line at 351.51 nm (not shown). The background corrected signal showed no peak, but the background was identical to the run using 20 ppm Pd and the Pd 340.5 nm line. This is indicative of an atomic Pd signal rather than scatter or broadband absorption by molecular species.

One last experiment was performed because of the difficulty in observing a blank signal which did not have memory effects from previous Pd sample runs. The effluent from the reaction cell was examined by inductively coupled plasma mass spectrometry (ICP-MS) analysis using a GBC Scientific Optimass 8000 in order to determine if Pd metal was remaining in the reaction cell after sample runs. The experiment used to generate the CASAA signal in Figure 4.7 was performed several times and is shown in Figure 4.9 with the monitoring of $^{108}\text{Pd}^+$ as well as $^{80}\text{ArAr}^+$ to give an idea of the plasma stability.

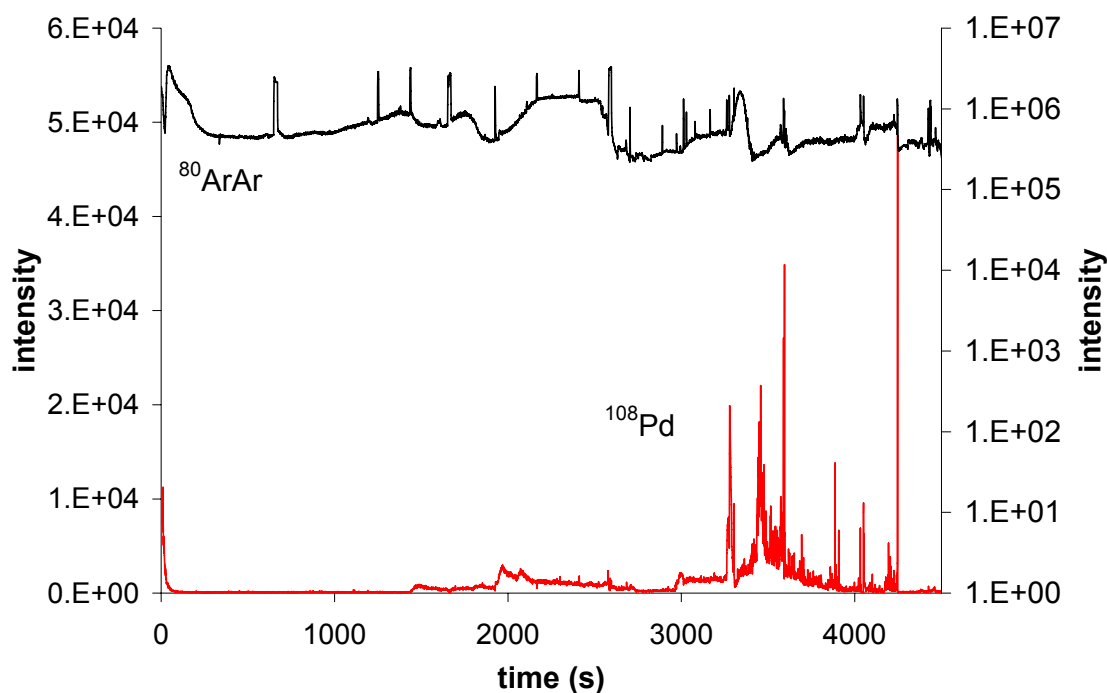


Figure 4.9 ICP-MS data for Pd^+ and Ar_2^+ (right y-axis) for procedure to produce CASAA signal. Large peak at 3500 s occurred from bubbles in reaction cell effluent, suggesting Pd is resident within the bubbles. 20 ppm Pd, 0.1% NaBH_4 /20% ethanol reducing solution, and 500 μL injection volume were used.

The procedure was performed the first time at ~ 1500 s. A small peak occurs as Pd is sent into the system. This signal decreases, but does not go to zero over 500 s. At ~ 2000 s the procedure was performed again in an acidic environment, causing minor bubble formation on reaction cell walls and giving a larger peak as the Pd from both runs gives a cumulative signal. At ~ 2600 s 1% HNO_3 is pumped through the cell and the resulting signal decrease can be seen. The procedure is performed one more time at ~ 3000 s and while a peak appears, the more significant effect is a large amount of additional bubble formation on cell walls due to the acid already in the cell reacting with the NaBH_4 reductant to form H_2 . The large signal from 3300 to 3700 s resulted from

these bubbles moving out of the cell as it was agitated by hand. The large Pd signal coincides with the exit of these bubbles out of the reaction cell. Figure 4.9 also shows from the Ar dimer signal that fluctuations in the plasma could have contributed to a false increase in the Pd intensity. The sharp plasma fluctuations were from large bubbles put into the system intentionally to determine when effluent from a particular experiment reached the plasma. The large Pd signal does coincide with a significant plasma perturbation, but other perturbations occurring before this suggest that the Pd signal obtained is accurate, and that Pd is indeed held within bubbles. The ICP is able to atomize and ionize Pd independent of the form it is in, so while the experiment detailed above cannot confirm that atoms were created, it is able to show the difficulty in cleaning the reaction cell between runs and that the Pd seems to be contained within bubbles in the system. The surprising stability of the atomic species within solution is implied by the studies involving delayed sparging of solutions containing Cd and Hg¹² as well as Rh, Pd, Au, and Cu¹³. Memory effects encountered in the CASAA generation experiments appear to be caused by the difficulty in cleansing the reaction cell of Pd species sequestered in bubbles attached to reaction cell surfaces.

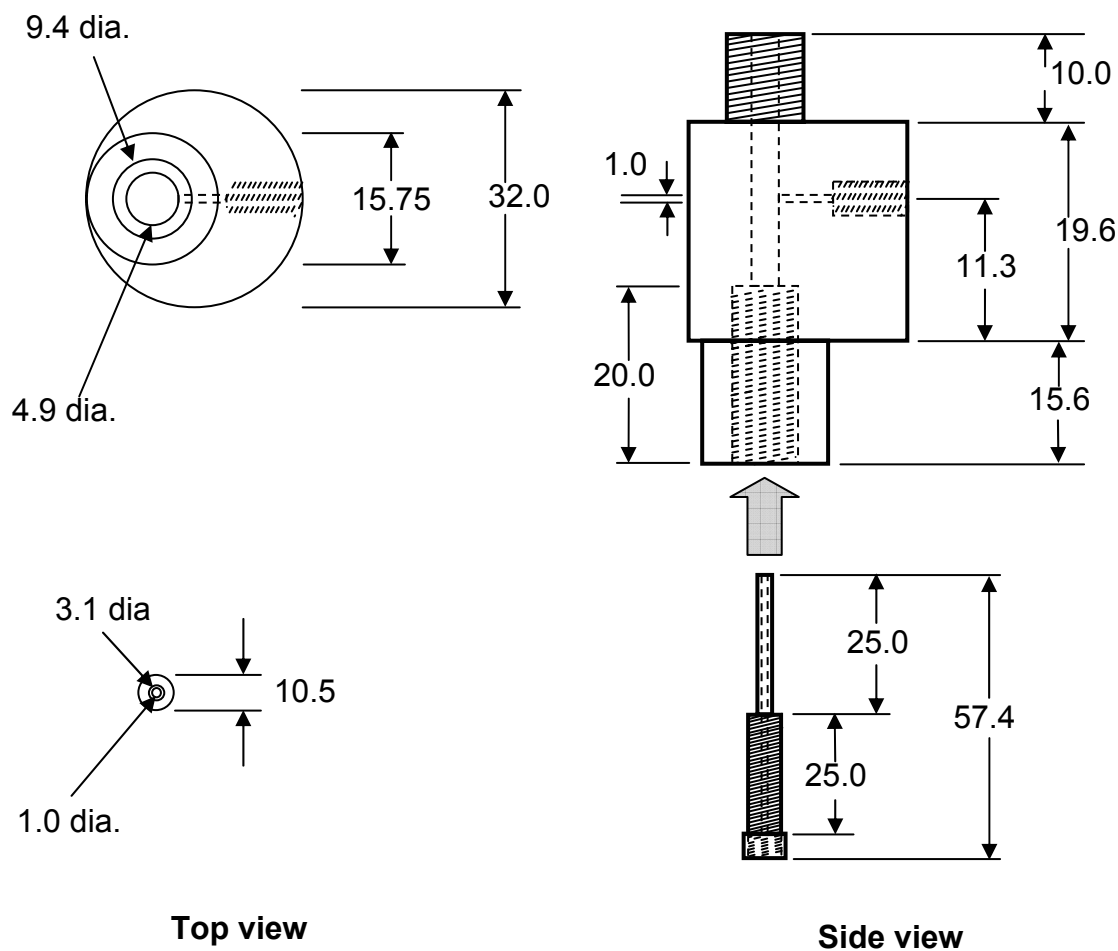
4.3.3 Parameters leading to signal enhancement

Figures 4.7 and 4.8 show that while the CASAA is well above the blank it is not very intense, even for considerable amounts of metal added to the system (10 µg). It would be useful to examine which parameters might lead to CASAA signal enhancement including changing the reagents to generate the bubbles, reducing agents, or the geometry of the reaction cell.

4.3.3.1 Other reaction cell designs

While the reaction cell displayed in the experimental section was used to collect the data presented in this chapter, several other designs were evaluated. Because the cell consisted of many detachable pieces, only the bottom PTFE piece needed to be replaced in order to accomplish this. The first design is shown in Figure 4.10.

Figure 4.10 Design of PTFE bottom piece to control solution flow into reaction cell. All measurements are in mm.



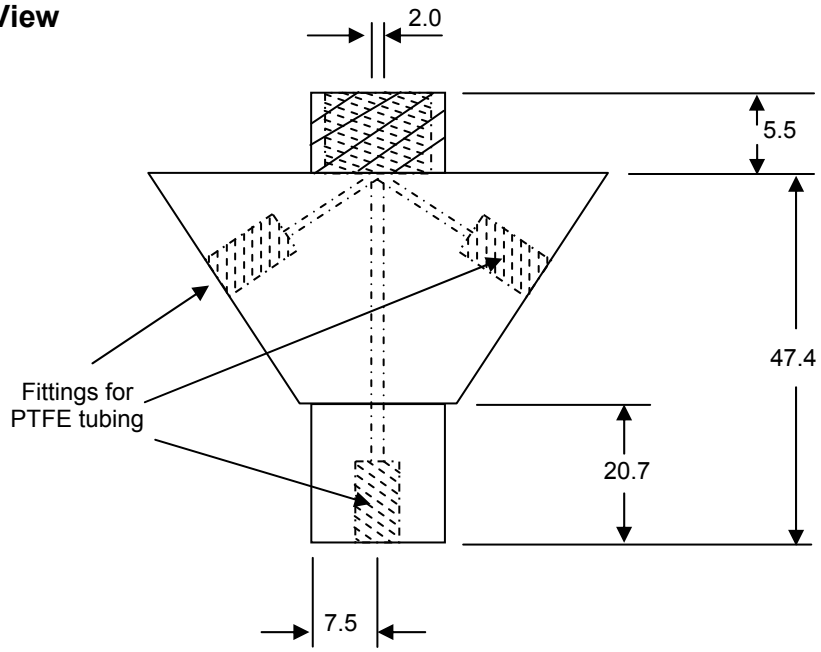
This design consisted of two PTFE pieces, with tubing from a pump attached to each one. This allowed solution flow from two different reagent containers

simultaneously in a concentric configuration and control of the distance between where the solution flows were combined and entry into the cell. The solution flow appeared to be more erratic and turbulent when the two solution flows met a large distance (>1 cm) below opening at the bottom of the cell. This resulted in the absence of any CASAA signal. Optimal performance occurred when the two solution flows met right at the bottom of the cell or if only one solution inlet were used. This led to the simpler design of the PTFE bottom piece shown in the experimental section.

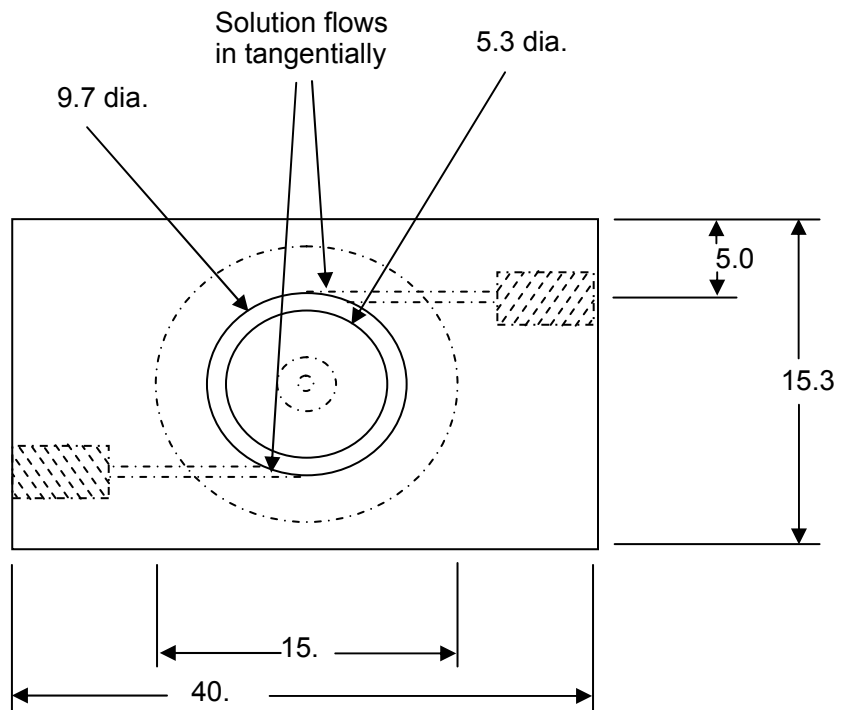
While the above discussion indicated that turbulence within the cell would impede the production of a CASAA signal, one more design was tested which intentionally caused solution turbulence. This design is shown in Figure 4.11. The design shown allowed for up to three different solutions to be pumped into the cell simultaneously. One inlet consisted of an undisturbed path straight into the cell while the other two inlets fostered mixing. The two inlets entered at an angle (60°) and joined the center channel tangentially. Furthermore, screw threading was added on the inside of the PTFE piece to further foster tangential mixing. This greatly increased the turbulence within the cell, but unfortunately impeded the production of any signal.

Figure 4.11 Schematic for cell bottom piece which fosters turbulence

Side View



Top View



4.3.3.2 Use of a commercially available cell design

In the interest of improving a weakness of the original experiment, reproducibility between different laboratories, a commercially available cell (Hellma, Catalog #130) was used to replace the custom built cell in the observation zone of the spectrometer. This was attempted in order to account for any small imperfections in the custom setup which might be contribute to the discussed signal. The cell was simply placed in the plexiglass frame and attached directly to Tygon tubing without the use of the PTFE pieces. The commercially available cell gave an atomic signal and background signal which were virtually identical to the custom built cell.

4.3.3.3 Metal concentration

Under the conditions discussed so far, Pd metal solutions produced a CASAA peak area with minimal linear correlation with Pd concentration for the reducing agents used, except perhaps SnCl_2 (Figure 4.12). The results using SnCl_2 reductant were counterintuitive since the signal peak area decreased exponentially with increasing metal concentration. A high background signal that increased with Pd concentration also reduced the transmitted light level to the point of producing an erroneous negative absorbance signals. In the case of NaBH_4 , it appeared that the peak area measurements were affected by Pd particle formation in solution as the peak area was significant above the blank, but remained relatively constant as the metal concentration increased. As the concentration of NaBH_4 was raised from 0.1% to 0.5%, an increase in the integrated signal was also observed. Figure 4.12 shows that this was the case even though maximum peak intensity for 0.5% NaBH_4 was identical to 0.1% NaBH_4 . The higher concentration of reducing agent fostered multiple peaks, typically with a second peak appearing on the rising edge of the background peak shown in Figure 4.7.

The lack of dependence of the signal on concentration for all reducing solutions shown in Figure 4.12 may indicate that a low bubble density in the system cannot contain the atoms produced because of transport limitations and/or homonucleation within the bubble. The pH is high enough that significant hydroxide precipitate formation should occur, but decreasing the pH of a solution when using NaBH_4 obscures the atomic absorption signal due to the copious amounts of H_2 gas produced. Lowering the pH with SnCl_2 results in erratic behavior of the absorption peak with changing concentration, and at high pH values using NaBH_4 , it is possible that the formation of the hydroxide precipitate is somehow beneficial to the atom formation process, but it must not be pivotal since a signal can be detected using SnCl_2 at a low pH. The authors who saw the atomic signal in solution previously were also working with a NaBH_4 solution at pH 11-12.⁵

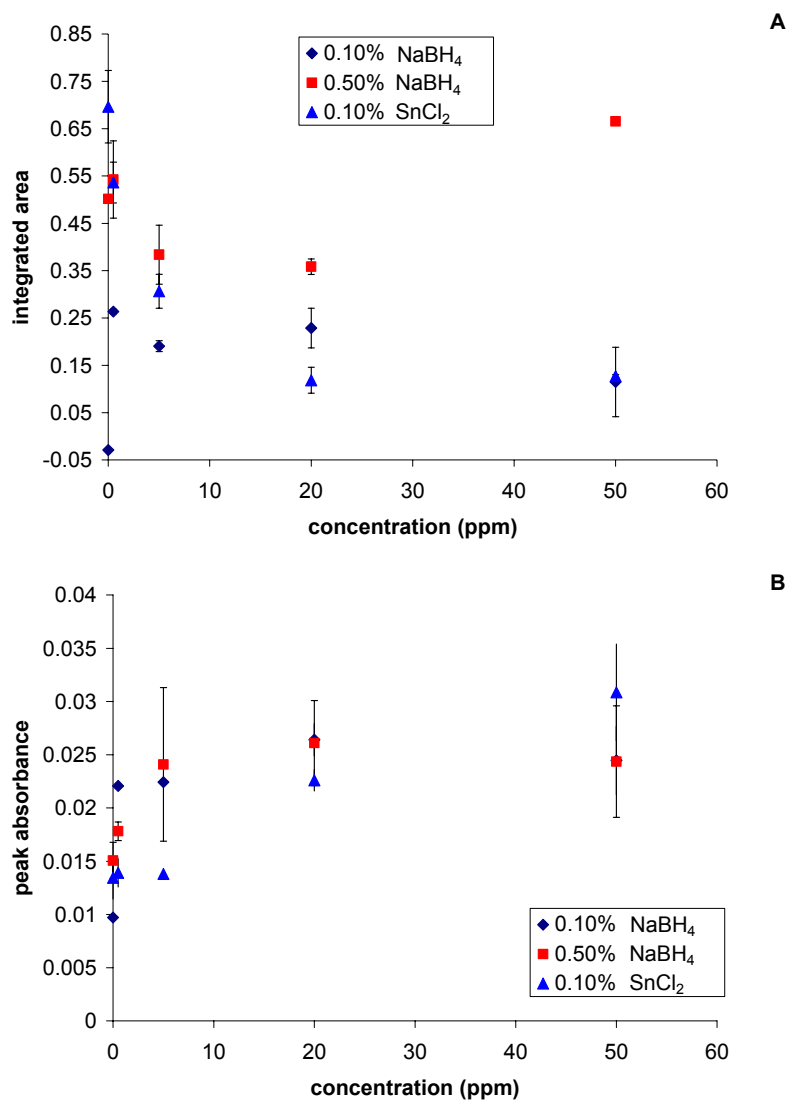


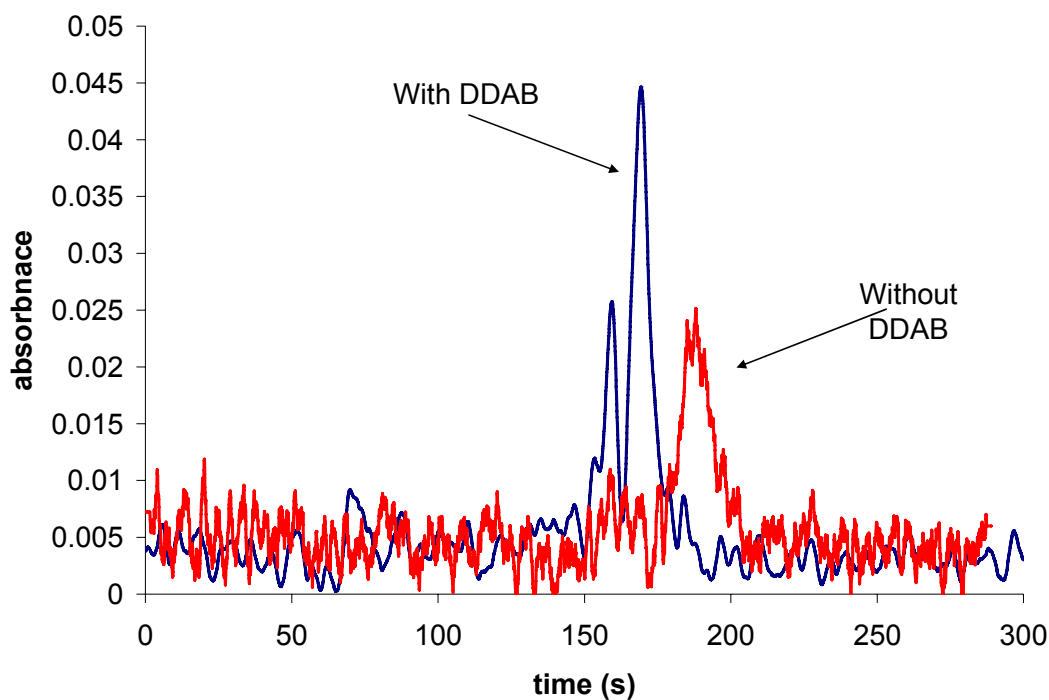
Figure 4.12 Calibration curve for Pd using a) integrated peak area and b) peak height
0.1% NaBH₄/20% ethanol reducing solution and a 500 μ L injection volume
were used

4.3.3.4 Addition of surfactant

DDAB has been used successfully in the literature to stabilize other chemical species in chemical vapor generation for signal enhancement.¹⁴ In this system, addition of 0.001 M DDAB produced a larger background, complex peak shape (i.e., multiple

peaks), and the peak signal intensity was enhanced by 50% (Figure 4.13), although probably not for the same reasons postulated by San-Medel et al in their study of cold vapor Cd production (i.e. formation of vesicles for stabilization of a hydride species¹⁴). In the present study DDAB likely lowers the surface tension of the solution making bubble generation easier. From earlier discussions, this could reduce broadening of the absorption line profile, giving a higher maximum absorbance value. DDAB molecules may also sterically hinder Pd metal cluster formation within solution, therefore providing more time for diffusion of atomic Pd to the bubble interface.

Figure 4.13 Signal enhancement from the addition of 0.001 M DDAB to 20 ppm Pd solution and using 0.1% NaBH₄/20% ethanol reducing solution and 500 μL injection volume.



4.3.3.5 Injection loop volume

The injected volume of metal (500 μL) using the procedure thus far has been significantly larger than that used by previous authors (7.5-30 μL),⁵ so the effect of using smaller injection loop sizes was investigated. The injection loop volume was varied from 100 to 500 μL and the results from monitoring the background and background corrected signals are shown in Figure 4.14. It is obvious from this that the CASAA signal is not changing over the range of injection volumes used. This would indicate that there is an excess of metal added to the system in the case of the 500 μL injection volume used in previous sections, and perhaps even in the 100 μL volume used in this study. However, the minimum volume for the experimental setup used was limited by the comparatively large volume of the injection loop itself and the parts used to attach it to the flow system. The increasing background signal with injection loop volume is indicative of higher amounts of molecular species forming with the higher amount of metal added to the system. The two possibilities which present themselves are that there are limitations related to the atom generation or bubble generation processes. The use of 0.5% NaBH_4 within this system was an attempt to insure the solution had enough reducing power to accommodate all the analyte ions when larger injection loop volumes are used. Figure 4.12 showed the signal enhancement occurring when higher concentrations of NaBH_4 solution were used, however further increases in concentration of reducing agent showed no additional enhancement, suggesting that the limitation observed in Figure 4.14 is caused by low bubble density within solution. If the reducing agent concentration is not limiting the signal, a higher metal ion concentration within solution could be fostering reactions which compete with atom formation, such as nucleation. Increasing the bubble density within the reaction cell becomes critical if the slow transport of elemental species must compete with these reactions.

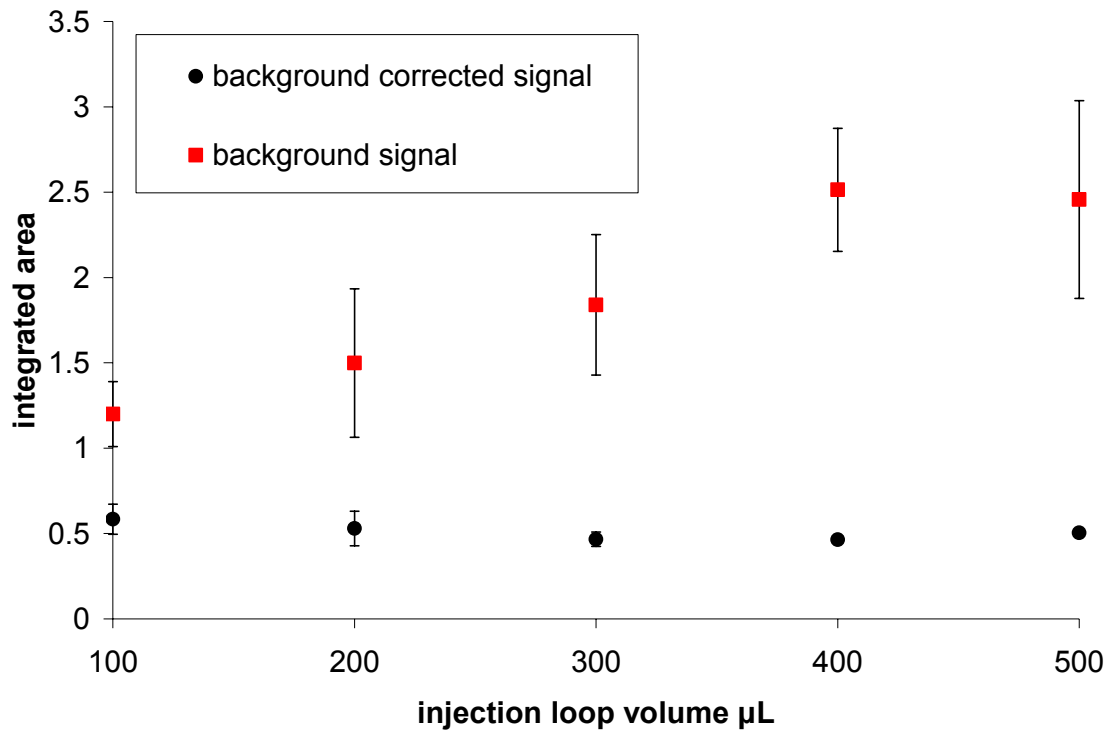


Figure 4.14 Integrated signal for 20 ppm Pd solution and 0.5% NaBH₄/20% ethanol reducing solution with changing injection loop volume

4.3.3.6 Stop flow experiments

Figure 4.15 shows the normalized absorbance signal obtained as a result of stopping the flow in the system once the metal plug was in the optical path. The pump was stopped when the metal plug was near the observation zone, and a micrometer driven translation stage moved the cell to the maximum atomic signal. The signal persisted for a long time (~5000 s) with a slow linear decay. The location of the maximum absorbance signal changed over time, as a likely consequence of the bubbles movement due to buoyant forces.

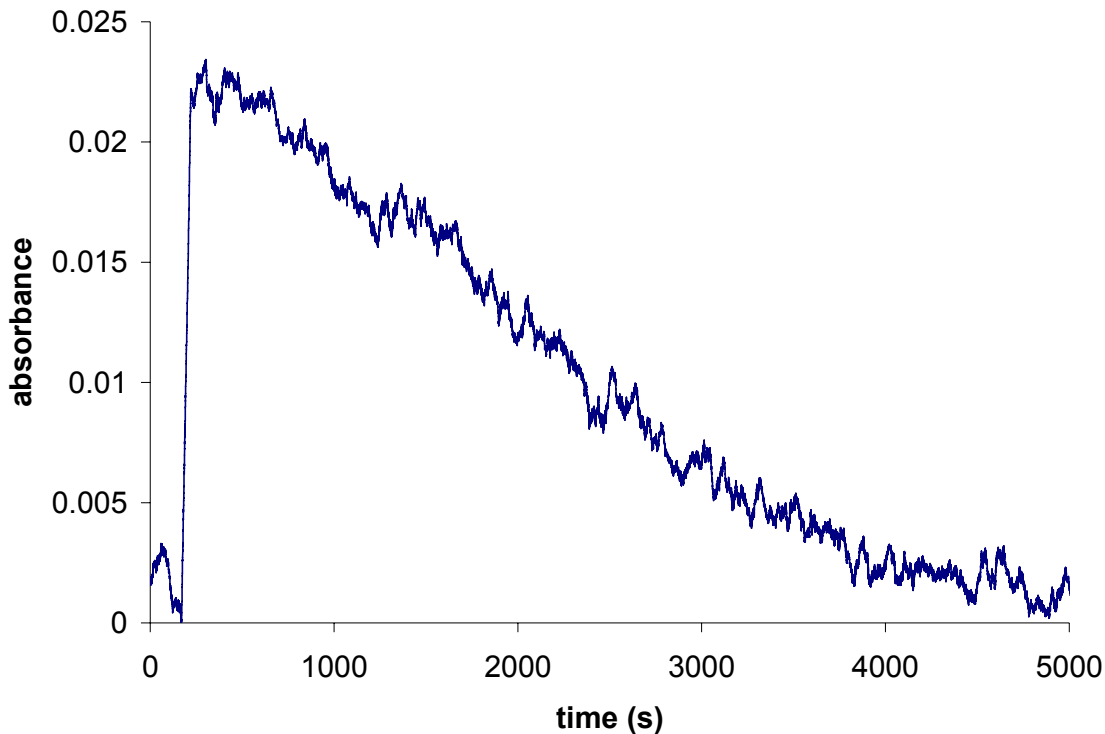


Figure 4.15 CASAA signal resulting from 100 μ L of 5 ppm Pd and using 0.1% SnCl₂/20% ethanol reducing solution if pump is stopped after atoms enter observation zone.

The cell was allowed to sit undisturbed for a period of time while the bubbles moved upward through the cell, and the new location of the maximum atomic signal and the delay time was used to estimate the bubble size because of their buoyancy. In this cell, with a 100 μ L injection volume of 5 ppm Pd and 0.1% SnCl₂ in 20% ethanol, the signal maximum moved 4.0 mm in 5900 s. This is an average velocity of 0.7 μ m/s allows bubble diameters to be calculated using the Navier-Stokes equation.¹⁵ For an air/water system, the average bubble diameter is calculated to be 800 nm. SnCl₂ was used as a reducing agent instead of NaBH₄ so that only bubbles emanating from the supersaturated air-water system could be considered, and so that bubble generation would be minimal after the solution flow had been stopped.

4.3.3.7 Signal integration

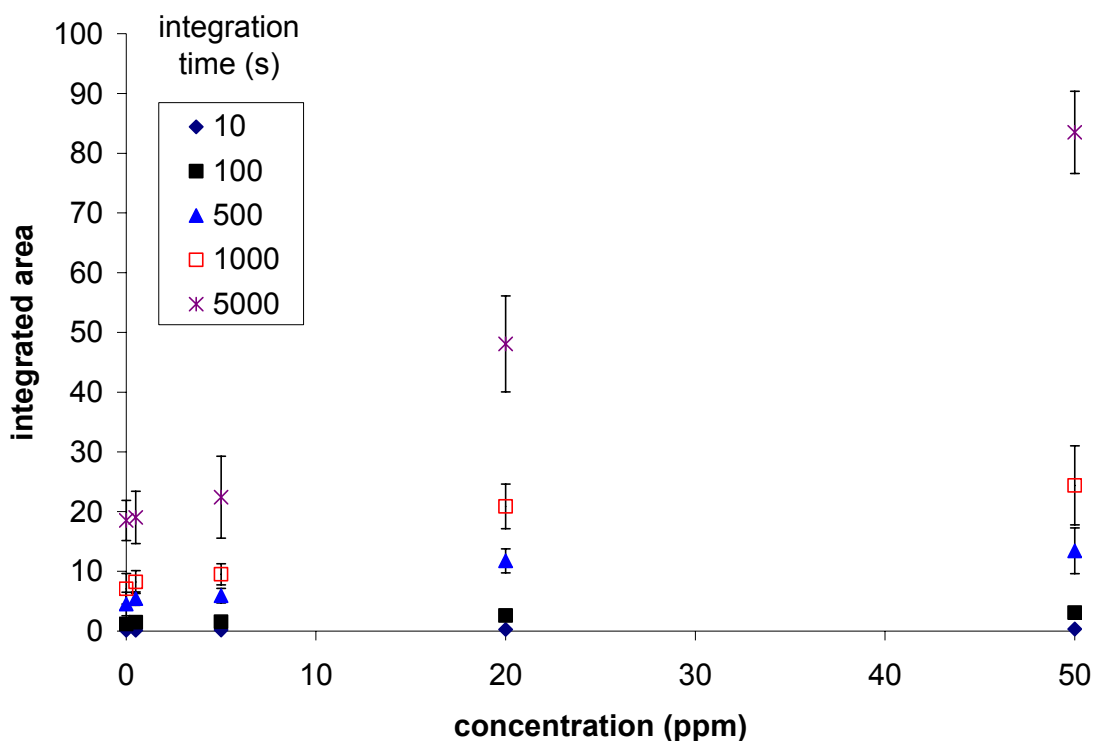


Figure 4.16 Calibration curve using integrated signal for different integration times using 0.1% NaBH₄/20% ethanol reducing solution and 100 μ L injection volume.

Many simple methods which would generate a higher bubble density such as raising the ethanol percentage would also change other important parameters such as bubble size, as well as leading to significant refractive index changes complicating signal observation and analysis. One way to get around the problem is to change the way the system is observed rather than changing the system itself. The decaying signal could be integrated over time with the pump stopped, rather than looking at absorbance only as the analyte is pumped through the cell. This might increase the efficiency of the detection scheme, as the residence time of the atomic species and bubbles within the observation zone is no longer a constraint. The CASAA signal was integrated 10 s, 100 s, 500 s,

1000 s, and 5000 s after halting the solution flow (Figure 4.16). For each of the integration times, a linear response was obtained for concentrations ranging 1 - 50 ppm giving sensitivity increases with larger integration times, but detection below 1 ppm was difficult because of the magnitude and precision of the integrated signal from the blank. While the results are not ideal, some correlation between Pd concentration and signal is present, an improvement over the flow experiments previously discussed.

Figure 4.17 shows the normalized data set for the signal for 3 different concentrations of Pd, all of which exhibit similar decay profiles. Results of Monte Carlo simulations (Figure 4.17) suggest that diffusion of the Pd metal ions throughout the cuvet plays a dominant role in affecting the shape and length of the decay. In this stochastic approach it has been shown that diffusion of a particle can be represented by the equation:¹⁶

$$\Delta d_i = R_{g_i} (2D_{T_i} \Delta t)^{1/2} \quad (4)$$

where R_{g_i} is a random number from a Gaussian distribution, D_{T_i} is the temperature dependent diffusion coefficient, and Δt is time increment used in the simulation. This equation gives the movements of a particle for each dimension within a multidimensional system. The parameters used in the simulation are shown in Table 4.1 and Visual Basic code for the simulation is given in Appendix B.

Table 4.1 Parameters used for Monte Carlo simulation of Pd particle diffusion in reaction cell

Parameter	Value
D_{Pd}	$2.0 \times 10^{-5} \text{ cm}^2/\text{s};$
	$8.3 \times 10^{-5} \text{ cm}^2/\text{s}$
Temperature	298.15 K

Δt	0.1 s
Total time	10,000 s
Starting metal plug width	0.5 cm
Reaction cell size	10 mm x 10 mm x 30 mm

Initially, $D_{Ti} = 8.30 \times 10^{-5} \text{ cm}^2/\text{s}$ was used since this is the observed value for Pd^{2+} species through aqueous solution. {Uemoto, 2000 #107 Because the diffusion might be affected by the ethanol present, and Pd atom diffusion might be slower because of an altered solvation sphere; the results were also evaluated using $D_{Ti} = 2.00 \times 10^{-5} \text{ cm}^2/\text{s}$.

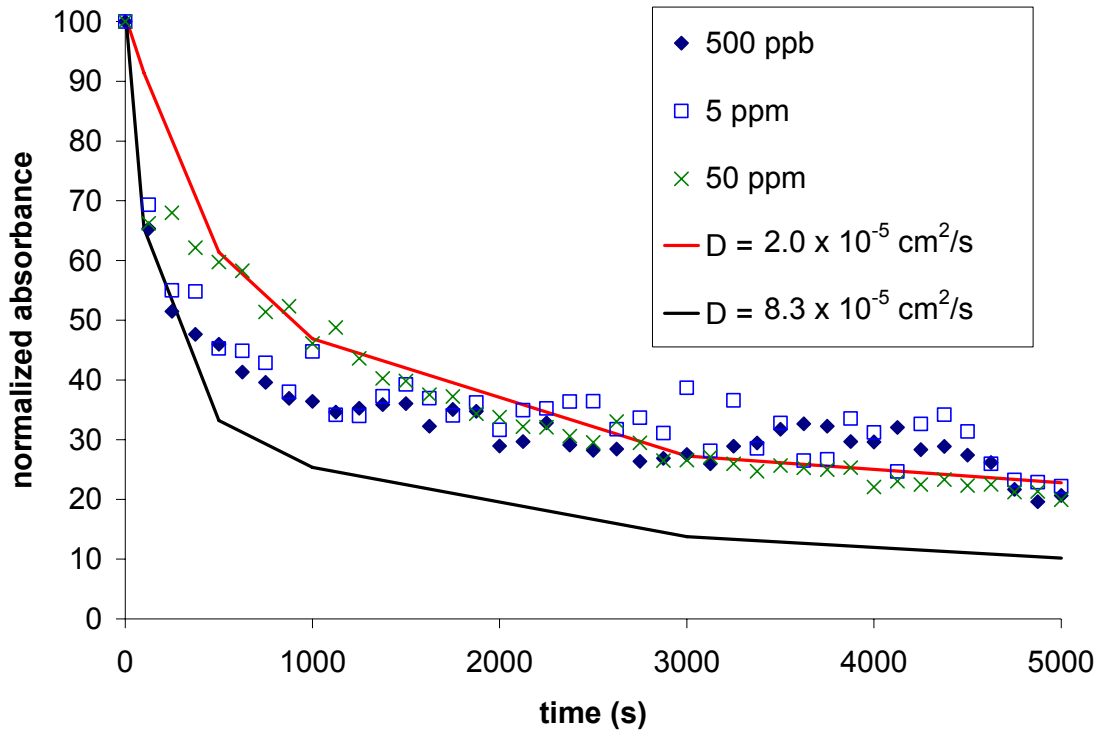


Figure 4.17 Comparison of Monte Carlo simulation results to experimental data using different concentrations of Pd and 0.1% NaBH₄/20% ethanol reducing solution and 100 μ L injection volume.

Nucleation leading to Pd particle formation in solution could also contribute to the signal decay modeled above. While studies have been conducted on Pd cluster formation, {Michaelis, 1992 #160} little information is available regarding the kinetics of the disappearance of atomic species, especially at the low metal concentrations of interest. Further study may show that metal cluster formation contributes significantly to the decay of the atomic species, but this is presently beyond the scope of our discussion.

It is obvious from Figure 4.17 that while not giving a perfect fit, the relatively simple simulation models the decay of the atomic Pd signal quite well. Thus, it is reasonable to assume that spatial dispersion and the subsequent decrease in signal within the cell might be attributable to diffusion rates of Pd.

4.3.3.8 Detection efficiency

Given the bubble size calculated above, the peak absorbance and absolute mass added to the system, it is possible to calculate the percentage of atoms added to the system which were detected, *viz.*, *detection efficiency*. Atomic line broadening equations^{1,7} show that the absorbance signal intensity due to pressure broadening inside a 800 nm bubble is reduced relative to signals measured at 1 atm by a factor of 4.5. Using the attenuation of the oscillator strength of the broadened absorption profile, the characteristic mass of Pd for GFAAS (40 pg)¹⁷ and the signal resulting from 50 ng Pd used in the CASAA experiment, it is estimated that ~0.2% of the sample added was detected for a 100 μ L injection volume of 500 ppb Pd.

Since attenuation from line broadening was accounted for, the procedure used to generate the atomic signal has much room for improvement and a few crucial variables could greatly improve the intensity of the CASAA signal. The factor of primary concern at this time is the low bubble density within solution. Atoms generated by the reducing agent are either converted to molecular species before reaching a bubble or are not able to reach a bubble before physically passing out of the observation zone of the spectrometer.

4.3.4 Increasing bubble density

Even though it proved to sensitivity for Pd, the extended measurement period and intended application to microfluidics makes signal integration less than ideal. Increasing bubble density should enhance the sensitivity, but simply increasing the ethanol concentration has deleterious effects on refractive index gradients at the interface and causes significant loss in S/N. An alternative is to replace the ethanol with a solvent which has higher gas solubility. Longer chain alcohols have higher gas solubilities than

ethanol,¹⁸ and the solubility increase comes with a proportionately smaller increase in refractive index than would be the case if the ethanol concentration were raised.¹⁹ The upper limit on chain length is imposed by miscibility of the alcohol in water.

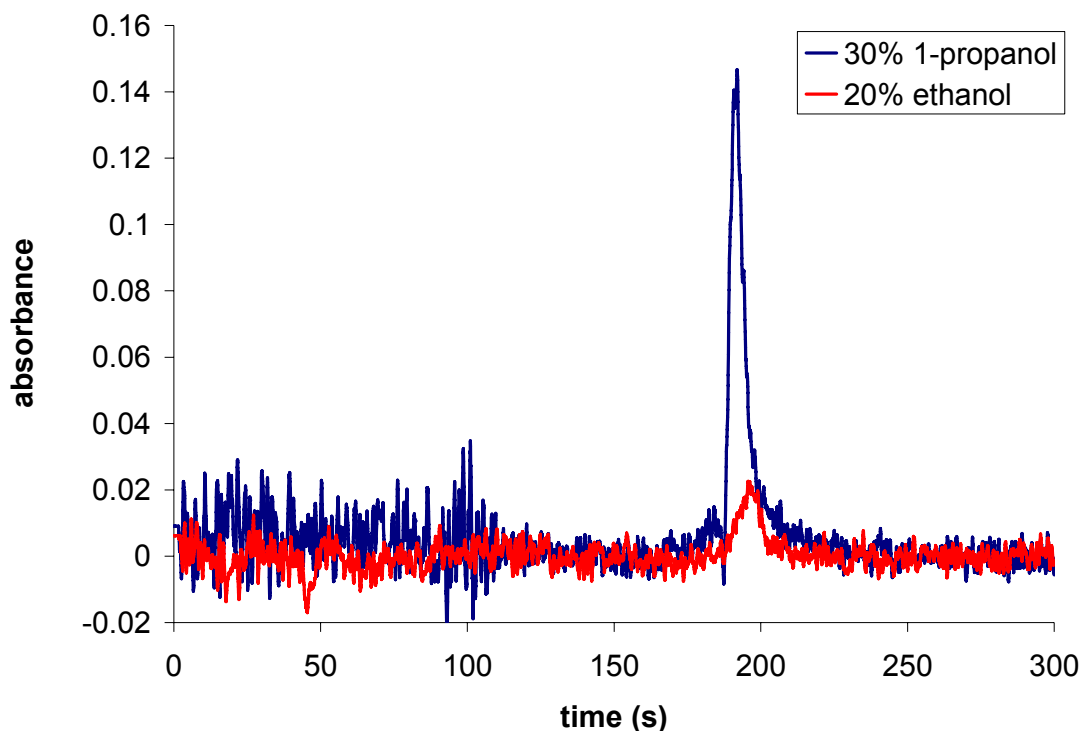


Figure 4.18 CASAA signal for 5 ppm Pd using 0.1% NaBH₄/30% 1-propanol reducing solution and 100 μL injection volume compared to data using ethanol.

1-propanol exhibits a 70% increase in gas solubility over ethanol¹⁸ and is very miscible with water. Thus, an aqueous solution containing 30% 1-propanol was selected as a good compromise of gas solubility and miscibility. Using the same procedure as before to generate the transient signal from a flowing solution, it was found that the peak shapes were similar to those produced with ethanol and the atomic absorption and background peak heights increased by 5-fold (Figure 4.18), which yielded a significant

sensitivity improvement was achieved (Figure 4.19). While poor response characteristics above 1 ppm Pd are shown, a reproducible, linear response is seen below 1 ppm.

The 1-propanol system yielded an average bubble diameter of ca. 900 nm, which is a 12% increase in diameter (i.e., a 40% increase in volume). Since an increase of 200% in signal area observed with the 1-propanol is higher than the 109% signal enhancement expected from reduced pressure within the larger bubbles, it is likely that more bubbles are also formed in the change to propanol. The detection efficiency for this system was determined to be 0.4% for 100 μ L of 500 ppb Pd solution. The system yields a detection limit for Pd of \sim 100 ppb in 100 μ L, based on $S/N=3$ using the standard deviation of the time-integrated blank level from a continuous flow run to determine N and the slope of the calibration curve to estimate S .

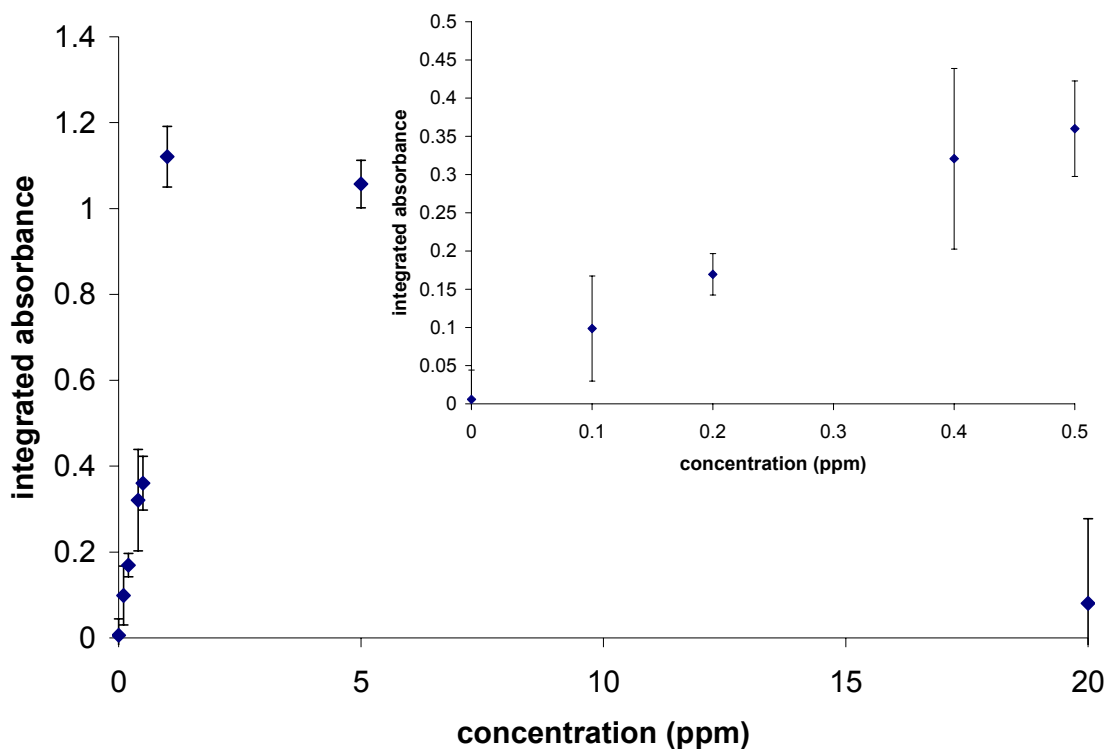


Figure 4.19 Calibration curve for Pd using 0.1% NaBH₄/30% 1-propanol reducing solution and 100 μ L injection volume.

While the CASAA signal intensity and detection efficiency were increased, the 0.4% efficiency indicates additional room for improvement. The creation of higher bubble density is an obvious target but increased alcohol/water ratios are accompanied by increased refraction (i.e., background and beam distortion) at the mixing interface. The current state of knowledge of the processes suggests the possible utility of rapid, complete mixing of the two solutions without loss in bubble density by dilution. The present system was designed with minimal convective mixing to permit elucidation of the mechanisms responsible for the signal production and to establish a repeatable experimental protocol as a point from which further optimizations could begin.

4.4 CONCLUSIONS

A means of reproducibly generating cold vapor metal atoms in solution has been developed, and strong evidence that the signal arises from free atoms trapped inside bubbles within the solution presented. Additionally, some insights into processes that are (and *are not*) limiting signal development have been clarified. Processes of homonucleation for reducible, nonvolatile metals such Pd compete with mass transport of solvated atoms to the bubble interface, and the solvated Pd obviously leads to elevated background levels as well. Increasing the bubble density should improve this situation. However, making a larger number of smaller bubbles from the same volume of gas can lead to elevated pressure within each bubble and significant pressure broadening of the atomic line. In short, the next advancement is optimization of bubble size and density within solution to facilitate atom transport into the bubbles. Similarly, successful translation of the concepts to a microfluidics-type design remains an obvious objective.

The approach of bubble formation by destabilizing gas solubilized in a water-alcohol solution is viable and reproducible, but the inherent refractive index change may significantly impact signal reproducibility with the use of a high aspect ratio cell, such as that found in microfluidics applications. More thorough mixing of the water and alcohol solutions might circumvent this problem but has yet to be tested. It also remains to determine whether the conditions used to form a CASAA signal for Pd are transferable to other metals.

REFERENCES

- (1) Lovett, R. J.; Parsons, M. L. *Applied Spectroscopy* **1977**, *31*, 424-434.
- (2) Lovett, R. J.; Parsons, M. L. *Spectrochim. Acta, Part B* **1980**, *35B*, 615-630.
- (3) Lovett, R. J. *Applied Spectroscopy* **1985**, *39*, 778-786.
- (4) Guell, O. A.; Holcombe, J. A. *Appl. Spectrosc.* **1991**, *45*, 1171-1176.

- (5) Panichev, N.; Sturgeon, R. E. *Analytical Chemistry* **1998**, *70*, 1670-1676.
- (6) Whiting, E. E. *J. Quant. Spectrosc. Radiat. Transfer* **1968**, *8*, 1379-1384.
- (7) Hannaford, P. *Spectrochimica Acta, Part B: Atomic Spectroscopy* **1994**, *49B*, 1581-1593.
- (8) Lou, S.-T.; Ouyang, Z.-Q.; Zhang, Y.; Li, X.-J.; Hu, J.; Li, M.-Q.; Yang, F.-J. *Journal of Vacuum Science & Technology, B: Microelectronics and Nanometer Structures* **2000**, *18*, 2573-2575.
- (9) Lou, S.; Gao, J.; Xiao, X.; Li, X.; Li, G.; Zhang, Y.; Li, M.; Sun, J.; Li, X.; Hu, J. *Materials Characterization* **2002**, *48*, 211-214.
- (10) Jones, S. F.; Evans, G. M.; Galvin, K. P. *Advances in Colloid and Interface Science* **1999**, *80*, 27-50.
- (11) Chen, S.; Huang, K.; Stearns, J. A. *Chemistry of Materials* **2000**, *12*, 540-547.
- (12) Feng, Y.-L.; Sturgeon, R. E.; Lam, J. W. *Analytical Chemistry* **2003**, *75*, 635-640.
- (13) Feng, Y.-L.; Sturgeon, R. E.; Lam, J. W. *Journal of Analytical Atomic Spectrometry* **2003**, *18*, 1435-1442.
- (14) Sanz-Medel, A.; Valdes-Hevia y Temprano, M. C.; Bordel Garcia, N.; Fernandez de la Campa, M. R. *Analytical Chemistry* **1995**, *67*, 2216-2223.
- (15) Clift, R. *Bubbles, drops, and particles*; Academic Press: New York, 1978.
- (16) Guell, O. A.; Holcombe, J. A. *Analytical Chemistry* **1990**, *62*, 529A-534A, 536A, 538A, 540A-542A.
- (17) L'Vov, B. V. *Spectrochimica Acta, Part B: Atomic Spectroscopy* **1990**, *45B*, 633-655.
- (18) Fogg, P. G. T.; W., G. *Solubility of Gases in Liquids*; John Wiley and Sons: New York, 1991.
- (19) *CRC Handbook of Chemistry and Physics*, 83 ed.; CRC Press: New York, 2002.

Chapter 5: Some preliminary explorations and future directions

5.1 POSSIBLE AVENUES FOR FUTURE RESEARCH

The research presented in this thesis will hopefully provide an impetus for further exploration of the production of metal vapor species within bubbles. It should provide a foundation which makes the technique easier to apply to other analytes or to modify experimental setup. Some ideas for future directions for this work are indicated in this chapter.

5.1.1 Increasing reaction cell path length

Increasing the path length of the reaction cell is one of the most obvious ways of increasing signal intensity for the procedure described in the previous chapter. The eventual goal of fabricating a long path length reaction cell on a chip also makes this a necessary avenue of research to explore. During the course of this thesis research, preliminary studies were undertaken using 5 cm path length quartz cells which met with mixed amounts of success.

The first cell design employed the use of a 3 mm diameter quartz tube with an inlet and outlet 5 mm from either end attached to the tube tangentially to foster mixing within the observation zone of the spectrometer. The tube was sealed at either end using 1 mm thick quartz windows made from microscope slides attached with silicone adhesive. This was mounted so that the length of the tube (5 cm) was in the observation zone of the spectrometer. This cell design gave no signal, because a minimal amount of light was able to pass through the cell and reach the detector. The low photon flux was caused by the diverging optics giving the relatively large observation zone (see Appendix C for mapping of beam intensities) used by the spectrometer. Furthermore, the design

with inlet and outlet at either end of the cell caused large bubbles to be trapped within the cell, scattering any light that was able to pass into the cell.

The cell was redesigned with a larger diameter and the inlet and outlet of the cell were aligned in the middle as shown in Figure 5.1.

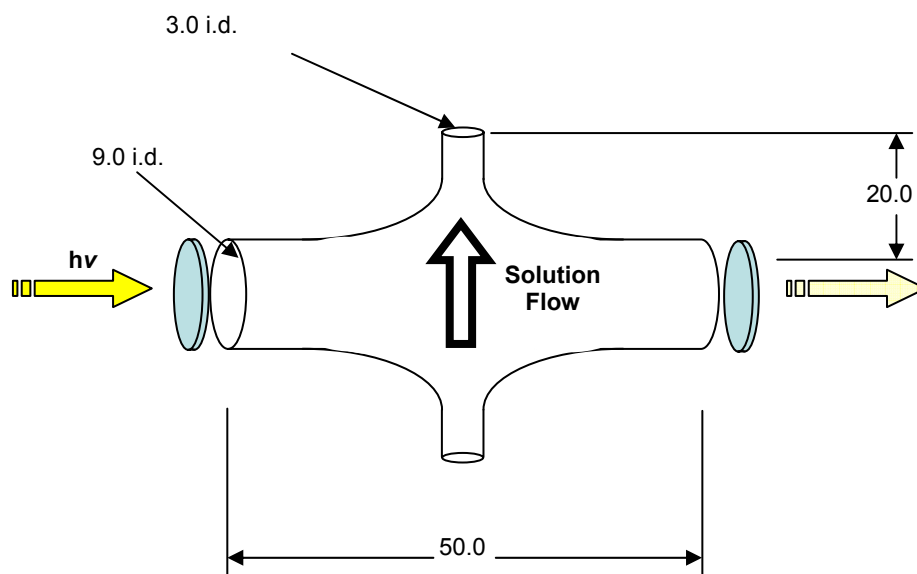


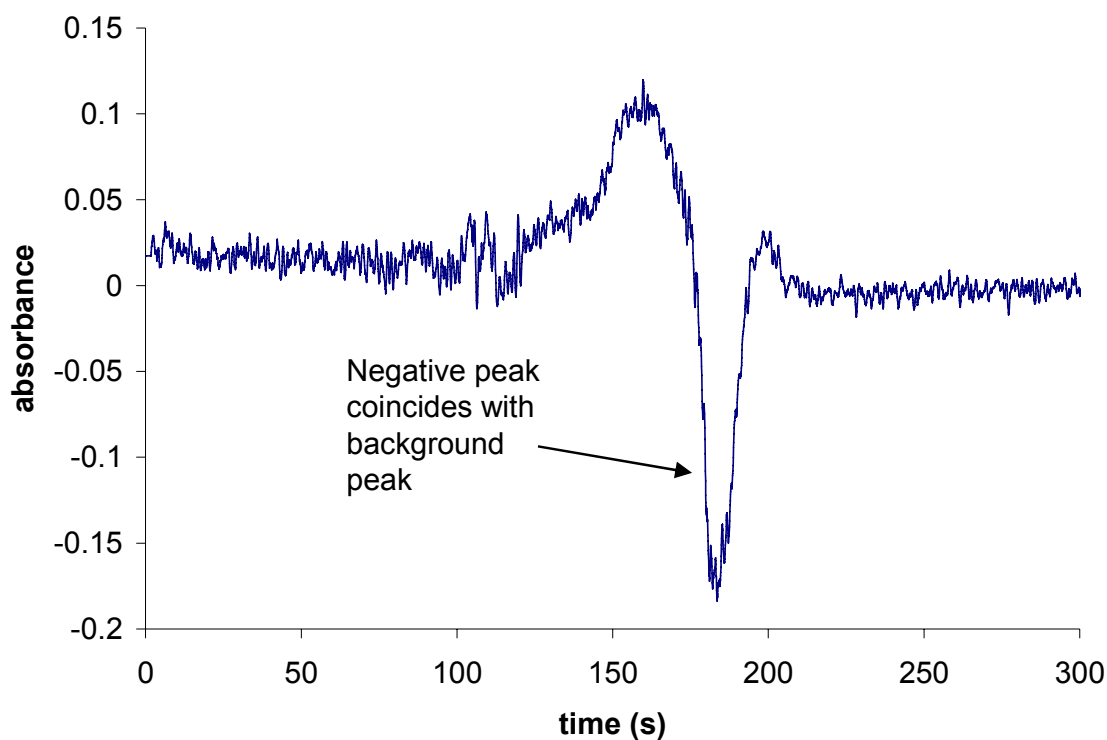
Figure 5.1 Cylindrical cell designed to increase effective path length. All measurements are in mm.

This cell design allowed any large bubbles generated from NaBH_4 or from changing reagent solutions to easily pass through and out of the cell with little interference in the observation of the absorption signal. Experiments using dye confirmed that the flow patterns from the top to the bottom of the cell were similar to that for the cell design used in the previous chapter, with the metal plug flowing upward in a discrete band.

Initial results using this cell design yielded a 5 fold increase in signal intensity, but also yielded over a 5 fold increase in background intensity. Figure 5.2 shows the results of producing a CASAA signal with 20 ppm Pd using 20% ethanol and 0.1%

NaBH₄ as a reducing solution. The negative peak was a result of an extremely intense background peak (~2.0 absorbance). In the case that very few photons are detected, the instrument measures a negative peak as the background correction overcompensates.

Figure 5.2 CASAA signal obtained for 100 μL of 20 ppm Pd for reaction cell with 5 cm path length



The results of this experiment were rather unfortunate given the ease of changing the reaction cell path length to increase signal intensity. However, these results are unavoidable without a radiation source with a higher photon flux. In addition to the ability to correct for background effects on a fast time scale, the use of a diode laser/photodiode detection scheme discussed in Chapter 1 would prevent the problems encountered above because of the higher photon flux and small spatial dimensions of the optical beam. Future research into applying a similar setup to detection of a CASAA

signal should be performed to lower detection limits with the longer path length as well as improve S/N and background correction capabilities through the use of diode lasers.

5.1.2 Increasing CASAA signal through more complete reagent mixing

The main thrust of the last portion of Chapter 4 indicated that bubble density may have been one of the biggest limits to increasing signal intensity. Experiments using propanol instead of ethanol for the production of bubbles showed a 5 fold increase in signal intensity and a 2 fold gain in detection efficiency. However, with the detection efficiency quite low (ca. 0.4%), increasing bubble density further without increasing average bubble size proportionally appears to be an avenue worthy of pursuit. Increasing the amount of mixing within the cell is one method of doing this, as bubble generation only appears to be occurring near the interface between DI water and ethanol/propanol solutions. As shown by the discussion of different cell designs in Chapter 4, mixing the solutions in a turbulent manner causes the CASAA signal to disappear altogether in many cases, however this appears to be the most obvious method of increasing bubble density, the parameter causing the single largest example of signal enhancement. Preliminary experiments have also been performed to increase mixing through out the cell, but thus far have had little success.

One of the first attempts at increasing bubble density through mixing was to change the order in which reagents were added to the system so that a metal plug in ethanol is added to a cell filled with DI water and reducing agent instead of the normal method of adding a metal plug to an ethanol filled cell. The advantage is that the ethanol solution would be going from 20% to <1% immediately instead of the normal procedure in which the ethanol goes through the same transition over a longer period of time as water is pumped into the system. It was rationalized that the faster transition would also cause rapid bubble formation, allowing atoms reduced to move into bubbles before

competing reactions could cause molecular species to form. This procedure gave no signal, and experiments using dye to monitor the movement of the ethanol plug revealed that the density difference between the ethanol and DI water solution caused the plug to rapidly rise through the cell and exit, with very little interaction between the plug and surrounding solution.

Other attempts at mixing reagent solutions within the cell were undertaken. Manually shaking the cell and placing it within the observation zone of the spectrometer showed some increases in signal, but results were understandably not reproducible from one run to the next. In order to adapt this idea further, a piezoelectric crystal was attached using epoxy to the cylindrical 5 cm path length cell detailed in Figure 5.1. When attached to a waveform generator and amplifier, it was hoped that mixing within the cell would be increased. Initial experiments with a dye plug indicated that the resonance frequency of the cell would be difficult to locate, but the presence of the formation of a standing wave within the dye plug at seemingly random time pointed toward the potential of this methodology. Unfortunately the devices controlling the piezoelectric crystal were home built and inadequate for producing substantial mixing. A further treatment of this method of mixing the cell contents with a more sophisticated experimental setup could prove useful in increasing the detection efficiency.

One last experiment should be noted to show the feasibility in pursuing this method of increasing the detection efficiency for a CASAA signal. The cell detailed in Figure 4.3 was modified so that a syringe needle (22 gauge, Fisher Scientific) was used for injecting the metal plug. The inlet at the bottom of the cell was only used to introduce 20% ethanol/0.1% NaBH₄ and then DI water after metal plug entry. The syringe tip was inserted into the cell from the top so that it touched the cell bottom increasing the linear velocity of the metal plug entering the cell as a consequence. In this way some mixing

within the cell was achieved. Figure 5.3 shows the results of this setup for 500 μL of 20 ppm Pd solution and 20% ethanol/0.1% NaBH_4 .

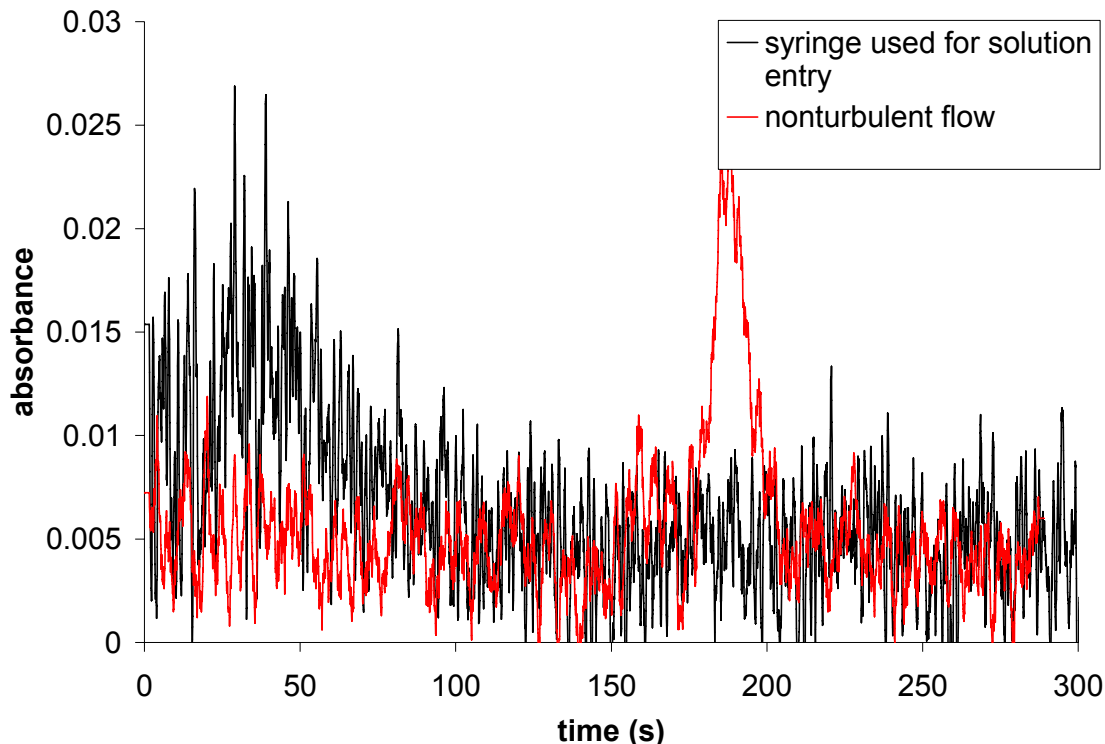


Figure 5.3 Results of turbulent mixing from use of syringe needle to facilitate turbulent entry of metal analyte plug.

For the run using the syringe needle for metal plug entry, time zero denotes the time at which the metal plug entered the cell. The nonturbulent flow curve is simply the result observed in the previous chapter in Figure 4.7 for an unmodified reaction cell. The most obvious result of changing the flow pattern is a peak which has a lower S/N but is considerably longer lasting. Integration of both signals shows that the mixing increases the peak area by 36%, indicative of more atoms being detected. Because the flow is so turbulent, bubble size calculations based on rise velocity performed in the previous chapter are not applicable. Therefore it is difficult to determine whether this method is

giving higher detection efficiency or simply attenuating the absorption line less because of the presence of larger bubbles. While agitation using a piezoelectric crystal might be a more sophisticated method of mixing and have a potentially bigger impact, initial success using the strategy shown in Figure 5.3 shows the most immediate promise.

5.1.3 Obtaining a CASAA signal for other metals

One of the largest drawbacks to the CASAA signal generation procedure discussed throughout this research is that it has only been applied to one metal, Pd, thus far. The most critical future work should be the application of the procedure to other elements. Without doing this, it has little applicability and has no advantage over miniature plasma sources discussed in Chapter 1. The work on which much of this research was based¹ showed a working procedure for 3 different elements, Ag, Pd, and Cu. Additional work performed in the same laboratory by Feng et al²⁻⁴ suggests that atomic species such as Au, Cd, Hg, and Rh are stable within solution, although no atomic signal has yet been reported. Pt also appears to be a likely candidate for future research because of a favorable E° for Pt^{2+} (1.18V)⁵ indicates that it should be easier to reduce than Pd^{2+} ($E^\circ = 0.915$).⁵

It is important to consider what limitations the procedure could potentially have when attempting to apply it to other elements. $NaBH_4$ and $SnCl_2$ are strong reducing agents capable of reducing many metals, but the largest limitation is likely imposed by the solvent. Many metals beyond those mentioned above can be reduced by these reagents, but the reduction of water would proceed first in many cases. This is even true for some of the metals discussed above. Using Cu as an example because it is one of the least reducible metals mentioned above, calculations using the Nernst equation considering the 0.1% $SnCl_2$ at pH 1 show that below concentrations of ~50 ppb reduction of water will become significant. Other, more easily reduced metals such as Pt should

not suffer from this limitation. Considering the reduction potentials, the elements As, Bi, Ge, Ir, Os, Sb and Ru can be added to the list of potential analytes, although some, such as Ge, would have to be present in significant amounts ($> 1\text{ppm}$) for the reaction to proceed. Similarly, hydride formation may be a competing product, especially with borohydride reductant. Future work in the area of expanding this procedure should commence with the elements discussed, and some leeway may be afforded if the pH of the system were raised above the pH 1 in order to make reduction of water less favorable. In order to expand the applicability to other elements, a procedure using a nonaqueous system with even stronger reducing agents such as LiAlH_4 would have to be devised.

5.2 CONCLUSIONS

The thesis research presented has discussed many of the fundamental processes occurring within systems containing metal vapor atoms. Much of the early work using Hg vapor in large scale bubbles has proven useful when considering how to produce and maintain atoms of Pd in a similar system on a much smaller scale. While initial goals included miniaturization and fabrication of the technique onto a chip, the complexity of such a system, not initially obvious, made the simple production of a reproducible CASAA signal a very involved undertaking.

Initial exploratory studies using Hg vapor in a bubble surrounded by flowing solution yielded insight into some of the parameters which could be important for maintaining a metal vapor within a bubble. Significant increases in decay times were observed for solutions with low densities and high ionic strengths. Reducing agent strength also proved to be an important parameter to control. Most importantly, experimental as well as theoretical studies showed that gas phase diffusion was not a parameter that dictated the signal decay time for Hg.

Studies centering on the decay of Hg out of a bubble within a stagnant system displayed the long amount of time an atomic signal could last due to slow diffusion and limited solubility of the elemental species. The feasibility of transporting metal vapor atoms into a bubble was also shown, although it was similarly slow. This initially proved the necessity of having elemental species travel small distances to the point of detection, and of having strong reducing agents in solution to keep species in their relatively insoluble elemental state. Simulations focusing on the transport of Hg species out of a bubble were able to give some insight into the system as well as yielding methods to calculate the diffusion coefficient and solubility of Hg species in aqueous solution.

The value of the research performed with Hg was demonstrated upon the successful detection of a reproducible CASAA signal for Pd. Initial experimental design suggested that the formation of many nanoscale bubbles would yield the optimal signal, however studies of absorption line broadening suggested that bubbles around 1 μm in diameter would prevent excessive attenuation of the signal. Bubble generation was accomplished from methods found in the literature,⁶ and simply depended upon the transfer of dissolved gases into another solvent, allowing bubbles to form. While the signal was initially quite small, signal enhancement was shown to occur with the addition of surfactant, and through the careful selection of bubble generation reagents. Studies using long integration times surprisingly showed signals lasting over 5000 s for Pd. Bubble density appeared to be the largest parameter affecting the detection efficiency of Pd in the system, with 20% ethanol solution yielding an efficiency of 0.2% and 30% 1-propanol giving 0.4% efficiency because of the increase in both the size and number of bubbles formed.

While much of the initial work to make CASAA signal production a reproducible analytical technique rather than a phenomenon, there is much future work that could be

performed. Mixing the reagents more completely should increase detection efficiency with the generation of higher bubble density, and longer path length absorption cells should contribute to higher signal intensity. Most importantly, application of this research to other elements is necessary if it is to be accepted as a feasible technique by the analytical community. This should be much easier with the work presented, and the inclusion of a diode laser-based atomic absorption system would make the development of the technique much smoother.

REFERENCES

- (1) Panichev, N.; Sturgeon, R. E. *Analytical Chemistry* **1998**, *70*, 1670-1676.
- (2) Feng, Y.-L.; Lam, J. W.; Sturgeon, R. E. *Spectrochimica Acta, Part B: Atomic Spectroscopy* **2004**, *59B*, 667-675.
- (3) Feng, Y.-L.; Sturgeon, R. E.; Lam, J. W. *Analytical Chemistry* **2003**, *75*, 635-640.
- (4) Feng, Y.-L.; Sturgeon, R. E.; Lam, J. W. *Journal of Analytical Atomic Spectrometry* **2003**, *18*, 1435-1442.
- (5) *CRC Handbook of Chemistry and Physics*, 83 ed.; CRC Press: New York, 2002.
- (6) Lou, S.-T.; Ouyang, Z.-Q.; Zhang, Y.; Li, X.-J.; Hu, J.; Li, M.-Q.; Yang, F.-J. *Journal of Vacuum Science & Technology, B: Microelectronics and Nanometer Structures* **2000**, *18*, 2573-2575.

Appendix A: Data collection setup

The spectrometer used (Varian SpectrAA 400Plus) did not have a method which allowed data output. The control software is DOS-based and exporting data through the software was not an option which could be explored without reprogramming the software in some way. The age of the instrument made the use of one computer for controlling the instrument and another computer for data collection and analysis necessary. The control computer required 1 free ISA slot for the control card and a hard drive no larger than 100 MB (or the software would read an error and lock up). The data collection computer was attached to the instrument directly as shown in Figure A.1.

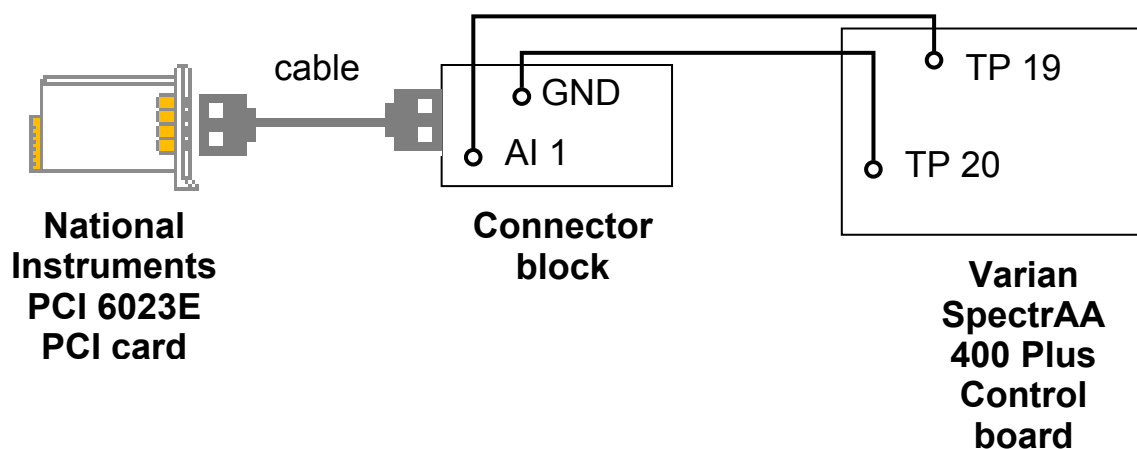


Figure A1 Schematic of data collection setup. Wires attached test point 19 on the control board of the spectrometer to Analog Input 1 on the connection block and test point 20 to ground on the connection block. The connection block was connected to a DAQ card via 68 pin cable.

Test point 19 on the spectrometer control board provided a signal at a rate of 16 Hz representing the absorbance signal of interest. This means that if background correction were turned on, the signal output would be a voltage representative of the

background corrected signal. If the background correction were turned off, the voltage would also reflect this. In this way the signal could be monitored by a data acquisition (DAQ) card made by National Instruments. However, since only this test point gave the signal, only one signal could be monitored at a time. Thus the background and background corrected signal could not be monitored simultaneously.

Data was acquired using Labview 7.0 software (National Instruments). The VI used was called Cont Acq to Spreadsheet File.vi and was built into Labview and shown in Figure A.2. The only modification made was to make the data collection rate 16 Hz or 4 Hz in the case of long runs. The data was output to a text file which had the time and voltage in 2 columns with the first row being the data collection rate.

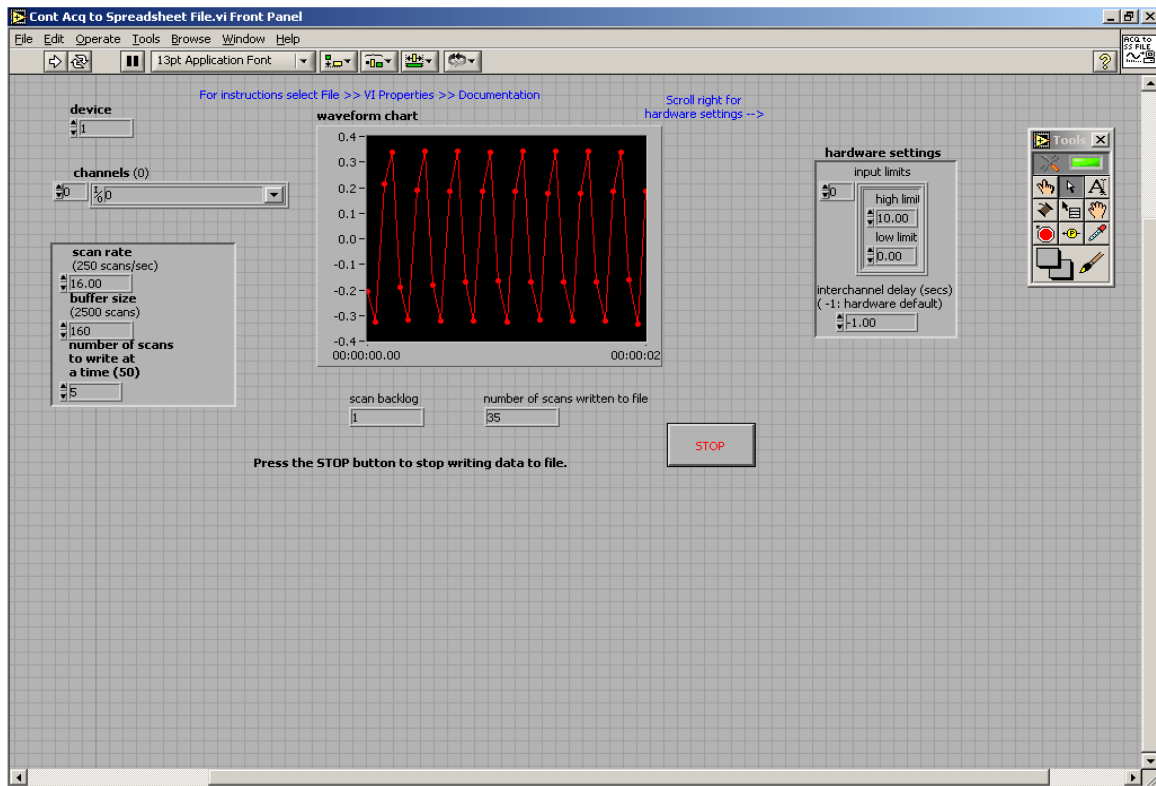


Figure A.2 Screenshot of Cont Acq to Spreadsheet File.vi

The voltage was converted to absorbance through the use of a calibration curve. This was constructed by placing various meshes within the observation zone of the spectrometer, tabulating the associated absorbance from the control computer, and correlating a voltage to this on the data collection computer. The calibration curve is shown in Figure A.3.

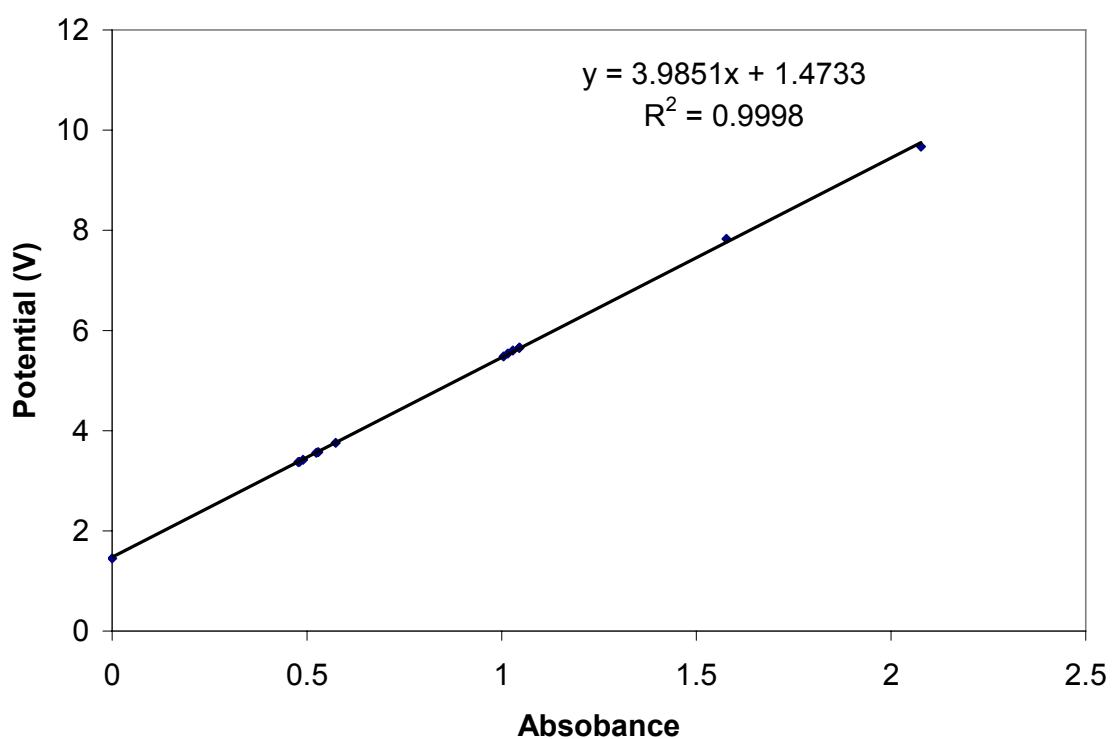


Figure A.3 Calibration curve for converting voltage to absorbance

Appendix B: Visual Basic code for simulations

B.1 MONTE CARLO SIMULATION TO DETERMINE TIME OF PARTICLE LOSS CONSIDERING ONLY GAS DIFFUSION RATES

The following is the Visual Basic (VB) code used to calculate the amount of time that it would take for Hg vapor to leave a 500 μL bubble assuming only that the gas diffusion rate is the limiting factor. This also calculates the “sticking coefficient” necessary for the simulation to match the data observed experimentally. Further details are available in Chapter 2

```
Sub random2()  
Dim Start, Finish, Totaltime  
Start = Timer  
Application.ScreenUpdating = True  
  
Dim RandomArray(9999)  
Dim count  
Dim n  
n is used in generating normally distributed random numbers  
  
Dim time, deltatime, diffcoeff, temp, numberofpart, percentsticking, radius  
these variables are input by the user  
  
Dim distx, disty, distz, Startpos, g, u, a, xpos, ypos, zpos  
  
Dim randomX, randomY, randomZ  
  
Dim PartTime(9999)  
This array contains the times that each particle is resident in the bubble  
  
radius = Range("B1").Value 'in meters  
temp = Range("B3").Value 'in Kelvin  
diffcoeff = Range("B2").Value 'm^2/s  
deltatime = Range("B4").Value 'seconds  
numberofpart = Range("B5").Value  
percentsticking = Range("B6").Value  
Randomize
```



```
n = 11
```

```
For z = 0 To 9999
```

```
count = 0
```

```
  For i = 1 To n
```

```
    count = count + Rnd
```

```
  Next i
```

This makes the uniform random numbers gaussian distributed, and puts them in an array

```
  RandomArray(z) = count - (n / 2)
```

```
Next z
```

The below loop is to iterate calculations for each particle

```
For k = 1 To numberofpart
```

```
  time = 0
```

```
  xpos = 1
```

```
  ypos = 1
```

```
  zpos = 1
```

The above initialization of x, y, and z positions as well as the below loop make sure that the starting position of each particle is not outside the bubble. The positions were initialized to 1 so the the do loop would occur the first time.

```
Do While ((xpos ^ 2 + ypos ^ 2 + zpos ^ 2) ^ (1 / 2)) > radius
```

```
  Startpos = ((radius * 2) * Rnd - radius)
```

```
  xpos = Startpos
```

X starting position is randomly decided

```
  Startpos = ((radius * 2) * Rnd - radius)
```

```
  ypos = Startpos
```

Y starting position is randomly decided

```
  Startpos = ((radius * 2) * Rnd - radius)
```

```
  zpos = Startpos
```

Z starting position is randomly decided

Loop

The below loop moves the particle with time and decides if the particle has left the loop. The variable g is randomly generated between 0 and 1 and helps determine if the particle sticks to the side of the bubble based on preset sticking percentage. The

variable a is used to randomly select an index of an array that contains normally distributed random numbers. The loop is exited when the particle leaves the bubble

Do Until Timer = 0

time = time + deltatime

Randomize

a = Int(9999 * Rnd)

randomX = RandomArray(a)

distx = randomX * (2 * diffcoeff * deltatime) ^ 0.5

Randomize

a = Int(9999 * Rnd)

randomY = RandomArray(a)

disty = randomY * (2 * diffcoeff * deltatime) ^ 0.5

Randomize

a = Int(9999 * Rnd)

randomZ = RandomArray(a)

distz = randomZ * (2 * diffcoeff * deltatime) ^ 0.5

xpos = xpos + distx

ypos = ypos + disty

zpos = zpos + distz

moves the particle some x, y, and z direction based upon previously generated random numbers

The below If statement checks to see if the particle is outside the bubble

$u = ((xpos^2 + ypos^2 + zpos^2) ^ (1 / 2))$

If u > radius Then

g = Rnd

The below if statement checks to see if the particle sticks to the side of the bubble and is lost. If it is, the loop is exited

If g * 100 <= percentsticking Then Exit Do

If the particle does not stick, it returns to its previous position

```

    If g * 100 > percentsticking Then
        xpos = xpos - distx
        ypos = ypos - disty
        zpos = zpos - distz
    End If
End If
Time is incremented for each time the particle moves
Loop

The time that each particle takes to leave the bubble is put into an array

PartTime(k - 1) = time

Range("B10").Select
Selection.Value = k

Next k
Range("G1").Select
Application.ScreenUpdating = False

The particle times are printed out

For x = 0 To numberofpart - 1
    Selection.Value = PartTime(x)
    ActiveCell.Offset(rowoffset:=1).Select
Next x

Finish = Timer
Totaltime = Finish - Start
Range("B11").Select
Selection.Value = Totaltime
Application.ScreenUpdating = True
End Sub

```

B.2 SIMULATION OF HG LEAVING BUBBLE IN STAGNANT SOLUTION

B.2.1 Explicit box method

The following is the VB code used to simulate the diffusion of Hg through solution, away from the interface. The program also allows different diffusion

coefficients in the first 10 boxes, in an effort to detect the effects of order at the interface.

Further details can be found in Chapter 3.

Sub diffusioninfluidisk2()

The parameters for the program are input

```
Start = Timer
deltat = Range("H2").Value 's
deltax = Range("H3").Value 'cm
Totaltime = Range("H4").Value
iterations = Totaltime / deltat
D = Range("H1").Value 'cm^2/s
DMA = Range("F2").Value
temperature = Range("M5").Value 'degrees Celsius
temperature = temperature + 273.15 'converts to K
radius = 0.49237 'cm
initconc = Range("M6").Value 'ppb
```

```
Jmax = Fix(Range("F3").Value)
```

makes sure the output will fit on the worksheet

```
If Jmax > 25000 Then
    Jmax = 25000
End If
If Jmax < 200 Then
    Jmax = 200
End If
```

```
concentration = (Range("M1").Value / (0.08257 * temperature)) * 200.59 * 1000000
converts partial pressure to microg/L
henry = Range("M2").Value 'unitless
volume = Range("M3").Value 'L
iterate = 0
report = Range("M4").Value
```

makes sure the output will fit on the worksheet

```
Do Until iterations / report < 40000
    report = report * 10
Loop
```

```
Dim bubble() As Double
Dim oldbox() As Double
Dim newbox() As Double
```

Dim diff(10) As Double

ReDim oldbox(Jmax + 1)
ReDim bubble(iterations + 2)
ReDim newbox(Jmax + 1)

Application.ScreenUpdating = False

For count = 0 To 9
Range("H6").Select
ActiveCell.Offset(count, 0).Select
diff(count) = Selection.Value
Next count

Make the initial conditions for mercury in solution

For count = 0 To Jmax + 1
 oldbox(count) = initconc
 newbox(count) = initconc
Next count

initmol = (initconc * 0.000001 * deltax ^ 3 / 200.59) 'mol per box
oldsum = 0
bubble(0) = concentration
oldbox(0) = concentration
surfvolume = (((radius) ^ 2 * 3.14159 * deltax)) / 1000
oldbox(1) = bubble(0) / henry

The below lines of code do the actual diffusion calculations with the for loop occurring once for every time increment

For iterate = 0 To iterations

Determine how much Hg is in the bubble by adding up Hg which diffused out

bubble(iterate + 1) = ((concentration * 0.000001 * volume / 200.59) - oldsum) *
200.59 * 1000000 / volume

the next few lines handle the situation where the concentration supposedly goes below 0 in the bubble

If bubble(iterate + 1) < 0 Then
 bubble(iterate + 1) = 0
End If

oldbox(0) is the volume pertaining to the amount of mercury in the bubble

oldbox(0) = bubble(iterate + 1)

oldsum sums the number of moles in the solution

oldsum = 0

oldbox(1) is the mercury on the bubble surface

oldbox(1) = bubble(iterate + 1) / henry

the volume next to the surface is calculated

newbox(2) = oldbox(2) + DMA * (diff(0) / D) * (2 * oldbox(1) - 3 * oldbox(2) + oldbox(3))

calculates diffusion for boxes near interface that may have different diffusion coefficients

For i = 3 To 11

newbox(i) = oldbox(i) + DMA * (diff(i - 2) / D) * (oldbox(i - 1) - 2 * oldbox(i) + oldbox(i + 1))

Next i

diffusion for all the other boxes is calculated

For i = 12 To Jmax

newbox(i) = oldbox(i) + DMA * (oldbox(i - 1) - 2 * oldbox(i) + oldbox(i + 1))

Next i

the data is saved to another array and the moles that have gone into solution are added up

For i = 2 To Jmax

oldbox(i) = newbox(i)

oldsum = oldsum + (oldbox(i) - initconc) * (((radius + deltax) ^ 2 * 3.14159 * deltax * i) / 1000 - (((radius + deltax) ^ 2 * 3.14159 * deltax * (i - 1))) / 1000) * 0.000001 / 200.59

Next i

Next iterate

The remaining part of the program prints out the mercury in the bubble at each time increment and the concentration profile at the last time increment

For x = 0 To iterations / report

Range("A1").Select

ActiveCell.Offset(x, 0).Select

Selection.Value = deltat * x * report

ActiveCell.Offset(0, 1).Select

If bubble((x * report) + 1) > 0 And concentration > 0 Then

Selection.Value = (bubble((x * report) + 1) / concentration) * 100

Else

Selection.Value = 0

End If

```

Next x

For x = 1 To Jmax
Range("A1").Select
ActiveCell.Offset(x, 2).Select
Selection.Value = deltax * (x - 1)
ActiveCell.Offset(0, 1).Select
Selection.Value = oldbox(x)
Next x

```

```

Finish = Timer
endtime = Finish - Start
Range("F4").Select
Selection.Value = endtime

```

```

End Sub

```

B.2.2 Crank Nicholson method

The following VB code uses the Crank-Nicholson method of calculating solution concentrations of Hg as it diffuses through solution. Details can be found in Chapter 3.

```

Sub CNbubblediffuse()

The parameters for the program are input
Start = Timer
deltat = Range("H2").Value 's
deltax = Range("H3").Value 'cm
Totaltime = Range("H4").Value
iterations = Totaltime / deltat
D = Range("H1").Value 'cm^2/s
DMA = Range("F2").Value
temperature = Range("M5").Value 'degrees Celsius
temperature = temperature + 273.15 'converts to K
radius = 0.49237 'cm
initconc = Range("M6").Value 'ppb

Jmax = Fix(Range("F3").Value)

makes sure the output will fit on the worksheet

```

If Jmax > 25000 Then

 Jmax = 25000

End If

If Jmax < 200 Then

 Jmax = 200

End If

concentration = (Range("M1").Value / (0.08257 * temperature)) * 200.59 * 1000000

converts partial pressure to microg/L

henry = Range("M2").Value 'unitless

volume = Range("M3").Value 'L

iterate = 0

report = Range("M4").Value

makes sure the output will fit on the worksheet

Do Until iterations / report < 40000

 report = report * 10

Loop

Dim bubble() As Double

Dim AD() As Double

Dim BD() As Double

Dim C() As Double

Dim diff(10) As Double

ReDim AD(Jmax + 1)

ReDim bubble(iterations + 2)

ReDim BD(Jmax + 1)

ReDim C(Jmax + 1)

Application.ScreenUpdating = False

For count = 0 To 9

 Range("H6").Select

 ActiveCell.Offset(count, 0).Select

 diff(count) = Selection.Value

Next count

Make the initial conditions for mercury in solution

For count = 0 To Jmax + 1

 C(count) = initconc

 AD(count) = 0

 BD(count) = 0

Next count


```

initmol = (initconc * 0.000001 * deltax ^ 3 / 200.59) 'mol per box
oldsum = 0
bubble(0) = concentration

```

```

surfvolume = (((radius) ^ 2 * 3.14159 * deltax)) / 1000

```

The below lines of code do the actual diffusion calculations with the for loop occurring once for every time increment

```

For iterate = 0 To iterations

```

Determine how much Hg is in the bubble by adding up Hg which diffused out

```

bubble(iterate + 1) = ((concentration * 0.000001 * volume / 200.59) - oldsum) *
200.59 * 1000000 / volume

```

the next few lines handle the situation where the concentration supposedly goes below 0 in the bubble

```

If bubble(iterate + 1) < 0 Then
    bubble(iterate + 1) = 0
End If

```

oldsum sums the number of moles in the solution

```

oldsum = 0

```

```

a = -2 / DMA * (1 + DMA)
A1 = -2 / DMA * (1 - DMA)

```

```

AD(Jmax) = a
BD(Jmax) = -C(Jmax - 1) + A1 * C(Jmax) - C(Jmax + 1) - initconc

```

```

C3 = C(Jmax)
C2 = C(Jmax - 1)
counter = Jmax - 1
Do Until counter = 0

```

```

    C1 = C(counter - 1)
    BI = -C1 + A1 * C2 - C3
    AD(counter) = a - 1 / AD(counter + 1)
    BD(counter) = BI - BD(counter + 1) / AD(counter + 1)
    C3 = C2
    C2 = C1
    counter = counter - 1

```

```

Loop

```

C(0) is the mercury on the bubble surface

```
C(0) = bubble(iterate + 1) / henry
```

```
For i = 1 To Jmax  
    C(i) = (BD(i) - C(i - 1)) / AD(i)  
Next i
```

the data is saved to another array and the moles that have gone into solution are added up

```
For i = 1 To Jmax  
    oldsum = oldsum + (C(i) - initconc) * (((radius + deltax) ^ 2 * 3.14159 * deltax *  
    i) / 1000 - (((radius + deltax) ^ 2 * 3.14159 * deltax * (i - 1))) / 1000) * 0.000001 /  
    200.59  
Next i  
Next iterate
```

The remaining part of the program prints out the mercury in the bubble at each time increment and the concentration profile at the last time increment

```
For x = 0 To iterations / report  
    Range("A1").Select  
    ActiveCell.Offset(x, 0).Select  
    Selection.Value = deltat * x * report  
    ActiveCell.Offset(0, 1).Select  
    If bubble((x * report) + 1) > 0 And concentration > 0 Then  
        Selection.Value = (bubble((x * report) + 1) / concentration) * 100  
    Else  
        Selection.Value = 0  
    End If  
Next x
```

```
For x = 1 To Jmax  
    Range("A1").Select  
    ActiveCell.Offset(x, 2).Select  
    Selection.Value = deltax * (x - 1)  
    ActiveCell.Offset(0, 1).Select  
    Selection.Value = C(x)  
Next x
```

```
Finish = Timer  
endtime = Finish - Start  
Range("F4").Select  
Selection.Value = endtime
```

```
End Sub
```

B.3 MONTE CARLO SIMULATION OF DIFFUSION THROUGH CUVET

The below VB code was used to simulate diffusion throughout a cuvet, and was used in Chapter 4.

```
Sub banddiffusion()
```

Macro present in file banddiffusion calc.xls

```
Dim RandomArray(9999)
```

```
Dim PartposZ(9999)
```

```
Dim PartposX(9999)
```

```
Dim PartposY(9999)
```

```
Dim count
```

```
Dim n
```

```
Dim time, deltatime, diffcoeff, temp, numberofpart
```

```
Dim distx, disty, distz, Startpos, g, u, a, xpos, ypos, zpos
```

these variables are input by the user

```
temp = Range("B3").Value 'in Kelvin
```

```
diffcoeff = Range("B2").Value 'cm2/s
```

```
deltatime = Range("B4").Value 'seconds
```

```
numberofpart = Range("B5").Value
```

```
totaltime = Range("B6").Value
```

```
plugwidth = Range("B8").Value
```

```
n = 11
```

```
For k = 1 To numberofpart
```

```
time = 0
```

particle starting positions are randomly selected within the height of the metal plug

```
xpos = Rnd
```

```
ypos = Rnd
```

```
zpos = Rnd * plugwidth
```

```
Do Until time > totaltime - deltatime
```

The following moves each particle in X, Y, and Z directions during each time increment.

```
count = 0
```

```
For i = 1 To n
```

```
count = count + Rnd
```

```
Next i
```

```
randomX = count - (n / 2)
```

```
distx = randomX * (2 * diffcoeff * deltatime) ^ 0.5
```

```

count = 0
For i = 1 To n
    count = count + Rnd
Next i
randomY = count - (n / 2)
disty = randomY * (2 * diffcoeff * deltatime) ^ 0.5

```

```

count = 0
For i = 1 To n
    count = count + Rnd
Next i
randomZ = count - (n / 2)
distz = randomZ * (2 * diffcoeff * deltatime) ^ 0.5

```

```

xpos = xpos + distx
ypos = ypos + disty
zpos = zpos + distz

```

The following code is used if a particle hits a cuvet wall. The particle put back to the position before it moved and is moved again in a different direction

```

Do While xpos > 1 Or xpos < 0
    xpos = xpos - distx
    count = 0
    For i = 1 To n
        count = count + Rnd
    Next i
    randomX = count - (n / 2)
    distx = randomX * (2 * diffcoeff * deltatime) ^ 0.5
    xpos = xpos + distx
Loop

```

```

Do While ypos > 1 Or ypos < 0
    ypos = ypos - disty
    count = 0
    For i = 1 To n
        count = count + Rnd
    Next i
    randomY = count - (n / 2)
    disty = randomY * (2 * diffcoeff * deltatime) ^ 0.5
    ypos = ypos + disty
Loop

```

Time is incremented for each time the particle moves
time = time + deltatime

Loop

```
PartposZ(k - 1) = zpos  
PartposX(k - 1) = xpos  
PartposY(k - 1) = ypos  
Range("B10").Select  
Selection.Value = k
```

Next k

Data output

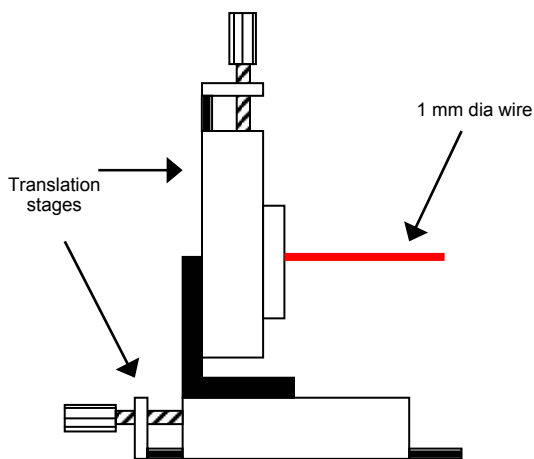
```
Range("G1").Select  
Application.ScreenUpdating = False  
For x = 0 To numberofpart - 1  
    Selection.Value = PartposX(x)  
    ActiveCell.Offset(columnoffset:=1).Select  
    Selection.Value = PartposY(x)  
    ActiveCell.Offset(columnoffset:=1).Select  
    Selection.Value = PartposZ(x)  
    ActiveCell.Offset(rowoffset:=1, columnoffset:=-2).Select  
Next x
```

End Sub

Appendix C: Alignment of Hollow Cathode and Deuterium lamps

The work detailed in Chapter 4 necessitated that the observation zones for Hollow Cathode and Deuterium lamps be the same volume of space. If this was not the case, an erroneous signal could be detected from scatter and/or broadband absorption. The apparatus used consisted of 2 translation stages (Newport) which moved 0.3 mm per turn and a wire 1 mm in diameter to block part of the lamp beam. A diagram is shown in Figure C.1.

Figure C.1 Apparatus for probing beam profile. Wire was scrolled across beam in vertical and horizontal directions for all lamps used using translation stages.



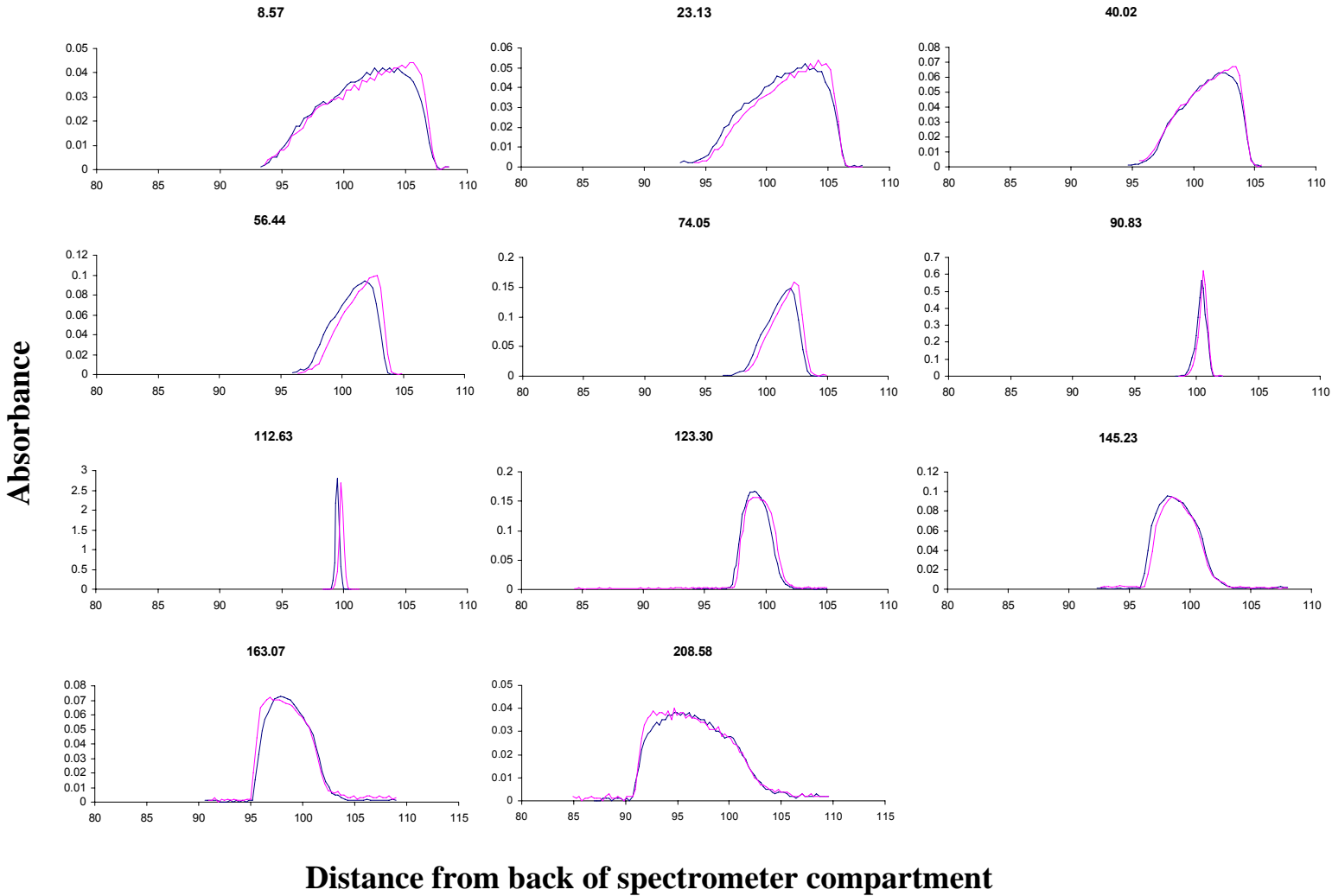
This apparatus was used to determine the beam profile as observed by the detector of the instrument. While a simple mapping of the beam could have been performed by visually inspecting where the beam was hitting the reaction cell, this method permitted the observation of what areas and intensities the detector was able to observe. The spectrometer has a working area where the burner apparatus would normally be installed. This compartment is 220 mm wide. The apparatus in Figure C.1 was used to map the

beam at various distances across this area in both the horizontal and vertical directions.

The absorbances in the horizontal direction are shown in Figure C.2.

Figure C.2 Horizontal beam profiles for Pd hollow cathode and deuterium lamps.

Number at the top of each graph is the distance along the beam from the side of the spectrometer compartment.



The diverging optics on the instrument cause the beam to decrease in width and height as it approaches the tangential and sagittal focal points at 113.36 mm and 108.37 mm.

mm respectively. Knowing these focal points allowed the reaction cell to be placed where they are present.

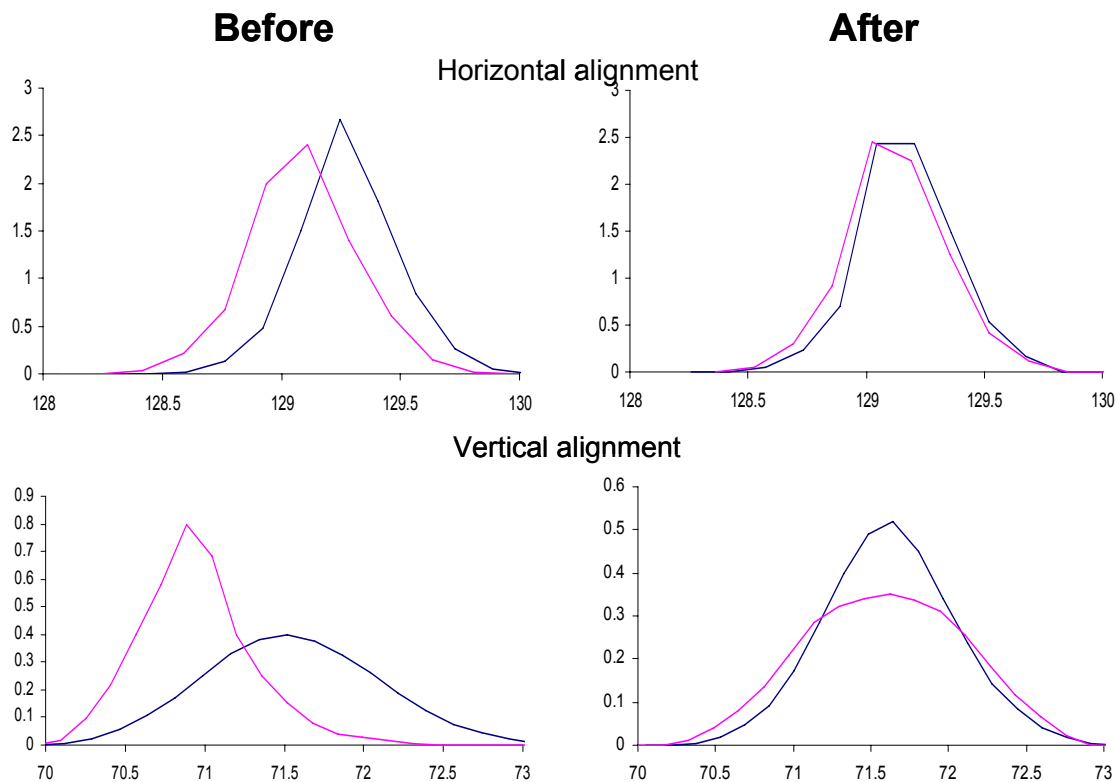


Figure C.3 Results of aligning Hollow Cathode and Deuterium lamp beams. Results shown are for Pd lamp. Darker line denotes deuterium lamp

The beam was aligned by moving the deuterium lamp to its optimal position, and moving the HCL away from optimum position, but aligned with the deuterium lamp. This procedure was used because the D₂ lamp intensity at the wave length of interest, 340.5 nm, was not intense. The results of aligning the beam are shown below in Figure C.3.

The alignment was repeated for every hollow cathode lamp used and any time a lamp was replaced. Alignment of all lamps was repeated after any replacement of the deuterium lamp.

Vita

John Leo Molloy was born February 15, 1979 in Dallas, Texas to Robert and Rebecca Molloy. He attended Bishop Lynch High school in Dallas and later graduated from Jack C. Hays High school in Buda, Tx in 1997. He attended Southwestern University in Georgetown, Tx and graduated with a Bachelors of Science in Chemistry in 2001. He started pursuing a PhD at The University of Texas at Austin in 2001, working for James A. Holcombe.

Permanent address: 415 W. 39th St. #308, Austin, Tx 78751

This dissertation was typed by the author.